UNIVERSITY *of*
TASMANIA
AUSTRALIA

School of Physical Sciences

Sal'nikov's reaction in a compressible gas

Rhys A Paul

BSc(Hons)

August 2017

Supervisors: Prof. Larry Forbes, Dr. Michael Brideson

Submitted in fulfilment of the requirements for the Degree of

Doctor of Philosophy

Declaration

This thesis contains no material which has been accepted for a degree or diploma by the University or any other institution, except by way of background information and duly acknowledged in this thesis, and to the best of my knowledge and belief no material previously published or written by another person except where due acknowledgement is made in the text of this thesis, nor does the thesis contain any material that infringes copyright.

Signed:

Rhys A. Paul

July 21, 2017

This thesis may be made available for loan and limited copying in accordance with the Copyright Act 1968

Signed:

Rhys A. Paul

July 21, 2017

Acknowledgements

I would like to thank my fiancée Gabby for supporting me over the years. Without her, this thesis would not be half of what it is, and nor would I.

I would also like to thank my supervisor Larry Forbes, who has been a wealth of patience, enthusiasm, and insight. Also to Michael Brideson, for providing somewhere to vent, to bounce ideas around, and to just talk.

Thanks also to Bryn Emptage and Jesse Swan, for all of the help with the more technical aspects of writing and typesetting, and for the laughter.

Finally, to my friends and family, a huge thank you for all of the support and understanding.

The following people contributed to the publication of work undertaken as part of this thesis:

Travelling waves and oscillations in Sal'nikov's reaction in a compressible gas

Rhys Paul 75%, Larry Forbes 25%

Combustion waves in Sal'nikov's reaction scheme in a spherically symmetric gas

Rhys Paul 80%, Larry Forbes 20%

Sal'nikov's reaction behind a spherical shock (Unsubmitted)
Rhys Paul 80%, Larry Forbes 20%

Signed:

Larry Forbes

Supervisor

School of Physical Sciences

University of Tasmania

Signed:

John Dickey

Head of School

School of Physical Sciences

University of Tasmania

Abstract

This thesis analyses a combustion reaction modelled by Sal'nikov's scheme in three geometries and contexts.

Chapter 1 considers the reaction as it occurs through a pipe of infinite length, so that the gas properties vary only in one dimension along the pipe's axis. Various asymptotic techniques are applied to reduce the governing equations to an approximate, weakly non-linear system to which travelling wave solutions are sought. These solutions are then compared to the results of a numerical scheme, which models the full, highly non-linear governing equations. Finally, the numerical scheme is used to explore behaviours beyond the scope of the asymptotic analysis.

Chapter 2 models the reaction in a spherically-symmetric cloud of gas, in which the gas properties are dependent only on the radial distance from the centre of the reaction. The governing partial differential equations are replaced by an approximate linear system, and solutions are found either as travelling waves or by using integral transforms, depending on the value of a bifurcation parameter which is also shown to determine the reaction stability. Again, these approximate solutions are compared to a numerical scheme to verify their accuracy.

In chapter 3, a similar radially-symmetric geometry is considered, but the reaction is now assumed to take place behind a shock. In this regime, the governing partial differential equations only hold between the centre of the reaction and the shock face, while the strength and propagation speed of the shock must satisfy a system of algebraic jump conditions. A novel numerical scheme is used to model the propagation of the shock, and its accuracy is compared to that of a classic shock-capturing method.

Contents

List of Figures

Introduction

In 1949 Sal'nikov analysed a simple chemical model, which now bears his name [1]. This model considered a mechanism in which a chemical species A decays to an inert product P by way of an intermediate stage X, with each step occurring at a temperature-sensitive rate. Using k_0 and k_1 to denote the (possibly temperature-dependent) rate of their respective reaction steps the system my be represented by the following simple schematic:

$$A \xrightarrow{k_0} X \xrightarrow{k_1} P. \tag{1}$$

The reaction system may be considered in isolation, such that the only dependent quantities are the chemical concentrations and temperature. This seemingly simple scheme can display highly varied behaviour and has been the subject of thorough study. It is well known that, in specific parameter spaces, a simple model considering only the concentration of the intermediate reagent and the temperature of the reaction system may exhibit limit-cycles; sustained periodic changes in concentration and temperature which are discussed in great detail in the series by Gray and Roberts [2] who also found similar behaviour in more complex reaction schemes [3], which were later visualised by Forbes [4]). Coppersthwaite et al [5] were able to produce similar oscillations experimentally , in a batch reactor containing molecular hydrogen and chlorine, and noted temperature excursions in excess of 200 Kelvin. In their formidable text on combustion reactions, Zel'dovich et al [6] derive governing equations for a combustion reaction in a non-homogeneous, compressible gas, by coupling the reaction equations with the basic equations of fluid mechanics. Such a model is known to support travelling wave solutions, a phenomenon which has roots in the study of reaction diffusion equations made famous by the work of Fisher [7] and Kolmogorov et al. [8]. In one-

dimensional flow the propagation of reaction fronts as travelling waves is a significant area of study, with particular interest in the modelling of flame velocity and on conditions for stability, and has been investigated in a variety of conditions, such as solid and gaseous fuel sources (Matkowsky and Sivashinsky [9] and Weber et al [10]) and through porous materials (Byrne et al. [11]).

Travelling waves with a sech-squared temperature profile were found by Forbes and Derrick [12] in one-dimensional reacting flow, who also showed that, under the right conditions, this solution evolved a steep shock front resulting in the complete exhaustion of the chemical components behind the reaction front. These sech-squared travelling waves were investigated further by Forbes [13] in the context of a competitive two-step reaction, in which the intermediate reagent may undergo one of two reactions to form different final products. Forbes made use of a weakly non-linear approximation to the full, highly non-linear governing partial differential equations, which then reduce to a system of ordinary differential equations in a travelling wave coordinate. That the resulting equations are ODEs and depend only on the travelling wave coordinate suggests that this analytical method is unable to capture solutions other than travelling waves.

In chapter 1, we adapt the method utilised by Forbes to a combustion reaction which proceeds according to Sal'nikov's scheme in an infinite pipe. The weakly non-linear approach is adapted to the fully non-linear governing partial differential equations but includes a second, slower time scale. This multiple-scale analysis allows the non-linear governing equations to be approximated with Burgers' equation, a PDE, which allows for a variety of

solution types, including travelling waves.

Moreover, reaction systems may exhibit both oscillatory and travelling wave behaviour simultaneously, manifesting as wave fronts which propagate with periodic amplitude and wave speed. Such solutions have been noted by Weber et al. [10] who used adaptive numerical techniques to model the evolution of combustion waves in gases and solids, and similar results have been observed by Matkowsky and Sivashinksy [9] and Bayliss and Matkowsky [14]; however, the authors assumed the fuel itself to be stationary within the reaction vessel. Further to the weakly non-linear analysis, chapter 1 also presents a numerical scheme which is used not only to verify the travelling wave solutions, but also to explore briefly the properties of some "pulsatile wave" solutions which are beyond the scope of the weakly non-linear analysis. The work contained in this chapter is presented much as it was published by the author and Forbes [15].

For many scenarios, reactions occurring in spherical geometries offer a more appropriate model and as such there is extensive literature on radially-symmetric combustion systems. Much as in the one-dimensional case, travelling waves in spherical geometries have seen extensive investigation. An early study is given by Sivashinsky [16] on an inward-travelling combustion wave and further analyses of outward-travelling fronts have been given by, among others, Frankel and Sivashinsky [17] and Ronney and Sivashinsky [18]. A typical configuration includes a "pre-heating" zone, wherein the approaching reaction front begins to warm the unburnt gas. Some authors, such as Ronney and Sivashinsky [18], treat all of the gas which is not in the preheating zone to be "active" and undergoing the reaction. Others such as Wu and

Chen [19] include an "active" and a "burnt" region, the latter remaining in chemical equilibrium. In models such as these the temperature profiles are assumed continuous but not necessarily differentiable at the interface of each domain. In chapter 2 of this thesis we analyse Sal'nikov's reaction process as it occurs in a compressible, radially-symmetric gas in which the temperature, concentration, density and gas velocity are assumed to be continuous and differentiable over the entire domain. Approximate solutions are found by linearising the governing non-linear partial differential equations around steady-state values, and two separate solution types are found, using two different techniques, depending on the value of a calculated quantity. This bifurcation parameter represents the linear approximation of the net heat produced by the reaction, and is also shown to be intricately linked to the stability of the reacting system. When this parameter is non-zero, the approximate linear equations are solved using spectral techniques. When it is zero, however, exact solutions to the linearised equations are found in terms of a travelling wave coordinate. The chapter also presents numerical solutions to the full governing equations, which are used to verify the approximate linear solutions. Much of this chapter can also be found in the publication by the author and Forbes [20].

When the combustible gas is ignited by an influx of energy of sufficient intensity the resulting combustion wave may propagate at super-sonic speeds. When this happens, the wave-front is no longer smooth, but instead manifests as a sharp jump discontinuity, as the wave moves into the unburnt gas faster than the super-heated burnt gas. While many properties of the gas are discontinuous across this shock interface, the usual conservation laws must

still apply but now take the form of the Rankine-Hugoniot jump conditions, so named for their formative publications on the subject in [21] and [22] respectively. These jump conditions describe the properties of the shock in terms of its propagation speed and conditions in the unburnt gas, and ensure that the necessary quantities are conserved. In the late 19th and early 20th centuries, Chapman [23] and Jouguet [24] independently described approximate conditions on the speed of the shock, which would form the basis of the ZND model, named for Zel'dovich [25], von Neumann [26] and Döring [27] who each described it during the 1940s. This one-dimensional shock model allowed for finite-rate reactions which depended on the local temperature and composition of reagents, in contrast to earlier models which assumed that the combustion occurs instantly in an infinitesimally small reaction zone at the shock front. Much of the interest of early research was in determining the limiting behaviour of the shock after the system has reached some steady-state solution using similarity techniques, for example Taylor [28] and Rogers [29], and are described in detail by Sedov [30]. These similarity solutions were highly successful in modelling shock propagation and allowed Taylor to publish a remarkably accurate approximation of the yield of the 1945 detonation of the world's first nuclear bomb in New Mexico [31].

Modern computing power has allowed for the development of various numerical techniques which are able to track accurately the behaviour of an evolving shock, and account for complex forcing terms and the influence of an ongoing combustion reaction. Such methods may broadly be divided into two camps: shock-capturing and shock-fitting. Shock-fitting methods build the discontinuity into the scheme and are generally better at resolving the shock

and its properties. This proficiency comes at the expense that they must assume the presence and number of shocks a priori, and are limited in their ability to resolve newly-formed discontinuities. Shock capturing methods, such as the method of Godunov [32], make no such assumption, and allow for the formation of shocks as the system evolves, though they are also less able to resolve the shock with the same accuracy as shock fitting methods, as the shock location is susceptible to numerical smearing (see Anderson [33, p.422]). Chapter 3 models the reaction scheme in a spherically-symmetric gas behind a shock which is propagating outwards from the centre of ignition. The governing equations in this case are as in chapter 2, though new conditions must be imposed to ensure the shock satisfies the expected conservation laws. A novel shock-fitting spectral method is developed, based loosely on the spherical Bessel transforms used in chapter 2. The governing equations are then solved numerically in the spectral space using a Runge-Kutta method, and the required solutions reconstructed. The results of this new numerical technique are verified by comparison with a Godunov scheme, a well known shock-capturing numerical technique.

Finally, we conclude this thesis with a review and discussion of the contained results, and consider some possible avenues of future research in section 4.

Chapter 1

Combustion in one spatial dimension

1.1 Introduction

In this chapter we consider the Sal'nikov model in a combustible gas which varies only in a single spacial dimension. In section 1.2 we present the model; four highly non-linear partial differential equations and an equation of state which govern the evolution of the combustion reaction.

In section 1.3 we employ asymptotic expansion techniques and the method of strained coordinates to derive a system of weakly non-linear partial differential equations which approximate the fully non-linear system. The resulting system of equations is then reduced to simply Burgers' equation for the gas speed. In doing so it will also prove necessary to account for a second, slower time scale, as this prevents the approximate system from degenerating to one of only ordinary differential equations.

The solutions to Burgers' equation are well documented, owing largely to the Cole-Hopf transform under which it reduces to the heat equation (see Whitham [34, p.97]). Of particular interest in this chapter are the travelling wave solutions, which manifest as a sech-squared temperature profile, and pulsatile solutions, in which the wave front propagates with periodic amplitude and wave speed.

When the viscosity term is small, Burgers' equation is capable of developing steep fronts, which become shocks in the inviscid limit. When two of these shocks interact, they are known to merge, forming a larger shock whose speed is between the speeds of the initial profiles. All of these behaviours are described by Whitham [34, pp.96-112] and are investigated in this chapter.

1.2 Combustion Model

Consider a pipe of infinite length positioned such that it extends along the x-axis. Inside the pipe a chemical species A reacts according the Sal'nikov's scheme, as in the schematic in (1). The gas flow is assumed to be one-dimensional and the only spatial variation in the gas properties is in the direction of the x-axis. It is also assumed that the concentration of species A is in such an excess that it remains effectively constant as the reactions proceed, the so-called 'pool-chemical' assumption (see Scott [35, p.31]). The gas density ρ is governed by the convection-diffusion equation which, assuming Fick's laws of diffusion and constant diffusion coefficient S, is given by

$$\frac{\partial \rho}{\partial t} + \frac{\partial}{\partial x}(\rho u) = S\frac{\partial^2 \rho}{\partial x^2} \tag{1.1}$$

in which u is the gas speed along the x-axis. A simple derivation of equation (1.1) is given by Stocker [36, p.56].

It follows from a similar argument that the concentration of species X, denoted $[X]$, satisfies the equation

$$\frac{\partial [X]}{\partial t} + \frac{\partial}{\partial x}(u[X]) = [A]\,k_0(T) - [X]\,k_1(T) + S\frac{\partial^2 [X]}{\partial x^2} \tag{1.2}$$

wherein $[A]$ is the molar concentration of A.

Denoting the pressure of the gas as p and its bulk viscosity ν, the Navier-Stokes equation for viscous and compressible fluids may be written

$$\frac{\partial}{\partial t}(\rho u) + \frac{\partial}{\partial x}\left(\rho u^2 + p\right) = \frac{4}{3}\nu\frac{\partial^2 u}{\partial x^2}. \tag{1.3}$$

We may also relate the pressure of the gas to its density and temperature using the ideal gas law

$$p = \rho R T \tag{1.4}$$

in which R is the universal gas constant. Finally, we consider the balancing of energy in the system. Defining γ to be the ratio of specific heats of the gas, B the rate of heat loss due to Newtonian cooling, w the rate of thermal diffusion, Q_0 and Q_1 the enthalpies of creation of X and P respectively and T_a the ambient temperature outside of the pipe, the energy equation is

$$\begin{aligned} &\frac{\partial}{\partial t}\left[\rho\left(\frac{\gamma RT}{\gamma-1}+\frac{1}{2}u^2\right)\right]+\frac{\partial}{\partial x}\left[u\rho\left(\frac{\gamma RT}{\gamma-1}+\frac{1}{2}u^2\right)\right]-\frac{\partial p}{\partial t} \\ &=w\frac{\partial^2 T}{\partial x^2}+\frac{4}{3}\nu\frac{\partial}{\partial x}\left(u\frac{\partial u}{\partial x}\right)+Q_0\left[A\right]k_0(T)+Q_1\left[X\right]k_1(T)-B\left(T-T_a\right). \end{aligned} \tag{1.5}$$

Equations (1.3) and (1.5) follow from the derivations given by Liepmann and Roshko [37, p.337] with a little algebra.

Far ahead of the reaction front we expect the system to attain its unperturbed state, and so we introduce the upstream boundary conditions

$$p\to\rho_0 RT_a \;\;;\;\; \rho\to\rho_0 \;\;;\;\; u\to 0 \;\;;\;\; T\to T_a \;\;;\;\; \left[X\right]\to\left[X\right]_0 \;\;\text{as}\;\; x\to\infty.$$

Before non-dimensionalising we must consider the forms of the reaction rates $k_0(T)$ and $k_1(T)$. Assuming Arrhenius reaction kinetics, these rates are

$$\begin{aligned} k_0(T) &= z_0 e^{-E_0/RT} \\ k_1(T) &= z_1 e^{-E_1/RT} \end{aligned}$$

where E_0 and E_1 are the activation energies of the respective reactions and z_0 and z_1 are the reaction coefficients. Although alternative forms for these rates may be chosen later, we will nevertheless make use of their activation energies and reaction coefficients to define dimensionless parameters.

We now proceed to introduce non-dimensional variables in relation to appropriate scales. The reference length is chosen to be $\sqrt{E_1}/z_1$, the time scale is

$1/z_1$ and, consequently, the speed scale is $\sqrt{E_1}$. Temperature is scaled relative to the quantity E_1/R and the upstream density ρ_0 provides the reference for the density. This then suggests the quantity $\rho_0 E_1$ as the natural choice to scale pressure. Finally, we scale concentration relative to the quantity $\rho_0 E_1/Q_1$. We now introduce nine new dimensionless parameters

$$\mu = \frac{4z_1\nu}{3\rho_0 E_1} \;\; ; \;\; \beta = \frac{B}{z_1\rho_0 R} \;\; ; \;\; \phi = \frac{z_1 w}{\rho_0 E_1 R} \;\; ; \;\; \zeta = \frac{z_0}{z_1}$$
$$q = \frac{Q_0}{Q_1} \;\; ; \;\; \epsilon = \frac{E_0}{E_1} \;\; ; \;\; \sigma = \frac{z_1 S}{E_1} \;\; ; \;\; \theta_a = \frac{RT_a}{E_1} \;\; ; \;\; A = \frac{[A]\,Q_1}{\rho_0 E_1}.$$

Here, the constant μ represents the dimensionless bulk viscosity, β the rate of Newtonian cooling, ϕ the rate of thermal diffusion, σ the rate of diffusion of X and ρ, A the dimensionless concentration of chemical A and θ_a the ambient temperature. The quantities ζ, q and ϵ represent the ratio of reaction coefficients, heat of reaction and activation energies of each of the reaction steps, respectively.

From here onwards we will drop the bracket notation used to denote concentration. As such, the transport equation (1.2) becomes

$$\frac{\partial X}{\partial t} + \frac{\partial}{\partial x}\left(uX\right) = \zeta A k_0\left(T\right) - X k_1\left(T\right) + \sigma\frac{\partial^2 X}{\partial x^2} \tag{1.6}$$

where the Arrhenius reaction rates k_0 and k_1 are now

$$\begin{aligned} k_0\left(T\right) &= e^{-\epsilon/T} \\ k_1\left(T\right) &= e^{-1/T}. \end{aligned} \tag{1.7}$$

The conservation of mass equation (1.1) becomes

$$\frac{\partial \rho}{\partial t} + \frac{\partial}{\partial x}\left(\rho u\right) = \sigma\frac{\partial^2 \rho}{\partial x^2} \tag{1.8}$$

while the momentum equation (1.3) yields

$$\frac{\partial}{\partial t}\left(\rho u\right) + \frac{\partial}{\partial x}\left(\rho u^2 + p\right) = \mu \frac{\partial^2 u}{\partial x^2}. \tag{1.9}$$

The energy equation (1.5) is

$$\begin{aligned} &\frac{\partial}{\partial t}\left[\rho\left(\frac{\gamma T}{\gamma - 1} + \frac{1}{2}u^2\right)\right] + \frac{\partial}{\partial x}\left[u\rho\left(\frac{\gamma T}{\gamma - 1} + \frac{1}{2}u^2\right)\right] \\ = &\frac{\partial p}{\partial t} + \phi\frac{\partial^2 T}{\partial x^2} + \mu\frac{\partial}{\partial x}\left(u\frac{\partial u}{\partial x}\right) + q\zeta A k_0(T) + X k_1(T) - \beta\left(T - T_a\right) \end{aligned} \tag{1.10}$$

and the gas law (1.4) has the form

$$p = \rho T. \tag{1.11}$$

Finally, the upstream boundary conditions become

$$p \to \theta_a \ ; \ \rho \to 1 \ ; \ u \to 0 \ ; \ T \to \theta_a \ ; \ X \to X_0 \ \text{ as } \ x \to \infty.$$

1.3 Weakly Non-Linear Analysis

In this section we use the method of strained coordinates with the method of multiple scales to derive a set of equations which approximate the behaviour of the model outlined in §1.2, for small amplitude perturbations. We do so by assuming that the values vary from their steady state solutions by a small value, characterised by the parameter κ. Much of this analysis is similar to the process used by Forbes [13] and, interestingly, the solutions are qualitatively similar, despite the addition of diffusion and viscosity into the model. Much of the notation in this analysis will be retained for ease of comparison.

First we introduce two strained coordinates given by

$$\tilde{t}_1 = \kappa t \quad ; \quad \tilde{x} = \kappa x.$$

We also introduce a second time-scale $\tilde{t}_2$ defined as

$$\tilde{t}_2 = \kappa^2 t.$$

The dependent variables are now expanded as power series in the small parameter κ around their steady states as follows:

$$\begin{aligned}
u &= \kappa u_1 + \kappa^2 u_2 + \mathcal{O}(\kappa^3) \\
\rho &= 1 + \kappa\rho_1 + \kappa^2\rho_2 + \mathcal{O}(\kappa^3) \\
T &= \theta_a + \kappa T_1 + \kappa^2 T_2 + \mathcal{O}(\kappa^3) \\
p &= \theta_a + \kappa p_1 + \kappa^2 p_2 + \mathcal{O}(\kappa^3) \\
X &= X_0 + \kappa X_1 + \kappa^2 X_2 + \mathcal{O}(\kappa^3).
\end{aligned}$$

The Arrhenius reaction rates in (1.7) are now approximated with the two rates

$$\begin{aligned}
k_0(T) &= \begin{cases} 0, & \text{if } T \leqslant \theta_a \\ 1 - e^{-\epsilon(T-\theta_a)}, & \text{if } T > \theta_a \end{cases} \\
k_1(T) &= \begin{cases} 0, & \text{if } T \leqslant \theta_a \\ 1 - e^{-(T-\theta_a)}, & \text{if } T > \theta_a. \end{cases}
\end{aligned} \tag{1.12}$$

Reaction rates such as these have been used previously by Forbes and Derrick [12]. The authors argue that these rates have the advantage of avoiding the "cold boundary problem", in which the Arrhenius rates are non-zero for arbitrarily low temperatures (see Williams [38, p.21]), while maintaining important qualitative behaviours of the Arrhenius rates; they have value zero for $T = 0$, have a finite bounding value for arbitrarily large temperature and maintain the three potential points of intersection with a line of appropriate slope. The same forms for the reaction rates have also been used by Forbes

[13]. For simplicity, the ignition temperatures (below which the reactions stop) are chosen to be equal to the ambient temperature θ_a. We may now expand these rates in powers of the parameter κ, yielding

$$\begin{aligned} k_0(T) =& \kappa\epsilon T_1 + \kappa^2\left(\epsilon T_2 - \frac{1}{2}\epsilon^2 T_1^2\right) + \mathcal{O}\left(\kappa^3\right) \\ k_1(T) =& \kappa T_1 + \kappa^2\left(T_2 - \frac{1}{2}T_1^2\right) + \mathcal{O}\left(\kappa^3\right) \end{aligned} \tag{1.13}$$

for $T > \theta_a$. These expansions are substituted into the dimensionless governing equations and quantities at each order in κ are collected. The order κ equation obtained from expanding the energy equation yields

$$T_1\left(\tilde{x}, \tilde{t}_1, \tilde{t}_2\right) \equiv 0$$

which, upon expanding the gas law (1.11), gives the relations

$$p_1 = \theta_a \rho_1 \;\; ; \;\; p_2 = T_2 + \theta_a \rho_2$$

at first and second orders in κ.

The second order temperature equation, coupled with the first order mass equation and the new reaction rate expansion (1.13), yields the equation

$$T_2\left(\tilde{x}, \tilde{t}_1, \tilde{t}_2\right) = -\omega\frac{\partial u_1}{\partial \tilde{x}} \tag{1.14}$$

in which we have defined the constant

$$\omega = \frac{\theta_a}{\beta - \zeta q \epsilon A - X_0}. \tag{1.15}$$

The resulting first order momentum and mass equations may be cross-differentiated to yield

$$\frac{\partial^2 u_1}{\partial \tilde{t}_1^2} = \theta_a \frac{\partial^2 u_1}{\partial \tilde{x}^2}. \tag{1.16}$$

Thus the fluid speed at first order obeys a linear wave equation with characteristic speed $\sqrt{\theta_a}$ on the short time scale.

Ahead of further analysis we define the following constant in terms of ω, outlined in (1.15):

$$\Gamma = \frac{1}{\mu + \sigma + \omega}.$$

Then, after some algebraic manipulation of the second order momentum and mass equations, it can be shown that the variable u_1 satisfies the partial differential equation

$$\frac{1}{\Gamma}\frac{\partial^2 u_1}{\partial \tilde{x}^2} - \frac{\partial}{\partial \tilde{x}}\left(u_1^2\right) - 2\frac{\partial u_1}{\partial \tilde{t}_2} = 0 \tag{1.17}$$

in the long time scale, of most interest here.

1.4 Travelling Waves

A travelling wave solution is now sought in terms of the variable

$$\eta = \tilde{x} - \sqrt{\theta_a}\tilde{t}_1 - m\tilde{t}_2. \tag{1.18}$$

This transformation satisfies equation (1.16) identically, and so that equation is considered no further. Equation (1.17) may now be integrated exactly, yielding

$$\frac{\mathrm{d}u_1}{\mathrm{d}\eta} = \Gamma\left(u_1 - 2m\right)u_1 \tag{1.19}$$

which has solution

$$u_1\left(\eta\right) = \frac{2m}{1 + \exp\left(2m\Gamma\eta\right)}. \tag{1.20}$$

Equation (1.14) now takes the form

$$T_2\left(\eta\right) = -\omega\frac{\mathrm{d}u_1}{\mathrm{d}\eta}. \tag{1.21}$$

Evaluating this expression using (1.20) gives

$$T_2(\eta) = m^2\omega\Gamma\mathrm{sech}^2(m\Gamma\eta) \tag{1.22}$$

and thus the asymptotic representation for temperature is

$$T(x,t) = \theta_a + \kappa^2 m^2\omega\Gamma\mathrm{sech}^2(\kappa m\Gamma(x-ct)) + \mathcal{O}\left(\kappa^3\right).$$

Here c is the wave speed in the physical coordinate x and t and it follows from (1.18) that along a characteristic of (1.16) c is given by

$$c = \frac{\mathrm{d}x}{\mathrm{d}t} = \sqrt{\theta_a} + \kappa m + \mathcal{O}\left(\kappa^2\right). \tag{1.23}$$

We may now make use of the first order mass equation and second order transport equation to find the forms of the density and concentration profiles. The resulting expressions are

$$\rho_1(\eta) = \frac{2m}{\sqrt{\theta_a}\left[1+\exp(2m\Gamma\eta)\right]}$$

and

$$X_1(\eta) = \frac{2m\left(X_0 - X_0\omega + \omega\zeta\epsilon A\right)}{\sqrt{\theta_a}\left[1+\exp(2m\Gamma\eta)\right]}.$$

Notice that the amplitude of the solution (1.22) could formally be negative, corresponding to a "cold soliton" if $\omega\Gamma < 0$. However, in the present model, this is precluded by the assumption $T > \theta_a$ in equation (1.13). Nevertheless, "cold soliton" solutions might be possible for more complex reaction systems in which the full Arrhenius reaction rates are included.

1.5 Numerical Analysis

We now proceed to analyse the full system of partial differential equations (1.6), (1.8) – (1.11) by approximating each of them with a system of ordinary

differential equations using the method of lines (see Ames [39, p.193]). We do so by approximating the infinite pipe with one of length $2L$, discretising the spatial coordinate $-L \leqslant x \leqslant L$ into N mesh points and replacing the corresponding spatial derivatives with appropriate centred finite differences. Using a j subscript to represent the value of a dependent variable at the j^{th} spatial mesh point, a prime to represent temporal derivatives and letting Δx be the width between mesh points, the governing equations may be approximated by

$$\begin{aligned}
\rho_j' =& \frac{\rho_j\left(u_{j-1}-u_{j+1}\right)+u_j\left(\rho_{j-1}-\rho_{j+1}\right)}{2\Delta x}+\sigma\left(\frac{\rho_{j+1}-2\rho_j+\rho_{j-1}}{\Delta x^2}\right)\\
u_j' =& \frac{2u_j\left(u_{j-1}-u_{j+1}\right)+T_{j-1}-T_{j+1}}{2\Delta x}\\
&+\frac{1}{\rho_j}\left[\frac{\left(T_j+u_j^2\right)\left(\rho_{j-1}-\rho_{j+1}\right)}{2\Delta x}-u_j\rho_j'+\mu\left(\frac{u_{j+1}-2u_j+u_{j-1}}{\Delta x^2}\right)\right]\\
T_j' =& \left(\gamma-1\right)\left\{u_j\left(\frac{J_{j-1}-J_{j+1}}{2\Delta x}-u_j'\right)+\frac{J_j\left(u_{j-1}-u_{j+1}\right)}{2\Delta x}\right.\\
&+\frac{1}{\rho_j}\left[\mu\left(\frac{u_j\left(u_{j+1}-2u_j+u_{j-1}\right)}{\Delta x^2}+\left(\frac{u_{j+1}-u_{j-1}}{2\Delta x}\right)^2\right)\right.\\
&+\frac{J_ju_j\left(\rho_{j-1}-\rho_{j+1}\right)}{2\Delta x}+\phi\left(\frac{T_{j+1}-2T_j+T_{j-1}}{\Delta x^2}\right)\\
&\left.\left.+\rho_j'\left(T_j-J_j\right)+X_jk_0\left(T_j\right)+\zeta qAk_1\left(T_j\right)-\beta\left(T_j-\theta_a\right)\right]\right\}\\
X_j' =& \zeta Ak_0\left(T_j\right)-X_jk_1\left(T_j\right)\\
&+\frac{X_j\left(u_{j-1}-u_{j+1}\right)+u_j\left(X_{j-1}-X_{j+1}\right)}{2\Delta x}+\sigma\left(\frac{X_{j+1}-2X_j+X_{j-1}}{\Delta x^2}\right)
\end{aligned} \tag{1.24}$$

for $1 \leqslant j \leqslant N$. In equation (1.24) we have defined the quantity

$$J_j = \frac{\gamma T_j}{\gamma-1}+\frac{1}{2}u_j^2,$$

the total enthalpy of the gas (see [37]) at the j^{th} mesh point, for convenience. The reaction rates may be used in their approximated form (1.12), evaluated at the mesh point x_j.

The best choice of boundary conditions is not obvious, since the only conditions on the original system were those which applied far upstream. For this analysis we have chosen to enforce zero-derivative conditions for each dependent variable at both ends of the mesh. This is achieved by introducing "false boundaries" at $x = -(L + \Delta x)$ and $x = L + \Delta x$, which correspond to mesh points at $j = 0$ and $j = N + 1$ respectively. Approximating the derivatives with appropriate central finite differences, these zero derivative conditions on the gas speed u reduce to

$$u_0 = u_2 \;\; ; \;\; u_{N+1} = u_{N-1}$$

with similar results holding for ρ, X and T. Further details of this technique are discussed in the text by Ames [39].

This system of $5N$ equations can now be integrated forwards in time using an appropriate method. For this analysis we have used ode45 routine in MATLAB [40], which uses fourth and fifth order Runge-Kutta methods and an adaptive time step to control the error.

The starting values are chosen such that the initial temperature has the form

$$T(x, 0) = \theta_a + A_T \text{sech}^2(\kappa m \Gamma (x + x_0))$$

where A_T is the amplitude of the initial temperature profile and x_0 is an offset for the location of the pulse. The value of x_0 is chosen to position the centre of the initial impulse away from the boundaries, minimising the effects of boundary conditions. The starting values of u, ρ and X are all chosen such

that they satisfy the weakly non-linear system derived in §1.3. As such they become

$$u(x,0) = \frac{2\kappa m}{1+\exp\left(2\kappa m\Gamma\left(x+x_0\right)\right)}$$

$$\rho(x,0) = 1+\frac{2\kappa m}{\sqrt{\theta_a}\left[1+\exp\left(2\kappa m\Gamma\left(x+x_0\right)\right)\right]}$$

$$X(x,0) = X_0+\frac{2\kappa m\left(X_0-X_0\omega+\omega\zeta\epsilon A\right)}{\sqrt{\theta_a}\left[1+\exp\left(2\kappa m\Gamma\left(x+x_0\right)\right)\right]}.$$

The parameter combination κm may be calculated using the relation

$$\kappa m = \sqrt{\frac{A_T}{\omega\Gamma}}.$$

Figure (1.1) displays the temperature above ambient as returned by the numerical solution obtained for parameters $\theta_a = 0.15$, $X_0 = 0.25$, $A = 1$, $\zeta = 0.4$, $q = 0.2$, $\epsilon = 0.75$, $\beta = 1$, $\sigma = 0.1$, $\mu = 0.03$, $\phi = 0.2$, $\gamma = 1.4$ for times $t = 0, 20, 40...500$. The grid spacing is $\Delta x = 0.02$, since this has been found sufficient for the convergence of the numerical results. The initial condition is given perturbation amplitude $A_T = 10^{-4}$ and initial displacement $x_0 = 100$ to the left of the origin. The solution increases slightly in amplitude at first, but continues travelling at a constant speed while maintaining a profile closely matching its initial shape. Analysis of the solution indicates an average wave speed of about 0.397. This value is calculated by simply taking the change in position of the maximum temperature divided by the final time of the numerical scheme (in this case 500). This measured value for the average wave speed is in close agreement with the predicted speed of

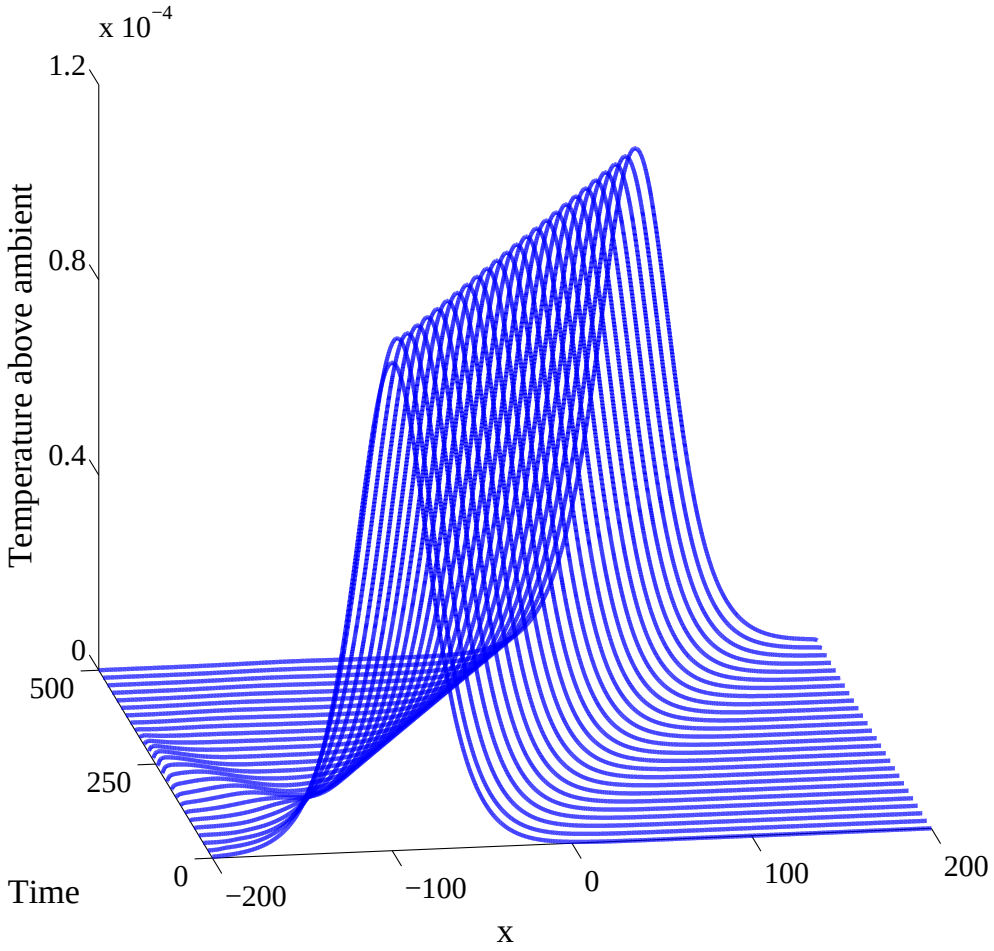

Figure 1.1: Travelling wave solution obtained by the numerical scheme, with parameter values given in the text.

$\sqrt{\theta_a} + \kappa m \approx 0.400$ in equation (1.23).

Figure (1.2) shows a comparison of the numerical solution (plotted with a solid blue line) with the asymptotic solution (1.22) (dashed red line) for the same parameters as figure (1.1), for times $t = 0, 200, 400...1000$. It can be seen that the two solutions are almost identical and there is little noticeable separation of the two until $t = 1000$. This confirms the usefulness of the weakly non-linear solution in section (1.3).

Forbes [13] showed that, in the weakly non-linear case, two sech-squared pulses with different amplitudes could run into each other and form a single larger pulse. To investigate whether this is also true for large-amplitude disturbances in the full system, figure (1.3) displays the numerical solution to the full system of partial differential equations given a two sech-squared pulse starting condition of the form

$$T(x,0) = \theta_a + A_{T1}\text{sech}^2\left(\kappa m_1 \Gamma\left(x - x_{01}\right)\right) + A_{T2}\text{sech}^2\left(\kappa m_2 \Gamma\left(x - x_{02}\right)\right)$$

where

$$\kappa m_1 = \sqrt{\frac{A_{T1}}{\omega\Gamma}} \quad ; \quad \kappa m_2 = \sqrt{\frac{A_{T2}}{\omega\Gamma}}.$$

Here the system parameters are chosen to be $\theta_a = 0.35$, $X_0 = 0.25$, $A = 1$, $\zeta = 0.4$, $q = 0.2$, $\epsilon = 0.75$, $\beta = 1$, $\sigma = 0.25$, $\mu = 0.1$, $\phi = 0.4$, $\gamma = 1.4$ with initial amplitudes $A_{T1} = 8 \times 10^{-3}$ and $A_{T2} = 2 \times 10^{-3}$. The two pulses were started at positions $x_{01} = 250$ and $x_{02} = 170$ along the negative x-axis. The solution is calculated using spacing $\Delta x = 0.02$ and is displayed at times $t = 0, 26, 52...650$. The figure shows that the larger, left-most pulse travels faster than the smaller, right-most pulse and the two eventually meet at around $t = 400$. After coinciding, the two merge to form a single, larger

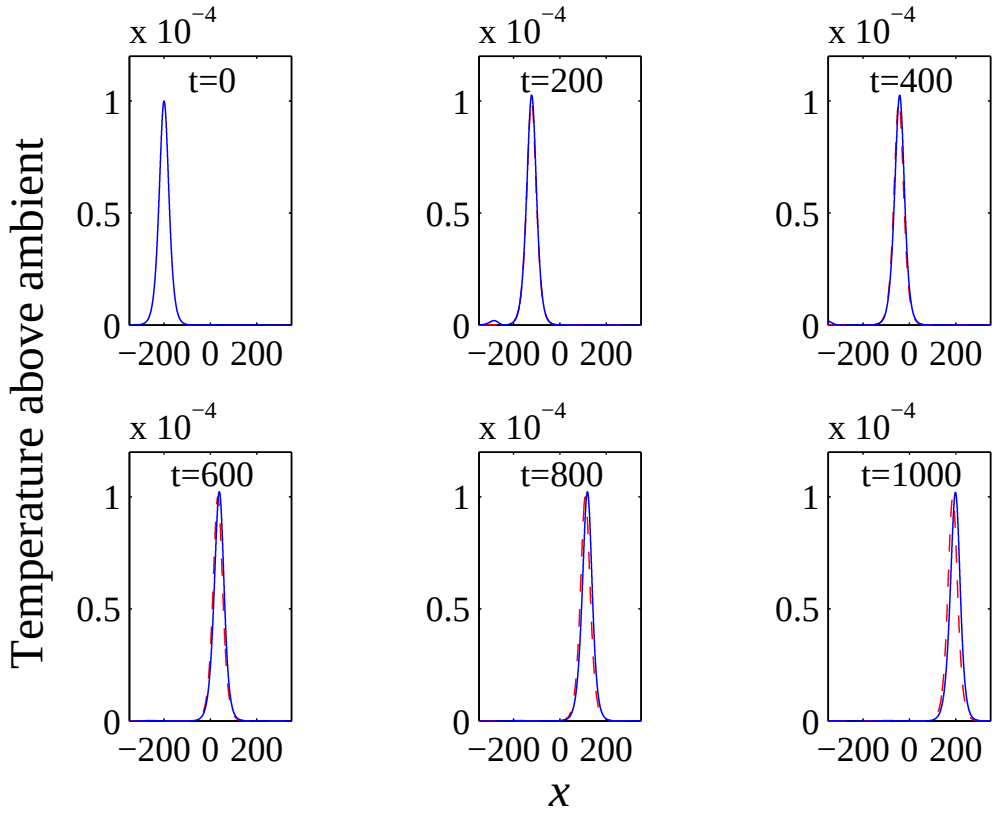

Figure 1.2: Comparison of numeric solution (solid blue line) to asymptotic solution (dashed red line), for the same parameter values illustrated in figure (1.1).

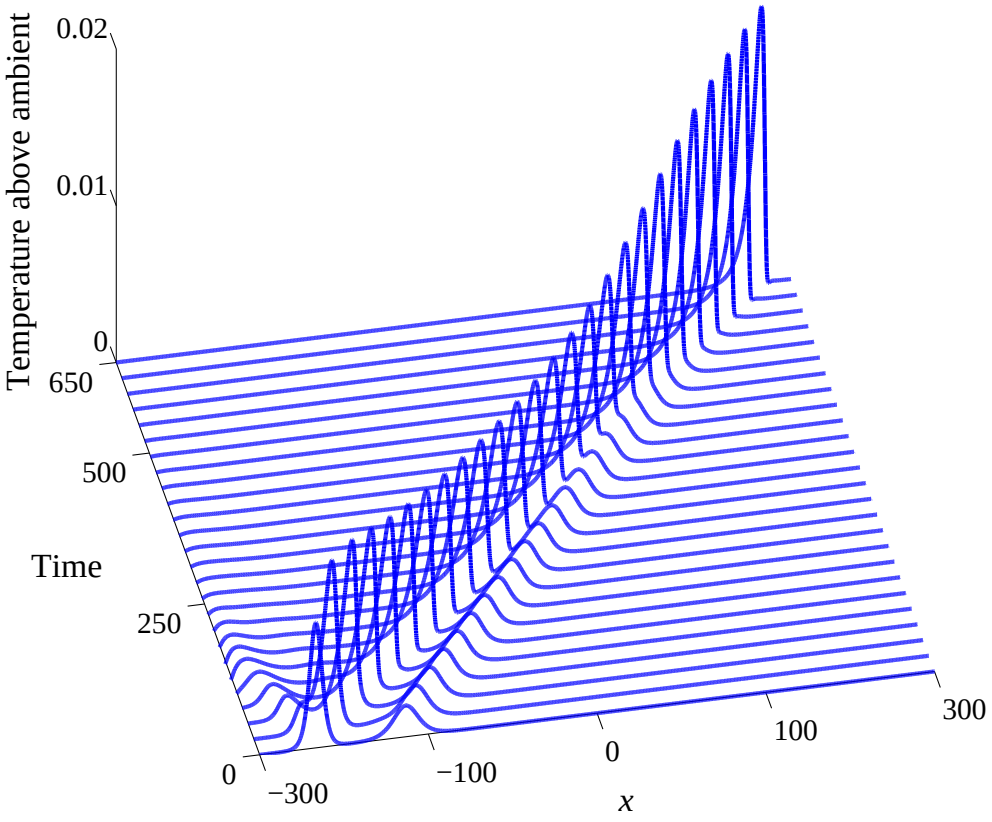

Figure 1.3: Evolution of two sech-squared pulses of differing amplitudes for the parameter values listed in the text.

pulse which continues travelling to the right.

Figure (1.4) displays the approximate speed of the larger pulse in figure (1.3). The wave speed at a point x_j, denoted v_j, was calculated by tracking the position of the maximum temperature in figure (1.3) at intervals of one time unit and numerically differentiating the results with a forward finite difference. The numerical differentiation produced rapid, low amplitude oscillations over several numerical mesh points. In order to reduce these variations, triangular smoothing was employed. The velocity at the position x_j, denoted v_j, was replaced with a weighted average of the nearby values, v_j^*, according to the rule

$$v_j^* = \frac{v_{j-2} + 3v_{j-1} + 5v_j + 3v_{j+1} + v_{j+2}}{13}. \tag{1.25}$$

Ten iterations of this procedure were needed before the majority of the variations were smoothed away. From figure (1.4) we can see that the speed increases rapidly before settling at a value of around 0.817. Some remaining small-amplitude oscillations may still be visible in this diagram. When the two waves interact at about $t = 400$, the wave speed decreases to about 0.769; this behaviour is consistent with that of confluent shocks in Burgers' equation (see Whitham [34]). While the equation for the gas speed given in (1.20) is not strictly a shock, it begins to look more like one as $m\Gamma$ becomes large. As such it is perhaps not too surprising that their behaviours are qualitatively similar.

In the interest of exploration, we have run this system for a different set of parameters but made use of the Arrhenius reaction rates as in (1.7). Figure (1.5) shows the solution under this scheme with parameter values $\theta_a = 0.15$, $X_0 = 0.4$, $A = 0.8$, $\zeta = 0.3$, $q = 0.1$, $\epsilon = 0.1$, $\beta = 1$, $\sigma = 0.3$, $\mu = 0.2$,

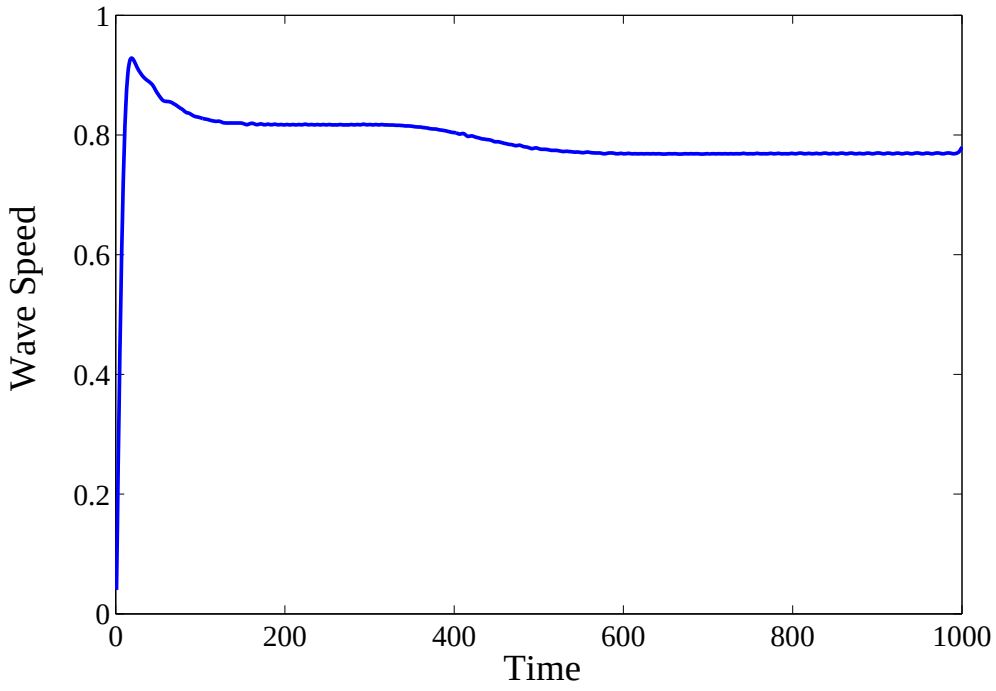

Figure 1.4: Approximate speed of the left pulse before and after it interacts with the smaller pulse displayed in figure (1.3).

$\phi = 0.5$, $\gamma = 1.4$, initial amplitude $A_T = 10^{-2}$ and offset $x_0 = 100$ to the left of the origin. The solution is displayed for $t = 0, 5, 10...350$ and has been calculated with a grid spacing $\Delta x = 0.02$. The temperature quickly increases in amplitude around $t = 60$ and reaches a temperature of $T \approx 2.15$. At this point the wave front (the location of the temperature peak) diverges, forming both forward and backward travelling waves with periodically varying amplitudes and wave speed. This behaviour continues, with more pulsatile wave fronts branching off in both the positive and negative x direction. Coinciding with each temperature spike are large increases in the reaction temperature along the upper and lower lengths of the pipe, independent of the behaviours of the reaction front. These oscillations are caused by the behaviour of the well-mixed reaction system, in which $u \equiv 0$ and there is no spatial variation. They are thus limit cycles in the purely temporal system, and come about through a Hopf bifurcation in the Sal'nikov reaction; further details are given in [41]. This behaviour did not occur if the Arrhenius rates were replaced with the approximate rates (1.12).

The periodic behaviour in the amplitude and wave speed is best illustrated by the right-most wave front. Figure (1.6) displays the amplitude of this front over time and its periodic nature is evident. Similar behaviour can be seen in the wave speed shown in figure (1.7). This plot was produced in much the same way as figure (1.4); numerically differentiating the wave position, and using one iteration of the smoothing scheming in (1.25) to reduce the rapid variations (some residual oscillations from the numerical differentiation may still be visible at early times). At around $t = 40$ the speed begins to increase rapidly and reaches a value of about 3.3 before decreasing to less

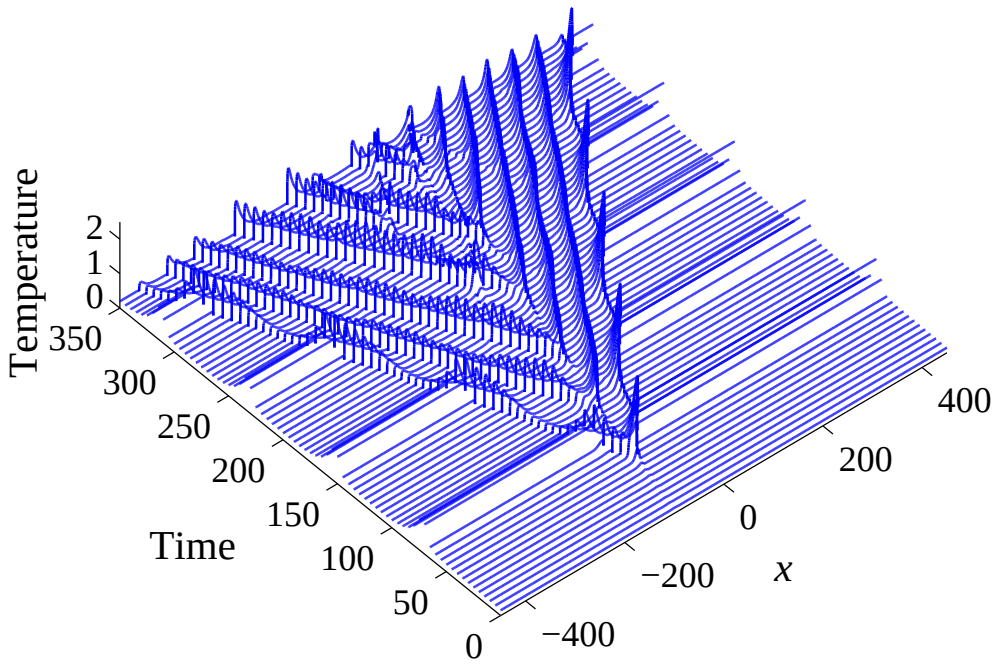

Figure 1.5: Pulsatile travelling wave solution with Arrhenius rates for parameters given in the text. The diagram shows periodic oscillations in time at all positions x, corresponding to the well-mixed system. In addition, a pulsatile travelling-wave system moving in each direction is also present.

than 1. These rapid increases and decreases in wave speed occur approximately every 65 time units, and direct comparison with figure (1.6) indicates that wave speed and amplitude maxima coincide. These plots were produced by finding the position and amplitude of the maximum temperature on the domain $[-L, L]$ at the initial time. At the next time step, this domain is updated to $[x_m, L]$, where x_m is the position of the maximum temperature at the previous step, and this process is repeated. This has the effect of tracking the right-most reaction-front.

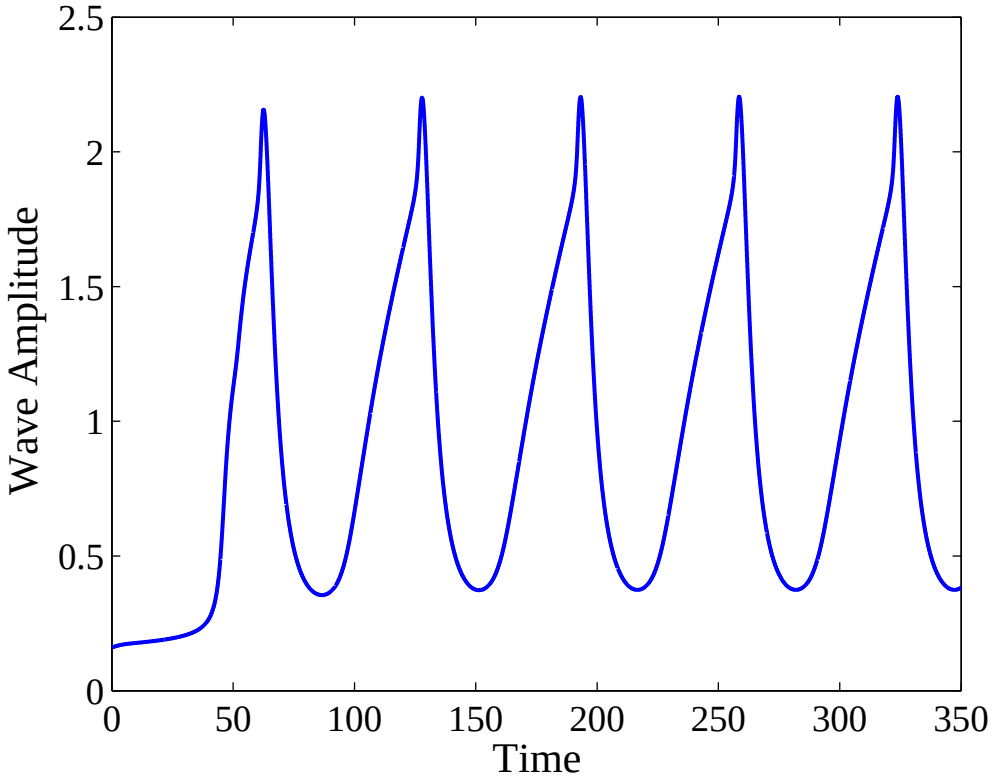

Figure 1.6: Amplitude of right-most wave front of pulsatile solution displayed in figure (1.5).

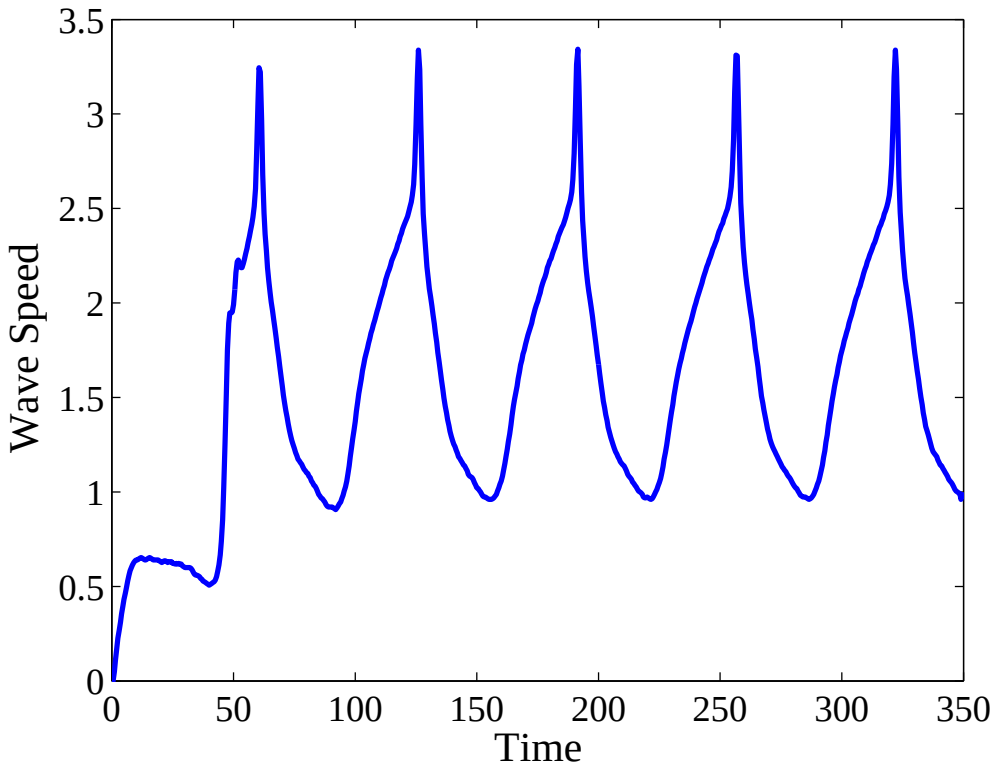

Figure 1.7: Approximate wave speed of the forward front in figure (1.5).

1.6 Conclusion

We have demonstrated a weakly non-linear analysis of a Sal'nikov reaction scheme in a viscous and diffusive compressible gas mixture using the method of strained coordinates and multiple scales. Interestingly, it was demonstrated that the solution to the weakly non-linear equations governing the system is a sech-squared travelling wave, qualitatively similar to that which was investigated by Forbes [13], despite the inclusion of strong fluid viscosity and diffusion.

It is possible to demonstrate the stability of these solutions by considering the behaviour of a perturbation of the form $u_1(\eta) + \hat{u}_1(\eta)$ in equation (1.19). This analysis is identical to the one provided by Forbes in the aforementioned paper and is discussed in the appendix to this chapter.

We have also made use of the method of lines to develop a numerical scheme to approximate accurately the behaviour of the full set of governing partial differential equations. Using this scheme we have numerically verified the conclusion of the weakly non-linear solution, demonstrating stable travelling wave solutions. In addition, the full non-linear system permits pulsatile travelling wave solutions, in which periodic oscillations in the well-mixed system are also present and such a case has been illustrated.

1.7 Appendix

1.7.1 Stability of Travelling Wave Solutions

In this chapter we discussed a particular sech-squared thermal soliton solution to the weakly non-linear system of ordinary differential equations given in (1.19) and (1.21). In this section we discuss the stability of the solutions, and show that the derived profiles are unconditionally stable. Thus we introduce a perturbation to the gas speed, in the form

$$u_1(\eta) + \delta u_1^*(\eta)$$

in which δ is a small parameter characteristic of the size of the perturbation. Substituting this perturbed quantity into equation (1.19), and retaining only the quantities of order δ yields

$$\frac{\mathrm{d}u_1^*}{\mathrm{d}\eta} = 2\Gamma(u_1 - m)u_1^*$$

which has solution

$$u_1^*(\eta) = A\exp\left[2\Gamma\int(u_1 - m)\,\mathrm{d}\eta\right] \tag{1.26}$$

where A is an arbitrary constant. This integral can be evaluated rather easily by rearranging equation (1.20) for u_1, noting that

$$\Gamma(u_1 - m) = \frac{1}{u_1}\frac{\mathrm{d}u_1}{\mathrm{d}\eta} + m\Gamma,$$

so that equation (1.26) may be equivalently written:

$$\begin{aligned} u_1^*(\eta) &= A\exp\left[2\int\left(\frac{1}{u_1}\frac{\mathrm{d}u_1}{\mathrm{d}\eta} + m\Gamma\right)\mathrm{d}\eta\right] \\ &= A\exp\left[\ln\left(u_1^2\right) + 2m\Gamma\eta\right] \\ &= A\exp(2m\Gamma\eta)\,u_1^2. \end{aligned}$$

Recalling the solution for u_1 given in equation (1.20), we now have

$$\begin{aligned} u_1^*(\eta) &= \frac{4m^2 A \exp(2m\Gamma\eta)}{[1+\exp(2m\Gamma\eta)]^2} \\ &= \frac{4m^2 A}{[\exp(-m\Gamma\eta)+\exp(m\Gamma\eta)]^2} \\ &= m^2 A \operatorname{sech}^2(m\Gamma\eta). \end{aligned}$$

Thus, since $\operatorname{sech}^2(m\Gamma\eta)$ vanishes as $\eta \to \pm\infty$, the solution is stable.

Chapter 2

Combustion in a spherically-symmetric gas

2.1 Introduction

In the following chapter of we model a combustion reaction as it proceeds according to the Sal'nikov two-step process in a radially-symmetric gas.
In section 2.2 we briefly describe the reaction model and present the governing equations for the combustion system. Interestingly, these equations may be linearised, and it is not necessary to seek weakly non-linear solutions as were required by the one-dimensional problem discussed in chapter 1, nor is it necessary to make use of strained coordinates nor multiple time scales. Thus we are able to write each of the relevant quantities as small perturbations about a steady state so that the full system of highly non-linear partial differential equations is approximated by a simpler, linear model.
In section 2.4 solutions are found which manifest as a combination of two separate profiles - an active part, which is reacting, and a "burnt" profile which remains after the reaction has progressed. Non-travelling-wave solutions are then considered in section 2.5 using integral transforms over a basis of spherical Bessel functions, and a brief stability analysis is also given. Finally, a numerical scheme is derived based on the method of lines to approximate the full non-linear system of differential equations and the linearised solutions predicted in sections 2.4 and 2.5 are compared with its results. This chapter concludes with a brief overview in section 2.8.

2.2 Model

We consider a spherical cloud of gas reacting according to Sal'nikov's scheme (1). As in chapter 1, we will impose the pool-chemical assumption that the

volume of initial species A is so large that its concentration $[A]$ remains effectively constant. Then the concentration of X at a distance r from the origin is governed by the reaction-convection equation in spherical coordinates:

$$\frac{\partial [X]}{\partial t} + \frac{1}{r^2}\frac{\partial}{\partial r}\left(r^2 u [X]\right) = [A]\, k_0(T) - [X]\, k_1(T) \tag{2.1}$$

in which braces denote concentration. In radially-symmetric spherical coordinates, the conservation of mass equation for a compressible fluid is

$$\frac{\partial \rho}{\partial t} + \frac{1}{r^2}\frac{\partial}{\partial r}\left(r^2 \rho u\right) = 0 \tag{2.2}$$

where ρ is the gas density and u is the velocity of the gas away from the origin. The Euler equation, governing the conservation of momentum for compressible fluids is

$$\rho\left(\frac{\partial u}{\partial t} + u\frac{\partial u}{\partial r}\right) + \frac{\partial p}{\partial r} = 0, \tag{2.3}$$

assuming no body forces. Here p is the gas pressure and, assuming the gas mixture to be ideal, can be related to the pressure and density by the gas law

$$p = \rho R T \tag{2.4}$$

where R is the universal gas constant. Finally, we have the equation for the conservation of enthalpy which again is given by Liepmann and Roshko [37, ch.7]. In spherical coordinates, after a little algebra, this equation takes the form

$$\rho\frac{D}{Dt}\left(\frac{\gamma R T}{\gamma - 1} + \frac{1}{2}u^2\right) = \frac{\partial p}{\partial t} + Q_0 [A]\, k_0(T) + Q_1 [X]\, k_1(T) - B\,(T - T_a) \tag{2.5}$$

where γ is the ratio of specific heats of the gas, Q_0 and Q_1 are the enthalpies of formation of X and P respectively, the constant B is the rate at which heat

is lost to ambient and T_a is the ambient temperature beyond the reaction front. The symbol $\frac{D}{Dt} = \frac{\partial}{\partial t} + u\frac{\partial}{\partial r}$ denotes the material derivative. Far from the centre of the reaction we expect the system to attain its back-ground values of velocity, temperature, density, chemical concentration and pressure. Representing these values with a subscript 0, we have the upstream conditions

$$\rho \to \rho_0; \quad u \to 0; \quad T \to T_0; \quad [X] \to [X]_0\,; \quad p \to \rho_0 R T_0 \ \text{ as } \ r \to \infty. \tag{2.6}$$

The upstream temperature T_0 and concentration X_0 satisfy the coupled non-linear algebraic equations

$$\begin{aligned} Q_0\,[A]\,k_0(T_0) + Q_1\,[X]_0\,k_1(T_0) - B\,(T_0 - T_a) =& 0 \\ [A]\,k_0(T_0) - [X]_0\,k_1(T_0) =& 0, \end{aligned}$$

as the steady-state solutions to equations (2.1) and (2.5), for use in boundary condition (2.6). We now consider the forms of the reaction rates k_0 and k_1. Perhaps the standard choice is to use Arrhenius reaction rates

$$\begin{aligned} k_0(T) =& z_0 \mathrm{e}^{-E_0/RT} \\ k_1(T) =& z_1 \mathrm{e}^{-E_1/RT} \end{aligned} \tag{2.7}$$

as in section (1.2), where E_0 and E_1 are the activation energies of their respective reaction steps and z_0 and z_1 are the pre-exponential reaction factors. These coefficients are useful for defining dimensionless quantities. We non-dimensionalise length and time with respect to $\sqrt{E_1}/z_1$ and $1/z_1$ respectively and this naturally gives $\sqrt{E_1}$ as the reference speed scale. Temperature is scaled relative to E_1/R and density to ρ_0. Finally, the reference pressure is chosen to be $\rho_0 E_1$ and concentration $\rho_0 E_1/Q_1$. Five new dimensionless parameters are now introduced:

$$\beta = \frac{B}{z_1 \rho_0 R}; \quad \alpha = \frac{z_0\,[A]\,Q_1}{z_1 \rho_0 E_1}; \quad q = \frac{Q_0}{Q_1}; \quad \epsilon = \frac{E_0}{E_1}; \quad \theta_a = \frac{R T_a}{E_1}. \tag{2.8}$$

Here β is the dimensionless rate of heat exchange to ambient, α, q and ϵ are the ratios of reaction constants, enthalpy of formation and activation energies and θ_a is the ambient temperature.

The governing equations are expressed in terms of these new variables and dimensionless parameters (2.8). Brackets denoting molar concentration are omitted, and in non-dimensional form, the system (2.1) - (2.5) becomes

$$\frac{\partial \hat{X}}{\partial \hat{t}} + \frac{1}{\hat{r}^2}\frac{\partial}{\partial \hat{r}}\left(\hat{r}^2 \hat{u}\hat{X}\right) = \alpha k_0(\hat{T}) - \hat{X}k_1(\hat{T}) \tag{2.9}$$

$$\frac{\partial \hat{\rho}}{\partial \hat{t}} + \frac{1}{\hat{r}^2}\frac{\partial}{\partial \hat{r}}\left(\hat{r}^2 \hat{\rho}\hat{u}\right) = 0 \tag{2.10}$$

$$\hat{\rho}\left(\frac{\partial \hat{u}}{\partial \hat{t}} + \hat{u}\frac{\partial \hat{u}}{\partial \hat{r}}\right) + \frac{\partial \hat{p}}{\partial \hat{r}} = 0 \tag{2.11}$$

$$\hat{\rho}\frac{D}{D\hat{t}}\left(\frac{\gamma \hat{T}}{\gamma - 1} + \frac{1}{2}\hat{u}^2\right) = \frac{\partial \hat{p}}{\partial \hat{t}} + q\alpha k_0(\hat{T}) + \hat{X}k_1(\hat{T}) - \beta\left(\hat{T} - \theta_a\right) \tag{2.12}$$

$$\hat{p} = \hat{\rho}\hat{T}. \tag{2.13}$$

The dimensionless upstream conditions, from equation (2.6), are

$$\hat{\rho} \to 1; \quad \hat{u} \to 0; \quad \hat{T} \to \hat{T}_0; \quad \hat{X} \to X_0; \quad \hat{p} \to \hat{T}_0 \text{ as } \hat{r} \to \infty.$$

While the Arrhenius rates in equation (2.7) were useful in non-dimensionalising the system, it is convenient in the following analysis to consider the alternative forms

$$\begin{aligned} k_0(T) &= \begin{cases} 0, & \text{if } T \leqslant \theta_a \\ 1 - e^{-\epsilon(T-\theta_a)}, & \text{if } T > \theta_a \end{cases} \\ k_1(T) &= \begin{cases} 0, & \text{if } T \leqslant \theta_a \\ 1 - e^{-(T-\theta_a)}, & \text{if } T > \theta_a, \end{cases} \end{aligned} \tag{2.14}$$

exactly as in equation (1.12) of the previous chapter.

2.3 Linearised System

We now proceed to linearise the system, expressing the dependent variables as small-order perturbations around their steady-states. Letting κ be a small parameter, we write

$$\begin{aligned}
\hat{u} &= \kappa u_1 + \mathcal{O}(\kappa^2) \\
\hat{\rho} &= 1 + \kappa \rho_1 + \mathcal{O}(\kappa^2) \\
\hat{T} &= \theta_a + \kappa T_1 + \mathcal{O}(\kappa^2) \\
\hat{p} &= \theta_a + \kappa p_1 + \mathcal{O}(\kappa^2) \\
\hat{X} &= X_0 + \kappa X_1 + \mathcal{O}(\kappa^2).
\end{aligned} \tag{2.15}$$

Substituting the appropriate expansions into the continuity equation (2.10) and retaining only the elements which are first order in κ yields

$$\frac{\partial \rho_1}{\partial t} + \frac{1}{r^2}\frac{\partial \left(r^2 u_1\right)}{\partial r} = 0. \tag{2.16}$$

A similar treatment of the gas law (2.13) gives

$$p_1 = \theta_a \rho_1 + T_1$$

which, upon substitution into the momentum equation (2.11), yields

$$\frac{\partial u_1}{\partial t} + \theta_a \frac{\partial \rho_1}{\partial r} + \frac{\partial T_1}{\partial r} = 0. \tag{2.17}$$

The non-Arrhenius reaction rates defined in (2.14) are also expanded as a power series to first order in κ, giving

$$\begin{aligned}
k_0(T) &= \kappa \epsilon T_1 + \mathcal{O}(\kappa^2) \\
k_1(T) &= \kappa T_1 + \mathcal{O}(\kappa^2)
\end{aligned}$$

and so the enthalpy equation (2.12) becomes

$$\frac{1}{\gamma-1}\frac{\partial T_1}{\partial t} = \theta_a \frac{\partial \rho_1}{\partial t} + \Omega T_1. \tag{2.18}$$

Finally, the linearised species-transport equation (2.9) is

$$\frac{\partial X_1}{\partial t} + \frac{X_0}{r^2}\frac{\partial \left(r^2 u_1\right)}{\partial r} = \mu T_1. \tag{2.19}$$

In the previous equations (2.18) and (2.19) we have defined the constants

$$\Omega = q\epsilon\alpha + X_0 - \beta \tag{2.20}$$

and

$$\mu = \epsilon\alpha - X_0$$

for simplicity.

2.4 $\Omega = 0$: Travelling Waves

In the previous section we derived a system of four linear partial differential equations (2.16), (2.17), (2.18) and (2.19) which approximate the full governing partial differential equations (2.9) – (2.13) to first order in the small parameter κ. It will prove necessary to consider the solution to this system in two separate cases which depend on the value of the key parameter Ω in equation (2.20). In this section we investigate the solution when $\Omega = 0$. Physically, this represents the situation in which there is no nett production or loss of heat energy to first order in κ. In this instance we see that equation (2.18) may be directly integrated with respect to time to give

$$T_1 = \theta_a \left(\gamma - 1\right) \rho_1 + L\left(r\right). \tag{2.21}$$

Here $L(r)$ is a yet unknown function only of r. Substituting this value for T_1 into equation (2.17) gives

$$\frac{\partial u_1}{\partial t} + \gamma\theta_a \frac{\partial \rho_1}{\partial r} + L'(r) = 0. \tag{2.22}$$

This is coupled with equation (2.16), and u_1 is eliminated to give the result

$$\frac{\partial^2 \rho_1}{\partial t^2} - \frac{1}{r^2}\frac{\partial}{\partial r}\left[r^2 \frac{\partial}{\partial r}(\gamma\theta_a\rho_1 + L)\right] = 0 \tag{2.23}$$

or equivalently

$$\frac{\partial^2}{\partial t^2}\left[r\left(\rho_1 + \frac{L(r)}{\theta_a\gamma}\right)\right] - \theta_a\gamma\frac{\partial^2}{\partial r^2}\left[r\left(\rho_1 + \frac{L(r)}{\theta_a\gamma}\right)\right] = 0.$$

This is the wave equation in spherical coordinates (see Whitham [34, p.215]). The reaction thus propagates with constant speed $\sqrt{\gamma\theta_a}$, which is also known to be the speed of sound in an isentropic gas at temperature θ_a (see, for example, Liepmann and Roshko [37, pp.65-70]). Writing $c = \sqrt{\theta_a\gamma}$ and introducing the two moving coordinates $\eta = r - ct$ and $\xi = r + ct$, the solution to the wave equation (2.23) is written

$$\rho_1(r,t) = \frac{f'(\eta) + g'(\xi)}{r} - \frac{L(r)}{c^2} \tag{2.24}$$

in which a prime indicates differentiation with respect to the relevant variable. These "differentiated forms" are used so as to simplify later equations. Substitution of the expression (2.24) for ρ_1 into (2.21) also yields the solution for T_1

$$T_1(r,t) = \theta_a(\gamma - 1)\left[\frac{f'(\eta) + g'(\xi)}{r}\right] + \frac{L(r)}{\gamma}. \tag{2.25}$$

Using (2.24) in (2.22) gives

$$\frac{\partial u_1}{\partial t} = c^2\left[\frac{f'(\eta) + g'(\xi)}{r^2} - \frac{f''(\eta) + g''(\xi)}{r}\right]$$

which may be integrated at once to give

$$u_1(r,t) = c\left[\frac{g(\xi) - f(\eta)}{r^2} + \frac{f'(\eta) - g'(\xi)}{r}\right]. \tag{2.26}$$

No arbitrary function of r is needed in (2.26), which follows from (2.16).

Finally, substituting the appropriate expressions for u_1 and T_1 (given in (2.26) and (2.25) respectively) into equation (2.19) and integrating with respect to t gives the solution for X_1 as

$$\begin{aligned} X_1(r,t) =& \frac{\mu\theta_a(\gamma-1)[g(\xi) - f(\eta)]}{cr} + \frac{X_0[f'(\eta) + g'(\xi)]}{r} \\ &+ \frac{(\mu\theta_a t - X_0)L(r)}{c^2} + M(r). \end{aligned} \tag{2.27}$$

Here $M(r)$ is another unknown function of r. Note that in this expression for X_1 the function L is multiplied by a term which is linear in t and, unless either μ or L are identically zero, the expression (2.27) is algebraically unstable with time.

The problem is now reduced to finding appropriate functions f, g, L and M based on the initial state of the system. It follows directly from equation (2.21), that L may be evaluated from the initial distributions of ρ_1 and T_1 according to the relation

$$L(r) = T(r,0) - \theta_a(\gamma-1)\rho_1(r,0).$$

From (2.24), (2.25) and (2.26) we have

$$\frac{\partial}{\partial r}\left\{\frac{1}{r}\int r[\theta_a\rho_1(r,0) + T_1(r,0)]\,\mathrm{d}r\right\} - cu_1(r,0) = 2c^2\frac{\partial}{\partial r}\left(\frac{g(r)}{r}\right).$$

By integrating with respect to r and simplifying we obtain

$$g(\xi) = \frac{1}{2c}\left\{\int^{\xi}\frac{r[\theta_a\rho_1(r,0) + T_1(r,0)]}{c}\mathrm{d}r - \xi\int^{\xi}u_1(r,0)\,\mathrm{d}r\right\} \tag{2.28}$$

and differentiating both sides of this gives

$$g'(\xi) = \frac{1}{2c}\left\{\frac{\xi\left[\theta_a\rho_1(\xi,0) + T_1(\xi,0)\right]}{c} - \xi u_1(\xi,0) - \int^{\xi} u_1(r,0)\,\mathrm{d}r\right\}. \quad (2.29)$$

Although a similar method may be used to find expressions for f and f', namely

$$f(\eta) = \frac{1}{2c}\left\{\int^{\eta} \frac{r\left[\theta_a\rho_1(r,0) + T_1(r,0)\right]}{c}\mathrm{d}r + \eta\int^{\eta} u_1(r,0)\,\mathrm{d}r\right\} \quad (2.30)$$

and

$$f'(\eta) = \frac{1}{2c}\left\{\frac{\xi\left[\theta_a\rho_1(\xi,0) + T_1(\xi,0)\right]}{c} + \eta u_1(\eta,0) + \int^{\eta} u_1(r,0)\,\mathrm{d}r\right\}, \quad (2.31)$$

care must be taken as using these equations would involve evaluating $\rho_1(r,0)$ and $u_1(r,0)$ for negative values of the radius r and a meaningful extension of these initial distributions is needed. Such an extension may be found by considering the behaviour of the solutions at the origin. In order to avoid singularities in ρ_1 and u_1 at $r = 0$ we impose the conditions

$$\lim_{r\to 0} r\rho_1(r,t) = \lim_{r\to 0} r^2 u_1(r,t) = 0$$

for all times $t \geqslant 0$. Thus we must have

$$\left.\begin{aligned} f'(-ct) &= -g'(ct) \\ f(-ct) &= g(ct) \end{aligned}\right\} t \geqslant 0.$$

For negative arguments, the values of f and its derivative f' are determined in terms of g and g' evaluated on positive arguments:

$$\begin{aligned} f(-|\eta|) &= g(|\eta|) \\ f'(-|\eta|) &= -g'(|\eta|). \end{aligned} \quad (2.32)$$

From equations (2.28) - (2.31) and (2.32) it follows that, for all values of η, f is given by

$$f(\eta) = \frac{1}{2c}\left\{\int^{|\eta|} \frac{r\left[\theta_a \rho_1(|r|,0) + T_1(|r|,0)\right]}{c}\mathrm{d}r + \eta\int^{|\eta|} u_1(r,0)\,\mathrm{d}r\right\}$$

and likewise that its derivative is

$$f'(\eta) = \frac{1}{2c}\left\{\frac{\eta\left[\theta_a \rho_1(|\eta|,0) + T_1(|\eta|,0)\right]}{c} + |\eta|\,u_1(|\eta|,0) + \int^{|\eta|} u_1(r,0)\,\mathrm{d}r\right\}.$$

Similar conditions on the solution to the spherical wave equation are considered by Whitham [34, p.216]. Finally, having found expressions for f and g, evaluating equation (2.27) at $t = 0$ allows for the calculation of M which, after a little simplification using (2.24) and (2.26), may be written

$$M(r) = X_1(r,0) - X_0\rho_1(r,0) + \frac{\mu(\gamma-1)}{\gamma}\int^{r} u_1(\hat{r},0)\,\mathrm{d}\hat{r}.$$

The solution discussed in this section may be viewed as having two major components, the travelling-wave component behaving as an "active region" modelled by f, g and their derivatives, and the "burnt" distribution, here written in terms of L and M, left behind after the reaction passes.

2.5 $\Omega \neq 0$: Solutions to the Linearised System and Stability

In this section we consider the solution to the linearised system derived in section 2.3, under the assumption $\Omega \neq 0$. Also included in this section is an analysis of the stability of the linear solution and a demonstration that the growth rate of unstable modes depends only on the parameter Ω in equation

(2.20). To begin, we focus on finding expressions for ρ_1, u_1 and T_1 and consider X_1 separately towards the end of this section.

A separation of variables argument is used to solve equations (2.16), (2.17), and (2.18) and solutions are found of the form

$$\begin{aligned} \rho_1(r,t) &= \int_0^\infty \mathcal{F}_m(t)\, j_0(mr)\, \mathrm{d}m \\ u_1(r,t) &= \int_0^\infty \mathcal{G}_m(t)\, j_1(mr)\, \mathrm{d}m \\ T_1(r,t) &= \int_0^\infty \mathcal{H}_m(t)\, j_0(mr)\, \mathrm{d}m \end{aligned} \tag{2.33}$$

where j_0 and j_1 are, respectively, the first kind spherical Bessel functions of zeroth and first order. The quantities $j_0(z)$ and $j_1(z)$ can be expressed in terms of elementary functions as

$$\begin{aligned} j_0(z) &= \frac{\sin(z)}{z} \\ j_1(z) &= \frac{\sin(z)}{z^2} - \frac{\cos(z)}{z} = -j_0'(z) \end{aligned}$$

(see Abramowitz and Stegun [42, p.438]). The spherical Bessel functions of the second kind with orders 0 and 1 also satisfy the radial part of these equations, but they are omitted as they are divergent at the origin. It follows from the closure relation for spherical Bessel functions (see Arfken [43, p.635]) and the equations in (2.33) that the temporal functions are given by

$$\begin{aligned} \mathcal{F}_m(t) &= \frac{2m^2}{\pi} \int_0^\infty r^2 \rho_1(r,t)\, j_0(mr)\, \mathrm{d}r \\ \mathcal{G}_m(t) &= \frac{2m^2}{\pi} \int_0^\infty r^2 u_1(r,t)\, j_1(mr)\, \mathrm{d}r \\ \mathcal{H}_m(t) &= \frac{2m^2}{\pi} \int_0^\infty r^2 T_1(r,t)\, j_0(mr)\, \mathrm{d}r. \end{aligned} \tag{2.34}$$

The functions of time satisfy a linear system of ordinary differential equations and, using a prime to denote a derivative with respect to time, these equations

are

$$\begin{aligned}\mathcal{F}'_m(t) + m\mathcal{G}_m(t) &= 0\\ \mathcal{G}'_m(t) - m\theta_a\mathcal{F}_m(t) - m\mathcal{H}_m(t) &= 0\\ \mathcal{H}'_m(t) - (\gamma-1)\theta_a\mathcal{F}'_m(t) - (\gamma-1)\Omega\mathcal{H}_m(t) &= 0.\end{aligned} \tag{2.35}$$

These three equations follow from (2.16), (2.17) and (2.18), respectively, after integration by parts in (2.33). Eliminating first $\mathcal{H}_m(t)$ and then $\mathcal{G}_m(t)$, these can be reduced to the ordinary differential equation for $\mathcal{F}_m(t)$, of third order:

$$\mathcal{F}'''_m(t) - (\gamma-1)\Omega\mathcal{F}''_m(t) + m^2\theta_a\gamma\mathcal{F}'_m(t) - m^2(\gamma-1)\Omega\theta_a\mathcal{F}_m(t) = 0. \tag{2.36}$$

Since (2.36) is a constant-coefficient equation, a solution is sought in the exponential form $\exp(\lambda t)$, for which the constant λ then satisfies the cubic characteristic equation

$$\lambda^3 - (\gamma-1)\Omega\lambda^2 + m^2\gamma\theta_a\lambda - m^2(\gamma-1)\Omega\theta_a = 0. \tag{2.37}$$

If λ_1, λ_2 and λ_3 are the roots of this polynomial, the solution to (2.36) may be written

$$\mathcal{F}_m(t) = A_m^{(1)}\mathrm{e}^{\lambda_1 t} + A_m^{(2)}\mathrm{e}^{\lambda_2 t} + A_m^{(3)}\mathrm{e}^{\lambda_3 t} \tag{2.38}$$

and it follows that the remaining temporal components have the forms

$$\begin{aligned}\mathcal{G}_m(t) &= B_m^{(1)}\mathrm{e}^{\lambda_1 t} + B_m^{(2)}\mathrm{e}^{\lambda_2 t} + B_m^{(3)}\mathrm{e}^{\lambda_3 t}\\ \mathcal{H}_m(t) &= C_m^{(1)}\mathrm{e}^{\lambda_1 t} + C_m^{(2)}\mathrm{e}^{\lambda_2 t} + C_m^{(3)}\mathrm{e}^{\lambda_3 t}.\end{aligned} \tag{2.39}$$

By substituting the expressions (2.39) into the first and second equations in (2.35) all of the coefficients can be written in terms of $A_m^{(j)}$;

$$\left.\begin{aligned}B_m^{(j)} &= -\frac{\lambda_j}{m}A_m^{(j)}\\ C_m^{(j)} &= -\frac{\left(m^2\theta_a + \lambda_j^2\right)}{m^2}A_m^{(j)}\end{aligned}\right\} j = 1, 2, 3. \tag{2.40}$$

The third equation in (2.35) gives the compatibility condition

$$\left[\lambda_j - (\gamma-1)\,\Omega\right] C_m^{(j)} - (\gamma-1)\,\theta_a \lambda_j A_m^{(j)} = 0,\ j = 1,2,3$$

which, using (2.40), reduces to equation (2.37). Before looking at the roots of the characteristic equation (2.37), we will analyse the discriminant, which will allow us to determine their nature. It will first prove useful to define the constants

$$\begin{aligned}\delta_1 =& \Omega\,(\gamma-1)\left(\Omega^2\,(\gamma-1)^2 - \frac{9}{2}\theta_a m^2\,(\gamma-3)\right)\\ \delta_2 =& 3m^2\gamma\theta_a - \Omega^2\,(\gamma-1)^2\end{aligned}$$

then, using Δ to represent the discriminant, we have

$$\Delta = \delta_1^2 + \delta_2^3.$$

This form of the discriminant is equivalent to the form given by Abramowitz and Stegun [42, p.17], up to a positive multiplying constant. We find (after some considerable algebra) that for $m > 0$ it satisfies the equation

$$\frac{64\gamma^3\Delta}{27m^2\theta_a} = \left[8\gamma^3\theta_a m^2 + \left(27 - 18\gamma - \gamma^2\right)(\gamma-1)^2\,\Omega^2\right]^2 + (9-\gamma)^3\,(\gamma-1)^5\,\Omega^4.$$

For $1 < \gamma < 9$ the right-hand side of this equation is strictly positive and therefore $\Delta > 0$. From this we conclude that the characteristic equation (2.37) has two complex roots, which are mutual conjugates, and without loss of generality we choose these roots to be λ_1 and λ_2. The third root, λ_3, is purely real and is given by

$$\lambda_3 = \frac{1}{3}\left[\Omega\,(\gamma-1) + \left(\delta_1 + \sqrt{\Delta}\right)^{1/3} - \frac{\delta_2}{\left(\delta_1 + \sqrt{\Delta}\right)^{1/3}}\right].$$

The roots λ_1 and λ_2 have real and imaginary parts given, respectively, by

$$\begin{aligned}
\mathrm{Re}\left(\lambda_1\right) = \mathrm{Re}\left(\lambda_2\right) =& \frac{\Omega\left(\gamma-1\right)}{3} + \frac{1}{6}\left[\frac{\delta_2}{\left(\delta_1+\sqrt{\Delta}\right)^{1/3}} - \left(\delta_1+\sqrt{\Delta}\right)^{1/3}\right] \\
\mathrm{Im}\left(\lambda_1\right) = -\mathrm{Im}\left(\lambda_2\right) =& \frac{1}{2\sqrt{3}}\left[\left(\delta_1+\sqrt{\Delta}\right)^{1/3} + \frac{\delta_2}{\left(\delta_1+\sqrt{\Delta}\right)^{1/3}}\right].
\end{aligned}$$

Finally, the problem is reduced to finding the values of the coefficients $A_m^{(j)}$, based on the equations for the initial data, given by

$$\begin{aligned}
\mathcal{F}_m\left(0\right) &= A_m^{(1)} + A_m^{(2)} + A_m^{(3)} \\
\mathcal{G}_m\left(0\right) &= B_m^{(1)} + B_m^{(2)} + B_m^{(3)} \\
\mathcal{H}_m\left(0\right) &= C_m^{(1)} + C_m^{(2)} + C_m^{(3)}.
\end{aligned}$$

These expressions are found by evaluating (2.38) and (2.39) at $t = 0$. Rewriting $B_m^{(j)}$ and $C_m^{(j)}$ in terms of the coefficients $A_m^{(j)}$ using (2.40), they are reduced to the system of three algebraic equations

$$\begin{aligned}
\mathcal{F}_m\left(0\right) &= A_m^{(1)} + A_m^{(2)} + A_m^{(3)} \\
\mathcal{G}_m\left(0\right) &= -\frac{1}{m}\left(\lambda_1 A_m^{(1)} + \lambda_2 A_m^{(2)} + \lambda_3 A_m^{(3)}\right) \\
\mathcal{H}_m\left(0\right) + \theta_a \mathcal{F}_m\left(0\right) &= -\frac{1}{m^2}\left(\lambda_1^2 A_m^{(1)} + \lambda_2^2 A_m^{(2)} + \lambda_3^2 A_m^{(3)}\right).
\end{aligned}$$

It then follows that the coefficients are given by

$$\begin{aligned}
A_m^{(1)} &= \frac{\left(m^2\theta - \lambda_2\lambda_3\right) F_m\left(0\right) - m\left(\lambda_2+\lambda_3\right) G_m\left(0\right) + m^2 H_m\left(0\right)}{\left(\lambda_3-\lambda_1\right)\left(\lambda_1-\lambda_2\right)} \\
A_m^{(2)} &= \frac{\left(m^2\theta - \lambda_1\lambda_3\right) F_m\left(0\right) - m\left(\lambda_1+\lambda_3\right) G_m\left(0\right) + m^2 H_m\left(0\right)}{\left(\lambda_1-\lambda_2\right)\left(\lambda_2-\lambda_3\right)} \\
A_m^{(3)} &= \frac{\left(m^2\theta - \lambda_1\lambda_2\right) F_m\left(0\right) - m\left(\lambda_1+\lambda_2\right) G_m\left(0\right) + m^2 H_m\left(0\right)}{\left(\lambda_2-\lambda_3\right)\left(\lambda_3-\lambda_1\right)}.
\end{aligned}$$

Notice that these three quantities are all related by a cyclic permutation of the indices. We now turn our attention to solving for X_1 using the remaining

linear equation (2.19). Equations (2.16) and (2.18) allow the substitutions

$$\frac{1}{r^2}\frac{\partial\left(r^2 u_1\right)}{\partial r} = -\frac{\partial \rho_1}{\partial t}$$

and

$$T_1 = \frac{1}{\Omega\left(\gamma - 1\right)}\frac{\partial T_1}{\partial t} - \frac{\theta_a}{\Omega}\frac{\partial \rho_1}{\partial t}$$

to be made into (2.19) and with a little simplification we obtain

$$\frac{\partial X_1}{\partial t} = \left(X_0 - \frac{\mu\theta_a}{\Omega}\right)\frac{\partial \rho_1}{\partial t} + \frac{\mu}{\Omega\left(\gamma - 1\right)}\frac{\partial T_1}{\partial t}$$

which may be integrated with respect to t, yielding

$$X_1\left(r,t\right) = \left(X_0 - \frac{\mu\theta_a}{\Omega}\right)\rho_1\left(r,t\right) + \frac{\mu}{\Omega\left(\gamma - 1\right)}T_1\left(r,t\right) + N\left(r\right).$$

Here $N\left(r\right)$ is a function purely of radius, r, and may be calculated from

$$N\left(r\right) = X_1\left(r,0\right) + \left(\frac{\mu\theta_a}{\Omega} - X_0\right)\rho_1\left(r,0\right) - \frac{\mu}{\Omega\left(\gamma - 1\right)}T_1\left(r,0\right). \qquad (2.41)$$

The stability of the linear solutions derived above depends on the sign of λ_3, $\mathrm{Re}\left(\lambda_2\right)$ and $\mathrm{Re}\left(\lambda_1\right)$; if, for any value of m, any of these three quantities is positive, the expressions in (2.38) and (2.39) will grow exponentially with time. Conversely, the solution will remain stable or decay if, for every value of m, they are all negative or zero. These considerations lead to the key result concerning stability of these solutions:

Theorem. *The solutions presented in section 2.5 to the linearised system derived in section 2.3 are stable if and only if* $\Omega < 0$.

Proof. The Routh-Hurwitz stability criterion (see Routh [44, p.27]) for the characteristic polynomial (2.37) reduces the requirements for stability to the

condition that $-\Omega(\gamma-1)$, $-\Omega(\gamma-1)m^2\theta_a$ and $-\Omega(\gamma-1)^2 m^2\theta_a$ must all be positive. All of these conditions are satisfied, for all m, if and only if $\Omega < 0$. □

Since Ω may be interpreted as the first order approximation of the net heat increase of the reaction, it is perhaps not too surprising that it determines the stability of the linear system. Thus the solutions are stable when the cooling rate to ambient temperature exceeds the rate at which heat is generated by the reaction.

2.6 Comparison with Numerical Results

In this section we use the method of lines to derive a numerical scheme to approximate the full non-linear system of partial differential equations, for comparison with the linear solution given previously. The infinite domain $[0,\infty)$ is replaced by the finite one $[0, r_{max}]$, which we divide into $N+1$ discrete, equally spaced points of width Δr. In the interior of the domain we replace the spatial derivatives in equations (2.9) - (2.12) with central

differences, yielding the system of ordinary differential equations

$$\begin{aligned}
\tilde{\rho}_j'(t) =& \frac{(j-1)\tilde{\rho}_{j-1}\tilde{u}_{j-1} - (j+1)\tilde{\rho}_{j+1}\tilde{u}_{j+1}}{2j\Delta r} \\
\tilde{u}_j'(t) =& \frac{\tilde{\rho}_{j-1}\tilde{T}_{j-1} - \tilde{\rho}_{j+1}\tilde{T}_{j+1}}{2\tilde{\rho}_j\Delta r} + \tilde{u}_j\left(\frac{\tilde{u}_{j-1} - \tilde{u}_{j+1}}{2\Delta r}\right) \\
\tilde{T}_j'(t) =& (\gamma-1)\left[\tilde{u}_j\left(\frac{J_{j-1} - J_{j+1}}{2\Delta r} - \tilde{u}_j'\right)\right. \\
&\left. + \frac{\tilde{T}_j\tilde{\rho}_j' + \tilde{X}_j k_1(\tilde{T}_j) + zqAk_0(\tilde{T}_j) - \beta\left(\tilde{T}_j - \theta_a\right)}{\tilde{\rho}_j}\right] \\
\tilde{X}_j'(t) =& \frac{(j-1)\tilde{X}_{j-1}\tilde{u}_{j-1} - (j+1)\tilde{X}_{j+1}\tilde{u}_{j+1}}{2j\Delta r} + zAk_0(\tilde{T}_j) - \tilde{X}_j k_1(\tilde{T}_j)
\end{aligned}$$

for $j = 1, 2, ..., N-1$. Here we have made the substitution $J_j = \gamma\tilde{T}_j/(\gamma-1) + \frac{1}{2}\tilde{u}_j^2$ for convenience. The behaviour of the numerical system at either boundary must be considered separately. Special consideration must be made of the radial derivatives in the continuity equation (2.10), to ensure boundedness at the origin. Using L'Hôpital's rule we may write

$$\begin{aligned}
\lim_{r\to 0^+}\frac{1}{r^2}\frac{\partial}{\partial r}\left(r^2\hat{\rho}\hat{u}\right) &= \lim_{r\to 0^+}\left[\frac{\partial}{\partial r}\left(\hat{\rho}\hat{u}\right) + \frac{2\hat{\rho}\hat{u}}{r}\right] \\
&= 3\frac{\partial}{\partial r}\left(\hat{\rho}\hat{u}\right)\Big|_{r=0}.
\end{aligned}$$

The existence of this limit, and the application of L'Hôpital's rule, requires and assumes that $\hat{\rho}\hat{u} \to 0$ as $r \to 0$. Applying the product rule for derivatives and setting $\hat{u}(0,t) = 0$, the above expression can be simplified to

$$\lim_{r\to 0^+}\frac{1}{r^2}\frac{\partial}{\partial r}\left(r^2\hat{\rho}\hat{u}\right) = 3\left(\hat{\rho}\frac{\partial\hat{u}}{\partial r}\right)_{r=0}$$

and a similar expression is derived for the radial derivative in the species transport equation (2.9). Approximating these derivatives with forward finite

differences gives

$$\begin{aligned}
\tilde{\rho}_0'(t) =& 3\tilde{\rho}_0 \left(\frac{\tilde{u}_2 - 4\tilde{u}_1}{2\Delta r} \right) \\
\tilde{u}_0'(t) =& 0 \\
\tilde{T}_0'(t) =& \frac{(\gamma - 1)}{\tilde{\rho}_0} \left[\tilde{T}_0 \tilde{\rho}_0' + \tilde{X}_0 k_1(\tilde{T}_0) + zqAk_0(\tilde{T}_0) - \beta \left(\tilde{T}_0 - \theta_a \right) \right] \\
\tilde{X}_0'(t) =& 3\tilde{X}_0 \left(\frac{\tilde{u}_2 - 4\tilde{u}_1}{2\Delta r} \right) + zAk_0(\tilde{T}_0) - \tilde{X}_0 k_1(\tilde{T}_0).
\end{aligned}$$

This difference scheme is chosen to approximate the derivatives to order Δr^2 (see Zwillinger [45, p.705] and Fornberg [46]). Far from the origin (at $j = N$) the radial derivatives of the quantities are set to 0, so that they are unaffected by the reaction front. As a result, the numerical scheme at this end is given by

$$\begin{aligned}
\tilde{\rho}_N'(t) =& 0 \\
\tilde{u}_N'(t) =& 0 \\
\tilde{T}_N'(t) =& \frac{(\gamma - 1)}{\tilde{\rho}_N} \left[\tilde{X}_N k_1(\tilde{T}_N) + zqAk_0(\tilde{T}_N) - \beta \left(\tilde{T}_N - \theta_a \right) \right] \\
\tilde{X}_N'(t) =& zAk_0(\tilde{T}_N) - X_N k_1(\tilde{T}_N).
\end{aligned}$$

The scheme is then numerically integrated with initial distributions given by the expressions

$$\rho_1(r,0) = T_1(r,0) = X_1(r,0) = 10^{-6}\mathrm{e}^{-r^2} \tag{2.42}$$

and

$$u_1(r,0) = 10^{-6} r \mathrm{e}^{-r^2}. \tag{2.43}$$

Comparison with the linearised solution of section 2.3 is made possible by evaluating the integrals in equation (2.34). We obtain

$$\mathcal{F}_m(0) = \frac{10^{-6} m^2 \mathrm{e}^{-m^2/4}}{2\sqrt{\pi}}$$
$$\mathcal{G}_m(0) = \frac{10^{-6} m^3 \mathrm{e}^{-m^2/4}}{4\sqrt{\pi}}$$
$$\mathcal{H}_m(0) = \frac{10^{-6} m^2 \mathrm{e}^{-m^2/4}}{2\sqrt{\pi}}$$

while equation (2.41) gives

$$N(r) = \left[1 - X_0 + \frac{\mu\theta_a}{\Omega} - \frac{\mu}{\Omega(\gamma - 1)}\right] 10^{-6}\mathrm{e}^{-r^2}$$

The parameter values were chosen to be $\alpha = 0.5$, $q = 0.2$, $\epsilon = 0.5$, $\theta_a = 0.1$, $\beta = 0.5$ and $X_0 = 0.3$. For the remainder of this section the ratio of specific heats, γ, will be given the value 1.4 (equal to that of a thermally perfect diatomic molecule; see John [47, p.227]). From the definition given in (2.20), the parameter Ω is calculated to be -0.15 and from the stability analysis in section 2.5 we expect the amplitude of the solution to decay with time.

The integrals presented in (2.34), necessary for calculating the linear solution at later times $t > 0$, will be evaluated numerically, due to the complicated dependence of the integrand on the integration variable m. The infinite upper bound is replaced with a sufficiently large finite value and with the help of von Winckel's Gauss-Legendre quadrature routine [48], the resulting integrals are approximated to a high degree of accuracy. For this particular case, we evaluated the quadratures with an upper bound of $m = 15$ and 5000 mesh points.

Figure (2.1) displays the velocity profile, as produced by the numerical scheme (plotted as a blue, solid line), with the linear approximation given in

(2.33) (plotted in the red, dashed line) up to the time $t = 50$. The general shape of the velocity profile remains largely unchanged as time progresses, with a larger positive spike leading a smaller dip as the reaction front progresses away from the origin. The magnitude of the velocity, however, decreases with time and with distance from the origin, as predicted by the sign of Ω. There is very little noticeable deviation between the two solutions at $t = 10$, but at $t = 30$ the linear solution can be seen to dip below the numerical output just behind the right-most reaction front. This discrepancy grows slowly as time progresses, but the two agree very closely for all other values of r.

A similar comparison of the temperature is made in figure (2.2). There are effectively two separate regions in each plot, with an area of relatively high temperature remaining around the origin, and a smaller, outward-travelling ripple. This travelling portion is similar in shape to that seen in the velocity profile in figure (2.1), with a positive spike leading a negative one as the reaction front moves in the direction of increasing radius.

We now employ the numerical scheme to investigate the system with all of the same parameter values but for the reduced rate of cooling to ambient $\beta = 0.35$. This gives the calculated value $\Omega = 0$ and the linear analysis in section 2.4 indicates that we should expect travelling wave solutions. The initial distributions are again chosen to be the same Gaussian distributions used (2.42) and (2.43), assumed previously. Following the analysis given in

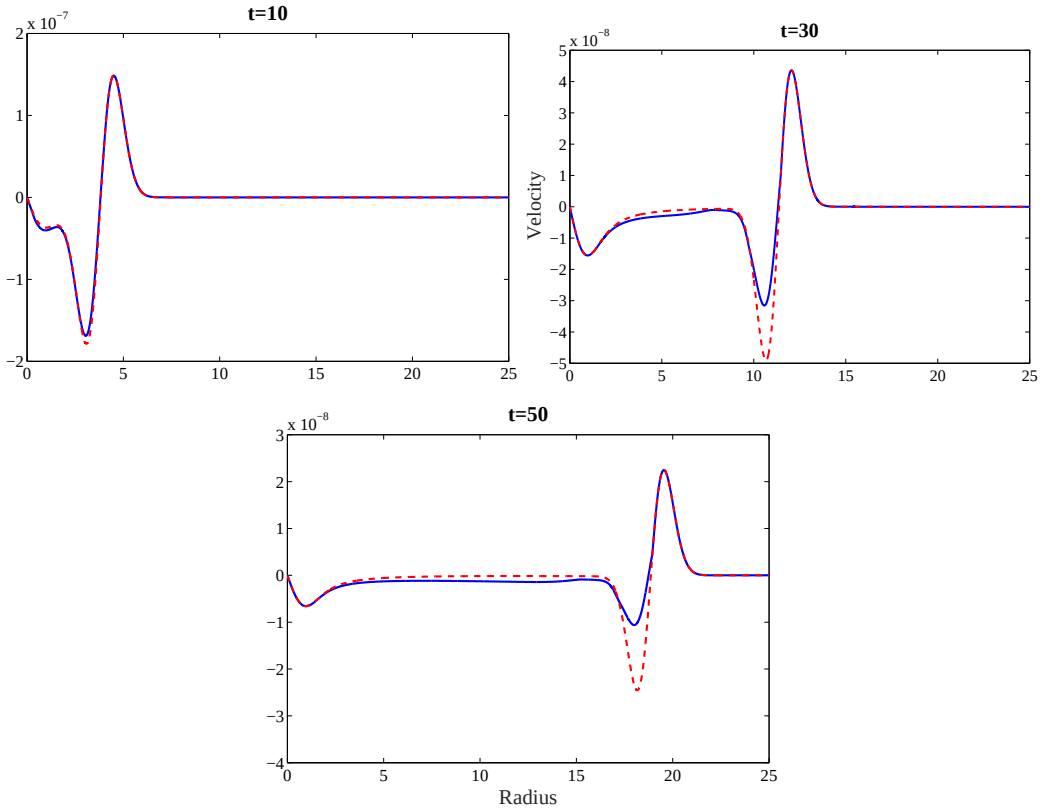

Figure 2.1: A comparison of the gas velocities predicted by the numerical scheme (solid blue line) and linearised equations (dashed red line), at various times up to $t = 50$. The two are virtually indistinguishable up to about $t = 20$.

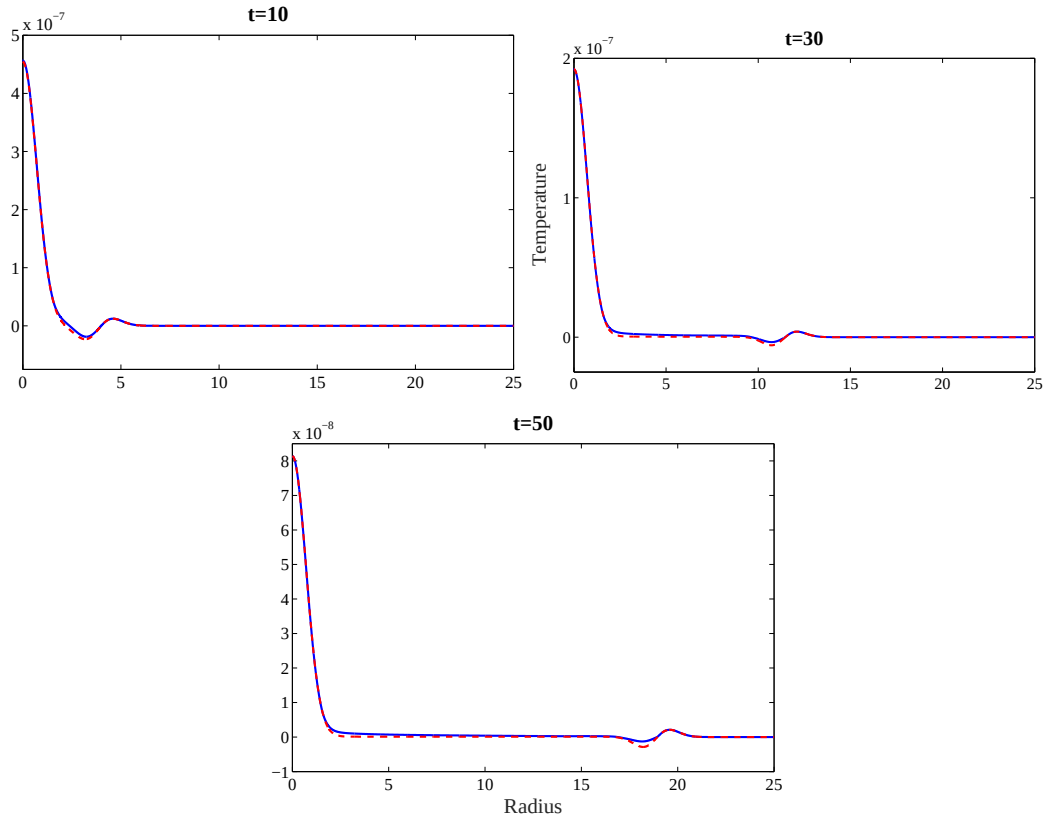

Figure 2.2: Temperature profiles produced by the numerical scheme plotted in a solid blue line compared with the linearised solution in the dashed red line. Comparisons are shown up to the time $t = 50$, and there is almost no noticeable deviation between the two. The temperature is displayed here as its level above ambient.

section 2.4, we derive the travelling wave functions

$$f(\eta) = -\frac{10^{-6}}{4c^2}(c\eta + \theta_a + 1)\,\mathrm{e}^{-\eta^2}$$
$$g(\xi) = \frac{10^{-6}}{4c^2}(c\xi - \theta_a - 1)\,\mathrm{e}^{-\xi^2}$$

and their derivatives are given by

$$f'(\eta) = \frac{10^{-6}}{4c^2}\left[2(1+\theta_a)\eta + 2c\eta^2 - c\right]\mathrm{e}^{-\eta^2}$$
$$g'(\xi) = \frac{10^{-6}}{4c^2}\left[2(1+\theta_a)\xi - 2c\xi^2 + c\right]\mathrm{e}^{-\xi^2}.$$

We also have the radial functions

$$L(r) = \left[1 - \theta_a(\gamma - 1)\right]10^{-6}\mathrm{e}^{-r^2}$$

as well as

$$M(r) = \left[1 - X_0 - \frac{\mu(\gamma-1)}{2\gamma}\right]10^{-6}\mathrm{e}^{-r^2}.$$

The gas density, velocity, temperature, and the concentration of species X may all be calculated as in equations (2.24) - (2.27). Here, as in previous sections, the wave-speed is given by $c = \sqrt{\theta_a\gamma} \approx 0.374$.

Figure (2.3) compares the velocity $u(r,t)$ given by the numerical scheme and linear analysis (plotted in the blue solid line and red dashed line respectively) up to the time $t = 50$. As time progresses the profiles move away from the origin as two positive peaks either side of a negative one, all three of which slowly decay in magnitude in successive plots. The two solutions agree very closely for the majority of the plotted range, although, as with previous plots, the linearised solution over-estimates the size of the dip behind the advancing peak. A similar comparison is made for the temperature in figure (2.4). The profiles are qualitatively quite similar to those seen in

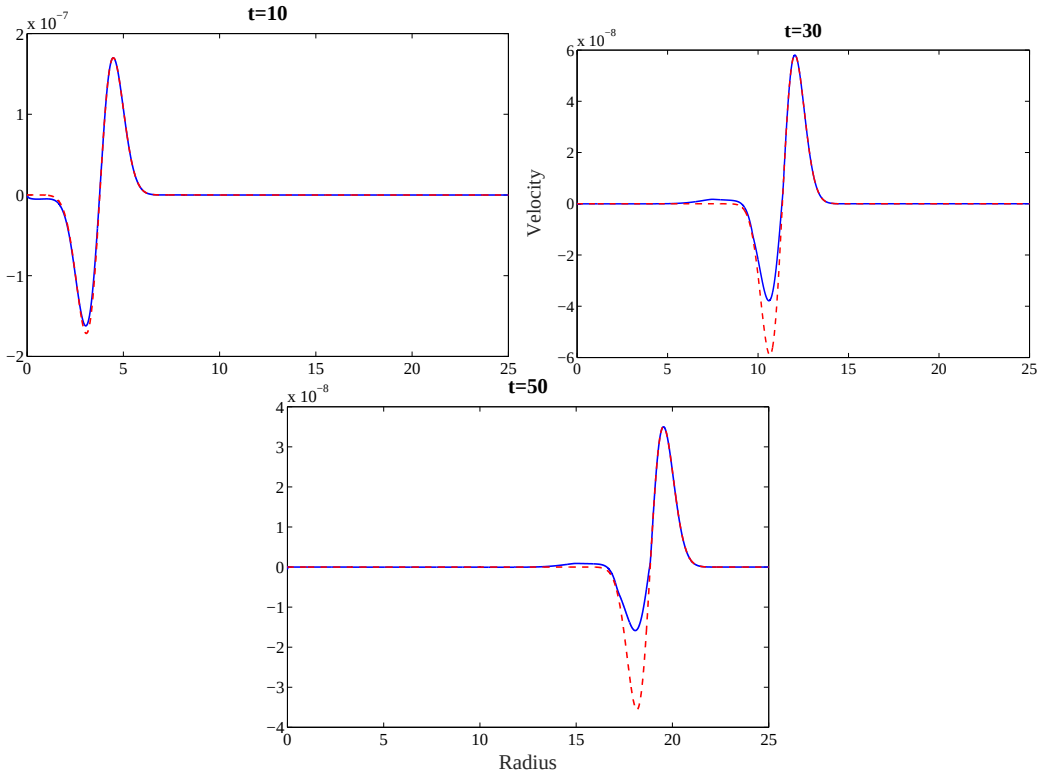

Figure 2.3: Velocity u of gas mixture in the numerical (blue, solid line) and linear, travelling-wave solution (red, dashed line) at various times up to $t = 50$.

the figures (2.2), with a region of high temperature around the origin and an outward-travelling reaction front consisting of an area of slightly higher temperature leading one of lower temperature. In this case, however, the travelling front appears to decay much more rapidly than in figure (2.2).

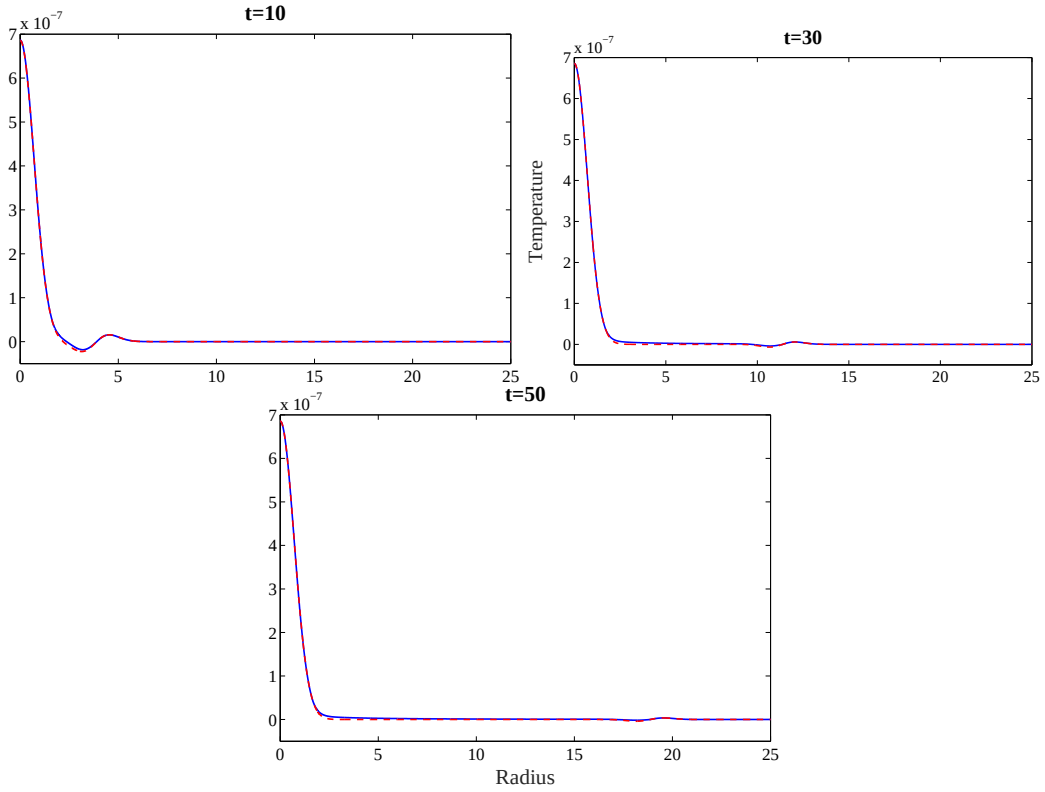

Figure 2.4: Temperature comparison of the predicted travelling-wave solution (red, dashed line) and the solution produced by the numerical scheme (blue, solid line) up to time $t = 50$.

2.7 Extension to a Diffusive Gas

In this section, which was not published along with the preceding chapters, we extend the previously derived linear method to a reaction in a diffusive gas. In dimensionless form, the transport equation (2.9), conservation of mass equation (2.10) and conservation of energy equation (2.12) now respectively become,

$$\begin{aligned}
\frac{\partial X}{\partial t} + \frac{1}{r^2}\frac{\partial}{\partial r}\left(r^2 u X\right) &= \frac{\sigma}{r^2}\frac{\partial}{\partial r}\left(r^2\frac{\partial X}{\partial r}\right) + \alpha k_0(T) - X k_1(T) \\
\frac{\partial \rho}{\partial t} + \frac{1}{r^2}\frac{\partial}{\partial r}\left(r^2 \rho u\right) &= \frac{\sigma}{r^2}\frac{\partial}{\partial r}\left(r^2\frac{\partial \rho}{\partial r}\right) \\
\rho\frac{D}{Dt}\left(\frac{\gamma T}{\gamma - 1} + \frac{1}{2}\right) &= \frac{\phi}{r^2}\frac{\partial}{\partial r}\left(r^2\frac{\partial T}{\partial r}\right) + \frac{\partial p}{\partial t} \\
&\quad + q\alpha k_0(T) + X k_1(T) - \beta\left(T - \theta_a\right)
\end{aligned}$$

wherein σ and ϕ are dimensionless diffusion parameters. The conservation of momentum equation (2.11) and equation of state (2.13) remain unchanged. When each variable is expanded in powers of the small parameter κ, as in (2.15), and the components of order κ^2 discarded, the linearised equations are

$$\begin{aligned}
\frac{\partial X_1}{\partial t} + \frac{X_0}{r^2}\frac{\partial\left(r^2 u_1\right)}{\partial r} &= \frac{\sigma}{r^2}\frac{\partial}{\partial r}\left(r^2\frac{\partial X_1}{\partial r}\right) + \mu T_1 \\
\frac{\partial \rho_1}{\partial t} + \frac{1}{r^2}\frac{\partial\left(r^2 u_1\right)}{\partial r} &= \frac{\sigma}{r^2}\frac{\partial}{\partial r}\left(r^2\frac{\partial \rho_1}{\partial r}\right) \\
\frac{1}{\gamma - 1}\frac{\partial T_1}{\partial t} &= \frac{\phi}{r^2}\frac{\partial}{\partial r}\left(r^2\frac{\partial T_1}{\partial r}\right) + \theta_a\frac{\partial \rho_1}{\partial t} + \Omega T_1 \\
\frac{\partial u_1}{\partial t} + \theta_a\frac{\partial \rho_1}{\partial r} + \frac{\partial T_1}{\partial r} &= 0
\end{aligned} \tag{2.44}$$

and with the linearised equation of state

$$p_1 = \theta_a \rho_1 + T_1. \tag{2.45}$$

Under these new linear equations, the travelling wave solution found in section 2.4 are no longer present, and so we make use of the transformation method discussed in section 2.5. Solutions are sought in terms of the same integral transformations presented in (2.33), that is we assume that the solutions may be written as

$$\begin{aligned}
\rho_1(r,t) &= \int_0^\infty \mathcal{F}_m(t)\, j_0(mr)\, \mathrm{d}m \\
u_1(r,t) &= \int_0^\infty \mathcal{G}_m(t)\, j_1(mr)\, \mathrm{d}m \\
T_1(r,t) &= \int_0^\infty \mathcal{H}_m(t)\, j_0(mr)\, \mathrm{d}m.
\end{aligned}$$

Assuming that the temporal function $\mathcal{F}$ is of the form *constant* $\times\, \mathrm{e}^{\lambda t}$, and similarly for $\mathcal{G}$ and $\mathcal{H}$, the exponent λ is found to satisfy the cubic polynomial equation

$$\lambda^3 + p_2\lambda^2 + p_1\lambda + p_0 = 0 \tag{2.46}$$

where the polynomial coefficients are given by

$$\begin{aligned}
p_2 &= m^2\phi(\gamma-1) + m^2\sigma - \Omega(\gamma-1) \\
p_1 &= m^4\phi\sigma(\gamma-1) - m^2\Omega\sigma(\gamma-1) + m^2\gamma\theta_a \\
p_0 &= m^2\theta_a(\gamma-1)\left(m^2\phi - \Omega\right).
\end{aligned} \tag{2.47}$$

Then by the Routh-Hurwitz stability criterion, the solution is stable if and only if the polynomial coefficients satisfy the inequalities

$$\begin{aligned}
p_2,\ p_0 \qquad &> 0 \\
p_2p_1 - p_0 \quad &> 0
\end{aligned} \tag{2.48}$$

for every value of $m > 0$. Clearly, if $\Omega > 0$, p_0 is negative when $m^2 < \Omega/\phi$ and thus the system is unstable when $\Omega > 0$. Conversely, if $\Omega \leqslant 0$, it can be

seen easily that both p_2 and p_0 are positive, and all we need to do is verify that the last stability condition holds. With some straight-forward algebra, we have

$$p_2 p_1 - p_0 = q_3 m^6 + q_2 m^4 + q_1 m^2 \tag{2.49}$$

where the polynomial coefficients are

$$\begin{aligned} q_3 &= \sigma\phi\,(\gamma-1)\,[\sigma + \phi\,(\gamma-1)] \\ q_2 &= \gamma\theta_a\sigma + \theta_a\phi\,(\gamma-1)^2 - \Omega\sigma\,(\gamma-1)\,[\sigma + 2\phi\,(\gamma-1)] \\ q_1 &= -\Omega\,(\gamma-1)^2\,(\theta_a - \sigma\Omega)\,. \end{aligned} \tag{2.50}$$

It is obvious that all of these coefficients are positive (or zero) if $\Omega \leqslant 0$, and therefore so is $p_2 p_1 - p_0$. Thus the system is stable if and only if $\Omega < 0$, regardless of the strength of the diffusion. The remainder of the method outlined in section 2.5 may now be adapted, with the appropriate changes, to complete the solution.

2.8 Conclusion

We have presented a linear analysis of a spherically symmetric gas, which is reacting according to Sal'nikov's reaction model. The form of the solution is dependent on the value of a derived parameter Ω, given in equation (2.20), which is a combination of various reaction parameters. Solutions with travelling wave components are found when this parameter has value zero, and exact solutions to the linearised equations are presented in terms of the initial conditions of the reaction. When this parameter is non-zero, the solutions are presented in terms of integrals over spherical Bessel functions.

A straight-forward numerical scheme has been derived using the method of lines and this has been used to compare non-linear results with the solutions predicted by the linear analysis and the two show very close agreement, although some minor deviation is seen behind a reaction front which travels outwards from the origin. It is also shown that the linear perturbations of density, gas velocity and temperature are all neutrally stable in the travelling wave case (when $\Omega = 0$). The amplitude of the concentration perturbation, however, will increase with time unless a second derived parameter, denoted μ, is zero or the initial temperature and density perturbations satisfy the relation $T_1(r,0) = \theta_a(\gamma - 1)\rho_1(r,0)$. When $\Omega \neq 0$, a brief analysis has also shown that the stability of the system is dependent solely on the sign of Ω, with the perturbations growing if the parameter is positive, and decaying if it is negative.

Finally section 2.7 gives a brief outline of how the transform method can easily be adapted to the case of a diffusive gas. Moreover, it also proves that the stability condition remains unchanged; irrespective of the strength of the diffusion, the system is stable if and only if $\Omega \leqslant 0$

Chapter 3

Combustion behind a spherical shock

3.1 Introduction

In the following chapter we model Sal'nikov's reaction scheme behind an outward-moving, spherically symmetric shock. The properties of the gas between the shock front and the centre of ignition are assumed to vary smoothly, so that the governing equations which hold in this region are much as they were in chapter 2; consisting of an algebraic equation of state, and partial differential equations for mass, momentum, energy and concentration of the intermediate reagent X. As we will discuss in more detail later, we will also include a fifth such equation for the initial reagent A, as it is deemed appropriate to drop the pool-chemical approximation discussed in the previous chapters 1 and 2. Across the shock however, the differential form for each of the governing equations is no longer appropriate as spatial become undefined across a jump discontinuity. On the shock it is necessary to consider the conservation equations in their integral forms, from which we derive an algebraic equation for each of the conserved quantities.

In the pages that follow we present a novel numerical scheme which is able to solve the governing differential equations behind the shock as well as the algebraic conditions on the shock discontinuity by building the shock equations into a spectral method built around specially chosen spherical Bessel functions, similar to those used in chapter 2. This yields a system of differential equations for the spectral coefficients and the shock strength, which are intricately linked by a requirement that the solution found behind the shock must be consistent with those which hold on the shock.

The resulting numerical method is shock-fitting, and thus provides clear resolution of the position and strength of the shock, but is occasionally suscep-

tible to the accumulation of numerical errors in the high-frequency modes. By comparison with the well-known method of Godunov, we show that a small amount of artificial diffusion is able to dampen these spurious growths in the higher order modes while maintaining an acceptable level of accuracy.

3.2 Model

In previous chapters we have invoked the "pool-chemical" approximation for the reagent A, allowing us to consider its concentration as constant and ignore dynamic effects on its distribution. In this chapter we will drop this simplifying approximation, as it seems likely that a reaction sufficiently strong to create a shock wave will also have a non-negligible effect in the distribution of initial fuel A. As such there is a need to also model the depletion of this reagent to the reaction and its movement through convection, by way of another partial differential equation. This additional equation is of a similar form to the reaction-convection equation used to model the distribution of the intermediate reagent X in the previous chapter.

The gas in which the reaction takes place is assumed to be spherically symmetric, so that the only spatial coordinate of interest is the radius r from the reaction centre, with a jump discontinuity at some distance $r = R_s(t)$ from the origin. Beyond the shock the gas attains its background values and remains stable. A sketch of this scenario in terms of the representative variable $V(r,t)$ can be seen in figure (3.1). In the reacting portion, then, the governing equations in dimensionless form are very much the same as those

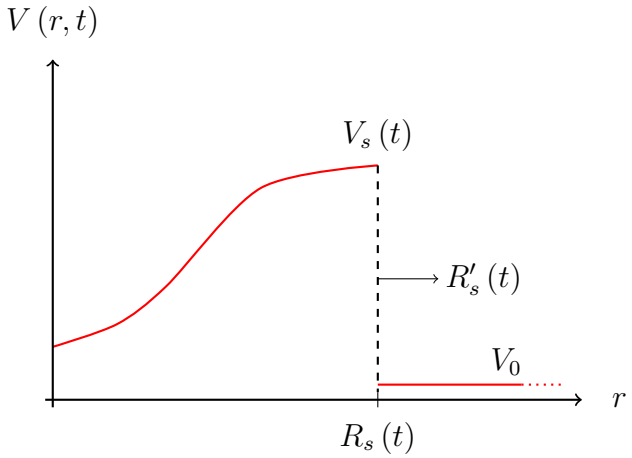

Figure 3.1: Snapshot of a variable behind a shock

in chapter 2.

Governing the conservation of mass is the equation

$$\frac{\partial \rho}{\partial t} + \frac{1}{r^2}\frac{\partial}{\partial r}\left(r^2 \rho u\right) = 0 \tag{3.1}$$

and Euler's momentum equation is

$$\frac{\partial u}{\partial t} + u\frac{\partial u}{\partial r} + \frac{1}{\rho}\frac{\partial p}{\partial r} = 0. \tag{3.2}$$

Here the variables are the same as in previous chapters, with ρ representing the total density, u the gas velocity and p the pressure, which is related to the density and temperature T by the gas law

$$p = \rho T. \tag{3.3}$$

The conservation of energy equation takes the form

$$\rho\frac{D}{Dt}\left(\frac{\gamma}{\gamma - 1}T + \frac{1}{2}u^2\right) - \frac{\partial p}{\partial t} = Q_T \tag{3.4}$$

where $\frac{D}{Dt} = \frac{\partial}{\partial t} + u\frac{\partial}{\partial r}$ is the material derivative, as in Batchelor [49, p.73]. Finally, the concentrations of X and A satisfy the equations

$$\frac{\partial X}{\partial t} + \frac{1}{r^2}\frac{\partial}{\partial r}\left(r^2 X u\right) = Q_X \tag{3.5}$$

and

$$\frac{\partial A}{\partial t} + \frac{1}{r^2}\frac{\partial}{\partial r}\left(r^2 A u\right) = Q_A. \tag{3.6}$$

In the three previous equations, Q_T, Q_X and Q_A are the source terms for T, X and A, respectively and will be discussed in more detail later. As they were in section 2.2 in chapter 2, these governing equations are based upon derivations given by Zel'dovich et al [6, p.238] and Liepmann and Roshko [37, p.337]. Equations (3.1) to (3.6) govern the behaviour of the gas in the region $0 \leqslant r < R_s(t)$. Outside the shock, in $r > R_s(t)$, the gas retains its background values:

$$\rho = 1; \quad u = 0; \quad T = \theta_a; \quad X = X_0; \quad A = A_0.$$

Here θ_a is the ambient temperature, X_0 is the background concentration of X and similarly for A_0. These equations, however, offer no information on the properties of the shock itself. In the next two sections we derive another set of equations governing the strength of the shock and the speed at which it propagates, by considering the conservation laws as they must hold across the shock boundary.

3.3 Weak solutions to PDEs in one spatial dimension

Before deriving the conservation conditions across the shock, we will introduce the concept of a weak solution to a partial differential equation. The method used will follow that given by Whitham [34, p.39] in a single spatial dimension, although Forbes and Krzysik have recently shown that this method can be extended to arbitrarily many dimensions [50]. A weak solution generalises the concept of a solution to a partial differential equation to one which holds even where derivatives may not necessarily exist. This will allow us to apply the conservation laws governing our system in the region of the shock, across which the spatial derivatives are undefined.

Consider the variable $V(x,t)$, which satisfies the partial differential equation

$$\frac{\partial V}{\partial t} + \frac{\partial F(V)}{\partial x} = C(x,t,V), \tag{3.7}$$

in some region $\mathcal{R}$ of space-time. In this equation x is a spatial coordinate, t is time, F is a continuous function of V, and C is a continuous function of x, t and V. Then $V(x,t)$ is a weak solution to (3.7) if it satisfies

$$\iint_{\mathcal{R}} V\frac{\partial \phi}{\partial t} + F(V)\frac{\partial \phi}{\partial x} + \phi C(x,t,V)\mathrm{d}x\mathrm{d}t = 0 \tag{3.8}$$

for an arbitrary differentiable function ϕ which vanishes on the boundary $\partial\mathcal{R}$ of the region $\mathcal{R}$. It can be shown that any solution to the integral equation (3.8) also satisfies the partial differential equation (3.7), provided the relevant derivatives exist. This brings us to the following theorem:

Theorem. *A solution $V(x,t)$ to the integral equation in* (3.8)*, where ϕ is an arbitrary differentiable function which vanishes on the boundary $\partial\mathcal{R}$ of*

the region $\mathcal{R}$, also satisfies the partial differential equation (3.7)*, provided all relevant derivatives exist.*

Proof. With a simple application of the product rule for differentiation we obtain

$$\begin{aligned}\iint_{\mathcal{R}} V\frac{\partial\phi}{\partial t} + F(V)\frac{\partial\phi}{\partial x} + \phi C(x,t,V)\mathrm{d}x\mathrm{d}t = \iint_{\mathcal{R}} \frac{\partial\phi V}{\partial t} + \frac{\partial\phi F(V)}{\partial x}\mathrm{d}x\mathrm{d}t \\ - \iint_{\mathcal{R}} \phi\left[\frac{\partial V}{\partial t} + \frac{\partial F(V)}{\partial x} - C(x,t,V)\right]\mathrm{d}x\mathrm{d}t.\end{aligned} \tag{3.9}$$

Applying Green's theorem in the plane to the first integral on the right-hand side of equation (3.9) gives

$$\iint_{\mathcal{R}} \left[\frac{\partial\phi V}{\partial t} + \frac{\partial\phi F(V)}{\partial x}\right]\mathrm{d}x\mathrm{d}t = \oint_{\partial\mathcal{R}} \phi\left[V\mathrm{d}x - F(V)\,\mathrm{d}t\right]$$

and since $\phi = 0$ on the boundary $\partial\mathcal{R}$, these integrals must vanish. As a result, equation (3.9) reduces to

$$\begin{aligned}\iint_{\mathcal{R}} V\frac{\partial\phi}{\partial t} + F(V)\frac{\partial\phi}{\partial x} + \phi C(x,t,V)\mathrm{d}x\mathrm{d}t = \\ - \iint_{\mathcal{R}} \phi\left[\frac{\partial V}{\partial t} + \frac{\partial F(V)}{\partial x} - C(x,t,V)\right]\mathrm{d}x\mathrm{d}t.\end{aligned}$$

Now, $V(x,t)$ is assumed to satisfy the integral equation (3.8), so we have

$$\iint_{\mathcal{R}} \phi\left[\frac{\partial V}{\partial t} + \frac{\partial F(V)}{\partial x} - C(x,t,V)\right]\mathrm{d}x\mathrm{d}t = 0.$$

Since ϕ is arbitrary, the result follows. □

The implication of this theorem is that the concept of a weak solution allows us to generalise the conservation laws in the presence of a shock, across

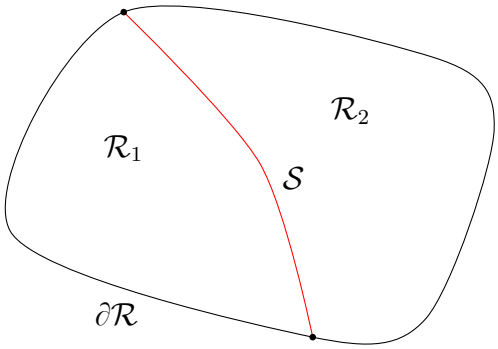

Figure 3.2: Schematic of a shock $\mathcal{S}$ through the region $\mathcal{R}$.

which the properties of the reacting gas experience a jump discontinuity.

We now consider a shock $\mathcal{S}$ passing through the region $\mathcal{R}$, dividing it into two non-overlapping regions $\mathcal{R}_1$ and $\mathcal{R}_2$, as in the diagram shown in figure 3.2. Following similar analysis to that outlined above, a weak solution to the partial differential equation (3.7) in the region $\mathcal{R}$ in the presence of the shock $\mathcal{S}$ satisfies

$$\begin{aligned} 0 &= \iint_{\mathcal{R}} V\frac{\partial\phi}{\partial t} + F(V)\frac{\partial\phi}{\partial x} + \phi C(x,t,V)\mathrm{d}x\mathrm{d}t \\ &= \oint_{\partial\mathcal{R}_1} \phi\left[V\mathrm{d}x - F(V)\,\mathrm{d}t\right] + \oint_{\partial\mathcal{R}_2} \phi\left[V\mathrm{d}x - F(V)\,\mathrm{d}t\right]. \end{aligned} \tag{3.10}$$

Again, as ϕ vanishes on the boundary $\partial\mathcal{R}$, all that remains of the integrals on the right-most side of equation (3.10) is the portion of the boundary integrals along the shock. Equation (3.10) thus reduces to

$$\int_{\mathcal{S}} \phi\left\{\left[F(V_2) - F(V_1)\right]\mathrm{d}t - \left[V_2 - V_1\right]\mathrm{d}x\right\} = 0 \tag{3.11}$$

wherein a subscript 1 or 2 indicates that a variable is evaluated on the side of the shock in region $\mathcal{R}_1$ or $\mathcal{R}_2$ respectively. As ϕ is arbitrary, it must be

that the quantity inside the braces in equation (3.11) is zero, and so, with a little simplification, we obtain the jump condition in its final form,

$$\frac{\mathrm{d}\chi}{\mathrm{d}t} = \frac{F(V_2) - F(V_1)}{V_2 - V_1}$$

where $\chi(t)$ is the spatial coordinate of the shock at time t.

3.4 Shock equations in one-dimensional spherical coordinates

In the previous section we introduced the concept of a weak solution to a partial differential equation, and showed that it allows the governing conservation equations to be generalised to regions in which the spatial derivatives are undefined, such as in the presence of a shock. In the following section we apply this method to our governing equations (3.1) to (3.6), and derive algebraic expressions for the value of the gas properties on the shock, as well as the speed of propagation of the shock front. Before deriving these conditions, the governing equations need to be written in conservative form so that they match the form of equation (3.7). It is well known that any differential equation may have multiple such conservative forms (see Whitham [34, p.40]), so it is important to ensure that each equation represents a physical quantity which is truly conserved. From the governing physics of the reaction problem, we know that each of the mass, momentum, energy and the amount of reagents A and X are conserved within any volume element. Thus the conserved quantities are ρ, ρu, $\rho\left(\frac{\gamma T}{\gamma-1} + \frac{1}{2}u^2\right)$, X and A, which thus satisfy

the conservative equations:

$$\frac{\partial \rho}{\partial t} + \frac{\partial}{\partial r}(\rho u) = -\frac{2\rho u^2}{r} \tag{3.12}$$

$$\frac{\partial}{\partial t}(\rho u) + \frac{\partial}{\partial r}\left[\rho\left(u^2 + T\right)\right] = -\frac{2\rho u^2}{r} \tag{3.13}$$

$$\frac{\partial}{\partial t}(\rho E) + \frac{\partial}{\partial r}(\rho u H) = Q_T - \frac{2\rho u H}{r} \tag{3.14}$$

$$\frac{\partial X}{\partial t} + \frac{\partial}{\partial r}(X u) = Q_X - \frac{2X u^2}{r} \tag{3.15}$$

$$\frac{\partial A}{\partial t} + \frac{\partial}{\partial r}(A u) = Q_A - \frac{2A u^2}{r}. \tag{3.16}$$

Here we have defined the specific energy $E = \frac{T}{\gamma - 1} + \frac{1}{2}u^2$ and specific enthalpy $H = \frac{\gamma T}{\gamma - 1} + \frac{1}{2}u^2$, for simplicity. Making use of the method given in section (3.3), we may now derive the shock conditions. Using a subscript s to indicate a value evaluated just inside the shock, and defining $R_s(t)$ to be the radial position of the shock front at time t, the jump conditions may now be written

$$(\rho_s - 1)\frac{\mathrm{d}R_s}{\mathrm{d}t} = \rho_s u_s \tag{3.17}$$

$$\rho_s u_s \frac{\mathrm{d}R_s}{\mathrm{d}t} = \rho_s\left(T_s + u_s^2\right) - \theta_a \tag{3.18}$$

$$\left(\rho_s E_s - \frac{\theta_a}{\gamma - 1}\right)\frac{\mathrm{d}R_s}{\mathrm{d}t} = \rho_s u_s H_s \tag{3.19}$$

$$(X_s - X_0)\frac{\mathrm{d}R_s}{\mathrm{d}t} = X_s u_s \tag{3.20}$$

$$(A_s - A_0)\frac{\mathrm{d}R_s}{\mathrm{d}t} = A_s u_s \tag{3.21}$$

in which $E_s = \frac{T_s}{\gamma - 1} + \frac{1}{2}u_s^2$ and $H_s = \frac{\gamma T_s}{\gamma - 1} + \frac{1}{2}u_s^2$.

The jump conditions (3.17) - (3.19) are equivalent to those given in the seminal text by Courant and Friedrichs [51, p.124], and conditions (3.20) and (3.21) are new, but analogous to (3.17). As this is a system of five equations in the six unknowns ρ_s, u_s, T_s, X_s, A_s and $\frac{\mathrm{d}R_s}{dt}$, all but one variable may be

eliminated such that five variables are expressed in terms of the sixth. It is of some use to write each of the other variables in terms of the shock speed $R_s'(t)$, in which case equations (3.17) - (3.21) become

$$\rho_s = \frac{(\gamma+1)(R_s')^2}{2\gamma\theta_a + (\gamma-1)(R_s')^2} \tag{3.22}$$

$$u_s = \frac{2\left[(R_s')^2 - \gamma\theta_a\right]}{(\gamma+1)R_s'} \tag{3.23}$$

$$T_s = \frac{\left[2(R_s')^2 - \theta_a(\gamma-1)\right]\left[(\gamma-1)(R_s')^2 + 2\gamma\theta_a\right]}{(\gamma+1)^2(R_s')^2} \tag{3.24}$$

$$X_s = \frac{X_0(\gamma+1)(R_s')^2}{2\gamma\theta_a + (\gamma-1)(R_s')^2} \tag{3.25}$$

$$A_s = \frac{A_0(\gamma+1)(R_s')^2}{2\gamma\theta_a + (\gamma-1)(R_s')^2} \tag{3.26}$$

where a prime is used to represent differentiation with respect to time. It is interesting to reconsider equation (3.22), written in the form

$$\rho_s = \frac{\gamma+1}{\gamma-1}\left[1 - \frac{2\gamma\theta_a}{2\gamma\theta_a + (\gamma-1)(R_s')^2}\right] < \frac{\gamma+1}{\gamma-1}.$$

We may interpret this as saying that, regardless of the shock strength, the gas density just behind the shock face is bounded by $\frac{\gamma+1}{\gamma-1}$. It is also of interest to rewrite equation (3.22), and solve for R_s' in terms of ρ_s, yielding

$$R_s' = \pm\sqrt{\frac{2\gamma\theta_a\rho_s}{\gamma+1-(\gamma-1)\rho_s}}. \tag{3.27}$$

Note that the expression on the right will not switch sign for $\rho_s > 0$ and so the direction of propagation of the shock will not change. While we may take either the positive value of equation (3.27) in the case of the outwards-moving shock, or the negative for an inwards-moving one, we will limit our

interest to just the positive case. It follows, based on an argument presented by Whitham [34, p.175], that such a wave must be compressive and that all of the relevant gas properties must decrease as we move from a position behind the shock to one in front of it. Thus we must have

$$\rho_s > 1; \quad u_s > 0; \quad T_s > \theta_a; \quad X_s > X_0; \quad A_s > A_0.$$

Taking $\rho_s > 1$ in equation (3.27), we also have the inequality

$$\begin{aligned} R_s' &= \sqrt{\frac{2\gamma\theta_a\rho_s}{\gamma+1-(\gamma-1)\,\rho_s}} \\ &> \sqrt{\frac{2\gamma\theta_a}{\gamma+1-(\gamma-1)}} \\ &= \sqrt{\gamma\theta_a}. \end{aligned}$$

As $\sqrt{\gamma\theta_a}$ is the speed of sound in the undisturbed gas, the shock must be supersonic when viewed from ahead.

3.5 Solution Approach

In this section we outline a method of solving the system of partial differential equations (3.1) - (3.6) in the region behind the shock, subject to the five jump conditions (3.22)-(3.26) on the shock $r = R_s(t)$. We will then present some preliminary results of the application of this method, followed by a discussion of these results. It is useful first to project the problem to a frame in which the shock is stationary, by making the change of variables

$$\xi = \frac{r}{R_s(t)}$$

so that the shock is always at $\xi = 1$. Radial derivatives may now be replaced by a derivative with respect to the new variable ξ, using the chain rule

$$\frac{\partial \bullet}{\partial r} = \frac{1}{R_s}\frac{\partial \bullet}{\partial \xi}$$

and the temporal derivative becomes

$$\left.\frac{\partial \bullet}{\partial t}\right|_r = \left.\frac{\partial \bullet}{\partial t}\right|_\xi - \xi\left(\frac{R_s'}{R_s}\right)\left.\frac{\partial \bullet}{\partial \xi}\right|_t . \tag{3.28}$$

In an attempt to avoid confusion due to the ambiguity in the temporal derivatives, a subscript has been used in equation (3.28) to indicate the variable being held constant in each derivative. For the remainder of this chapter, all derivatives with respect to t will be assumed to hold ξ constant, unless otherwise stated. With some minor algebra the governing equations in the new $\xi - t$ space become

$$\frac{\partial \rho}{\partial t} + \frac{1}{R_s}\left[(u - \xi R_s')\frac{\partial \rho}{\partial \xi} + \frac{\rho}{\xi^2}\frac{\partial}{\partial \xi}\left(\xi^2 u\right)\right] = 0 \tag{3.29}$$

$$\frac{\partial u}{\partial t} + \frac{1}{R_s}\left[(u - \xi R_s')\frac{\partial u}{\partial \xi} + \frac{1}{\rho}\frac{\partial p}{\partial \xi}\right] = 0 \tag{3.30}$$

$$\frac{\partial T}{\partial t} + \frac{1}{R_s}\left[(u - \xi R_s')\frac{\partial T}{\partial \xi} + (\gamma - 1)\frac{T}{\xi^2}\frac{\partial}{\partial \xi}\left(\xi^2 u\right)\right] = \frac{(\gamma - 1)}{\rho}Q_T \tag{3.31}$$

$$\frac{\partial X}{\partial t} + \frac{1}{R_s}\left[(u - \xi R_s')\frac{\partial X}{\partial \xi} + \frac{X}{\xi^2}\frac{\partial}{\partial \xi}\left(\xi^2 u\right)\right] = Q_X \tag{3.32}$$

$$\frac{\partial A}{\partial t} + \frac{1}{R_s}\left[(u - \xi R_s')\frac{\partial A}{\partial \xi} + \frac{A}{\xi^2}\frac{\partial}{\partial \xi}\left(\xi^2 u\right)\right] = Q_A. \tag{3.33}$$

Equation (3.31) is the result of some heavier simplification, using equations (3.1) and (3.2) to remove time derivatives of ρ and u from equation (3.4) before making the transformation from r to ξ. The source terms Q_T, Q_X

and Q_A are each given by the expressions

$$\begin{aligned} Q_T &= qAk_0(T) + Xk_1(T) \\ Q_X &= Ak_0(T) - Xk_1(T) \\ Q_A &= -Ak_0(T) \end{aligned}$$

where q is a dimensionless parameter given by the ratio of formation enthalpies of A and X, as in previous chapters. The quantities $k_0(T)$ and $k_1(T)$ are the temperature dependent reaction rates for the respective steps of the reaction scheme (1), which are assumed to be given by

$$\begin{aligned} k_0(T) &= \begin{cases} \zeta \exp\left(\dfrac{-\epsilon}{T-\theta_a}\right), & \text{if } T > \theta_a \\ 0, & \text{if } T \leqslant \theta_a \end{cases} \\ k_1(T) &= \begin{cases} \exp\left(\dfrac{-1}{T-\theta_a}\right), & \text{if } T > \theta_a \\ 0, & \text{if } T \leqslant \theta_a \end{cases} \end{aligned} \tag{3.34}$$

The parameters ζ and ϵ are dimensionless numbers expressing the ratio of pre-multiplying factors and activation energies respectively. These expressions have many of the desirable properties of the reaction rates in (1.12) in chapter 1 and (2.14) chapter 2. Most notably, they avoid the cold-boundary problem and are zero below the "ignition temperature", which has been chosen to be equal to the ambient temperature, θ_a, for convenience. However, these expressions are also infinitely differentiable at $T = \theta_a$, which is not true of the forms discussed in the previous chapter.

Solutions to the governing equations (3.29) - (3.33) are sought in the form

$$\rho(\xi,t) = \rho_s(t) + \sum_{m=1}^{\infty} \mathcal{A}_m(t)\, j_0(m\pi\xi) \tag{3.35}$$

$$u(\xi,t) = \xi u_s(t) + \sum_{m=1}^{\infty} \mathcal{B}_m(t)\, j_1(\alpha_m\xi) \tag{3.36}$$

$$T(\xi,t) = T_s(t) + \sum_{m=1}^{\infty} \mathcal{C}_m(t)\, j_0(m\pi\xi) \tag{3.37}$$

$$X(\xi,t) = X_s(t) + \sum_{m=1}^{\infty} \mathcal{D}_m(t)\, j_0(m\pi\xi) \tag{3.38}$$

$$A(\xi,t) = A_s(t) + \sum_{m=1}^{\infty} \mathcal{E}_m(t)\, j_0(m\pi\xi), \tag{3.39}$$

where ρ_s, u_s and so on are the values at the shock $\xi = 1$. For the numerical scheme, it will be necessary to truncate these series, and the infinite bound will be replaced with a suitably-large finite value denoted M.

The functions j_0 and j_1 are, respectively, the zeroth- and first-order spherical Bessel function of the first kind, as were used in the linear solutions in chapter 2 and may be written rather simply as

$$j_0(z) = \frac{\sin(z)}{z} \tag{3.40}$$

and

$$j_1(z) = \frac{\sin(z)}{z^2} - \frac{\cos(z)}{z}. \tag{3.41}$$

The parameter α_m is the m^{th} positive root of j_1, of which there are infinitely many, and will need to be found numerically. Note that, when m is an integer,

$$j_1\left[\frac{(2m-1)\,\pi}{2}\right] = (-1)^{m+1}\left[\frac{2}{(2m-1)\,\pi}\right]^2$$

so it is clear j_1 is continuous and changes sign in the interval

$$\left(\frac{(2m-1)\,\pi}{2}, \frac{(2m+1)\,\pi}{2}\right),$$

and thus there exists at least one root within this range. To see that there is exactly one root in this interval, consider the function

$$f(z) = \frac{z^2 j_1(z)}{\cos(z)} = \tan(z) - z.$$

Then the non-zero roots of f are exactly the roots of j_1, and its derivative satisfies

$$\begin{aligned} f'(z) &= \sec^2(z) - 1 \\ &= \tan^2(z) \\ &\geqslant 0. \end{aligned}$$

It follows that $f(z)$ is increasing, and so there is at most one root in every interval over which it is continuous. As f is discontinuous at each half-integer multiple of π, and continuous elsewhere, we conclude that $j_1(z)$ has exactly one root in every interval $\left(\frac{(2m-1)\pi}{2}, \frac{(2m+1)\pi}{2}\right)$, where m is an integer. The roots can thus be reliably found to high accuracy with a bracketing numerical scheme such as the bisection method.

As an aside, it is also interesting to explore the asymptotic behaviour of the roots α_m. From the definition of α_m, we know that it satisfies the equation

$$j_1(\alpha_m) = \frac{\sin(\alpha_m)}{\alpha_m^2} - \frac{\cos(\alpha_m)}{\alpha_m} = 0. \tag{3.42}$$

For large values of m (and thus large values of α_m), the sine term will decrease in magnitude faster than the cosine term and equation (3.42) becomes

$$\frac{\cos(\alpha_m)}{\alpha_m} \sim 0.$$

It follows then that α_m behaves like the roots of cosine, and we must have

$$\alpha_m \sim \frac{(2m+1)\,\pi}{2}. \tag{3.43}$$

Seeking solutions in the form of (3.35) - (3.39) effectively builds the shock value into the solution, as they clearly satisfy the conditions

$$\rho\,(1,t) = \rho_s\,(t)\,; \quad u\,(1,t) = u_s\,(t)$$

etc. by design. The series solutions also have the advantage that the spatial derivatives may be written (in principle, at least) in closed form, since

$$j_0'\,(z) = -j_1\,(z) \tag{3.44}$$

$$\frac{1}{z^2}\frac{\mathrm{d}}{\mathrm{d}z}\left[z^2 j_1\,(z)\right] = j_0\,(z) \tag{3.45}$$

as can be verified from the relations in (3.40) and (3.41). The derivative of j_1 is not as straightforward as these, but can still be written as a rational combination of trigonometric functions in the form

$$\begin{aligned} j_1'\,(z) &= \frac{\sin\,(z)}{z} + \frac{2\cos\,(z)}{z^2} - \frac{2\sin\,(z)}{z^3} \\ &= j_0\,(z) - \frac{2j_1\,(z)}{z}. \end{aligned} \tag{3.46}$$

The sets of spherical Bessel functions $j_0\,(m\pi\xi)$ and $j_1\,(\alpha_m\xi)$ form orthogonal bases with respect to the weight function ξ^2 over the interval $[0,\ 1]$.
Making use of the trigonometric expressions for j_0 and j_1 in (3.40) and (3.41), as well as some trigonometric identities yields to following orthogonality expressions:

$$\int_0^1 \xi^2 j_0\,(m\pi\xi)\, j_0\,(n\pi\xi)\,\mathrm{d}\xi = \delta_{mn} \tag{3.47}$$

and

$$\int_0^1 \xi^2 j_1(\alpha_m \xi)\, j_1(\alpha_m \xi)\, \mathrm{d}\xi = \delta_{mn}. \tag{3.48}$$

Here δ_{mn} is the Krönecker symbol, taking the value 1 when $m = n$ and 0 when $m \neq n$. Full derivations of the orthogonality equations (3.47) and (3.48) are included in the appendix to this chapter, in section 3.10.

Using the orthogonality conditions in equations (3.47) and (3.48) allows us to find the coefficients $\mathcal{A}_m(t)$, $\mathcal{B}_m(t)$ etc. in equations (3.35) - (3.39), such that

$$\begin{aligned} \mathcal{A}_m(t) &= 2m^2\pi^2 \int_0^1 \xi^2 (\rho - \rho_s)\, j_0(m\pi\xi)\, \mathrm{d}\xi \\ &= 2m\pi \int_0^1 \xi (\rho - \rho_s) \sin(m\pi\xi)\, \mathrm{d}\xi \end{aligned} \tag{3.49}$$

and similarly for $\mathcal{C}_m(t)$, $\mathcal{D}_m(t)$ and $\mathcal{E}_m(t)$. In much the same way, we can find the coefficients $\mathcal{B}_m(t)$ with

$$\begin{aligned} \mathcal{B}_m(t) &= \frac{2\alpha_m^2}{\sin^2(\alpha_m)} \int_0^1 \xi^2 (u - \xi u_s)\, j_1(\alpha_m \xi)\, \mathrm{d}\xi \\ &= \frac{2}{\sin^2(\alpha_m)} \int_0^1 (u - \xi u_s) \left[\sin(\alpha_m \xi) - \alpha_m \xi \cos(\alpha_m \xi)\right] \mathrm{d}\xi \end{aligned} \tag{3.50}$$

With all of the coefficients and shock values known at the current time step, we can also calculate the spatial derivatives, with

$$\frac{\partial \rho}{\partial \xi} = -\pi \sum_{m=1}^{M} m \mathcal{A}_m(t)\, j_1(m\pi\xi)$$

and a similar form for the derivatives of T, X and A. For the gas velocity u we have

$$\frac{\partial u}{\partial \xi} = u_s(t) + \sum_{m=1}^{M} \alpha_m \mathcal{B}_m(t)\, j_1'(\alpha_m \xi)$$

where the derivative $j_1'(\alpha_m \xi)$ is as given in (3.46). Then, evaluating the conservation of mass equation (3.1) using the series form (3.35) for the density

to simplify the temporal derivative, gives a differential equation for ρ_s:

$$\frac{\mathrm{d}\rho_s}{\mathrm{d}t} + \sum_{m=1}^{M} \mathcal{A}'_m(t)\, j_0(m\pi\xi) = \frac{1}{R_s}\left[(\xi R'_s - u)\frac{\partial\rho}{\partial\xi} - \frac{\rho}{\xi^2}\frac{\partial}{\partial\xi}\left(\xi^2 u\right)\right]. \quad (3.51)$$

Evaluating this equation as $\xi \to 1^-$ and using the series form to evaluate the spatial derivatives of ρ and u gives an equation for the time derivative of just the shock value:

$$\frac{\mathrm{d}\rho_s}{\mathrm{d}t} = \frac{1}{R_s}\sum_{m=1}^{M}\left[(u_s - R'_s)\, m\pi\mathcal{A}_m(t)\, j_1(m\pi) - \rho_s\alpha_m\mathcal{B}_m(t)\, j_0(\alpha_m)\right]. \quad (3.52)$$

This may be simplified somewhat by recalling the alternate form for j_0 and j_1, as in (3.40) and (3.41), so that we have

$$j_1(m\pi) = \frac{\sin(m\pi)}{m^2\pi^2} - \frac{\cos(m\pi)}{m\pi} = -\frac{(-1)^m}{m\pi}$$

and also

$$j_0(\alpha_m) = \frac{\sin(\alpha_m)}{\alpha_m}.$$

Then with a little simplification we have finally

$$\frac{\mathrm{d}\rho_s}{\mathrm{d}t} = \frac{1}{R_s}\sum_{m=1}^{M}\left[(-1)^m(R'_s - u_s)\,\mathcal{A}_m(t) - \rho_s\sin(\alpha_m)\,\mathcal{B}_m(t)\right].$$

There is no immediate reason as to why this method could not be applied to find $u'_s(t)$, $T'_s(t)$, $X'_s(t)$ or $A'_s(t)$, other than the fact that we need to ensure that the jump conditions (3.22)-(3.26) are satisfied. To that end, it is actually useful to rewrite the four latter of these equations in terms of ρ_s,

such that

$$u_s(t) = (\rho_s - 1)\sqrt{\frac{2\gamma\theta_a}{\rho_s\left[\gamma + 1 - (\gamma - 1)\rho_s\right]}} \tag{3.53}$$

$$T_s(t) = \frac{\theta_a}{\rho_s}\left[\frac{1 - \gamma + (\gamma + 1)\rho_s}{\gamma + 1 - (\gamma - 1)\rho_s}\right] \tag{3.54}$$

$$X_s(t) = X_0\rho_s \tag{3.55}$$

$$A_s(t) = A_0\rho_s. \tag{3.56}$$

The time derivatives u_s', T_s', X_s' and A_s' may then be found by applying the chain rule for differentiation to equations (3.53) - (3.56), so that with a little algebra we have

$$\begin{aligned}\frac{\mathrm{d}u_s}{\mathrm{d}t} &= \frac{\mathrm{d}u_s}{\mathrm{d}\rho_s}\frac{\mathrm{d}\rho_s}{\mathrm{d}t} \\ &= \sqrt{\frac{\gamma\theta_a}{2}}\frac{1 + \gamma + (3 - \gamma)\rho_s}{\left\{\rho_s\left[\gamma + 1 - (\gamma - 1)\rho_s\right]\right\}^{3/2}}\frac{d\rho_s}{dt}\end{aligned} \tag{3.57}$$

and by a similar method we find an expression for T_s'

$$\frac{\mathrm{d}T_s}{\mathrm{d}t} = \frac{\theta_a(\gamma - 1)\left[(\gamma + 1)\rho_s^2 - 2(\gamma - 1)\rho_s + \gamma + 1\right]}{\rho_s^2\left[(\gamma - 1)\rho_s - (\gamma + 1)\right]^2}\frac{\mathrm{d}\rho_s}{\mathrm{d}t}. \tag{3.58}$$

Finally, for the concentration of the two reagents, we have the much simpler results

$$X_s'(t) = X_0\frac{\mathrm{d}\rho_s}{\mathrm{d}t}$$

$$A_s'(t) = A_0\frac{\mathrm{d}\rho_s}{\mathrm{d}t},$$

with the intention to solve for ρ_s' at the current time and use the above equations to find u_s', T_s', X_s' and A_s'. Now that we know all of the coefficients $\mathcal{A}_m$, $\mathcal{B}_m$, $\mathcal{C}_m$, $\mathcal{D}_m$ and $\mathcal{E}_m$, as well as the shock values ρ_s, u_s, T_s, X_s, A_s and their time derivatives, we can then solve for the derivatives of the coefficients.

Rearranging equation (3.51) gives

$$\sum_{m=1}^{M} \mathcal{A}'_m(t)\, j_0(m\pi\xi) = \frac{1}{R_s}\left[(\xi R'_s - u)\frac{\partial \rho}{\partial \xi} - \frac{\rho}{\xi^2}\frac{\partial}{\partial \xi}\left(\xi^2 u\right)\right] - \frac{\mathrm{d}\rho_s}{\mathrm{d}t}.$$

The orthogonality condition (3.47) allows for the isolation of $\mathcal{A}'_m(t)$ in the form

$$\mathcal{A}'_m(t) = 2m\pi \int_0^1 \xi I_\rho \sin(m\pi\xi)\,\mathrm{d}\xi$$

wherein we have defined the term I_ρ in the integrand to be

$$I_\rho = \frac{1}{R_s}\left[(\xi R'_s - u)\frac{\partial \rho}{\partial \xi} - \frac{\rho}{\xi^2}\frac{\partial}{\partial x}\left(\xi^2 u\right)\right] - \frac{\mathrm{d}\rho_s}{\mathrm{d}t}. \tag{3.59}$$

Similarly, writing

$$I_u = \frac{1}{R_s}\left[(\xi R'_s - u)\frac{\partial u}{\partial \xi} - \frac{T}{\rho}\frac{\partial \rho}{\partial \xi} - \frac{\partial T}{\partial \xi}\right] - \xi\frac{\mathrm{d}u_s}{\mathrm{d}t} \tag{3.60}$$

$$I_T = \frac{1}{R_s}\left[(\xi R'_s - u)\frac{\partial T}{\partial \xi} - (\gamma - 1)\frac{T}{\xi^2}\frac{\partial}{\partial \xi}\left(\xi^2 u\right)\right] + \frac{(\gamma - 1)}{\rho}Q_T - \frac{\mathrm{d}T_s}{\mathrm{d}t} \tag{3.61}$$

$$I_X = \frac{1}{R_s}\left[(\xi R'_s - u)\frac{\partial X}{\partial \xi} - \frac{X}{\xi^2}\frac{\partial}{\partial \xi}\left(\xi^2 u\right)\right] + Q_X - \frac{\mathrm{d}X_s}{\mathrm{d}t} \tag{3.62}$$

$$I_A = \frac{1}{R_s}\left[(\xi R'_s - u)\frac{\partial A}{\partial \xi} - \frac{A}{\xi^2}\frac{\partial}{\partial \xi}\left(\xi^2 u\right)\right] + Q_A - \frac{\mathrm{d}A_s}{\mathrm{d}t} \tag{3.63}$$

we find the time derivatives for the remaining coefficients:

$$\mathcal{B}'_m(t) = \frac{2}{\sin^2(\alpha_m)}\int_0^1 I_u\left[\sin(\alpha_m\xi) - \alpha_m\xi\cos(\alpha_m\xi)\right]\mathrm{d}\xi \tag{3.64}$$

$$\mathcal{C}'_m(t) = 2m\pi\int_0^1 \xi I_T \sin(m\pi\xi)\,\mathrm{d}\xi \tag{3.65}$$

$$\mathcal{D}'_m(t) = 2m\pi\int_0^1 \xi I_X \sin(m\pi\xi)\,\mathrm{d}\xi \tag{3.66}$$

$$\mathcal{E}'_m(t) = 2m\pi\int_0^1 \xi I_A \sin(m\pi\xi)\,\mathrm{d}\xi. \tag{3.67}$$

In producing the figures to be shown in sections 3.7 and 3.8, these spatial integrals are approximated quickly and accurately using von Winckel's Gauss-Legendre quadrature routine [48]. With the help of an appropriate numerical integrator, this system of equations may be integrated forwards in time to find each of the spectral coefficients, the value of the gas properties on the shock, and the position of the shock at a new time step.

3.6 Consistency conditions on spatial derivatives approaching the shock

There is no guarantee, given the current construction of the solution method, that the value found for, say, u_s' using equation (3.60) matches the value we would expect to get from evaluating equation (3.30) as $\xi \to 1^-$ using the series form in (3.36), and there is a need to enforce a consistency condition so that the two do agree. The result is that, at least when deciding on the initial conditions of our system, we are not necessarily free to pick every aspect of the initial reaction profile, and will need to ensure the behaviour driven by the governing partial differential equations is consistent with that predicted by the shock conditions. In other words, we need to ensure that

$$\begin{aligned} &\sqrt{\frac{\gamma\theta_a}{2}} \frac{1+\gamma+(3-\gamma)\,\rho_s}{\{\rho_s\left[\gamma+1-(\gamma-1)\,\rho_s\right]\}^{3/2}} \frac{\mathrm{d}\rho_s}{\mathrm{d}t} \\ &= \frac{\mathrm{d}u_s}{\mathrm{d}t} \\ &= \lim_{\xi\to 1^-} \frac{1}{R_s}\left[(R_s'-u)\,\frac{\partial u}{\partial \xi} - \frac{T}{\rho}\frac{\partial \rho}{\partial \xi} - \frac{\partial T}{\partial \xi}\right] \end{aligned} \tag{3.68}$$

where the first equality comes from equation (3.57) and the second from the evaluation of (3.30) as $\xi \to 1^-$. This is effectively a linear equation in the quantities $\frac{\mathrm{d}\rho_s}{\mathrm{d}t}$, $\left.\frac{\partial \rho}{\partial \xi}\right|_{\xi\to 1^-}$, $\left.\frac{\partial u}{\partial \xi}\right|_{\xi\to 1^-}$ and $\left.\frac{\partial T}{\partial \xi}\right|_{\xi\to 1^-}$. This process may be repeated for the temperature, using equations (3.31) and (3.58), giving

$$\begin{aligned}
&\frac{\theta_a\left(\gamma-1\right)\left[\left(\gamma+1\right)\rho_s^2-2\left(\gamma-1\right)\rho_s+\gamma+1\right]}{\rho_s^2\left[\left(\gamma-1\right)\rho_s-\left(\gamma+1\right)\right]^2}\frac{\mathrm{d}\rho_s}{\mathrm{d}t}\\
&=\frac{\mathrm{d}T_s}{\mathrm{d}t}\\
&=\frac{1}{R_s}\left[\left(R_s'-u\right)\frac{\partial T}{\partial \xi}-\left(\gamma-1\right)T\frac{\partial u}{\partial \xi}-2\left(\gamma-1\right)T_s u_s\right]_{\xi\to 1^-}\\
&\quad+\frac{\left(\gamma-1\right)}{\rho_s}Q_{Ts}.
\end{aligned} \tag{3.69}$$

Evaluating equation (3.51) as $\xi \to 1^-$ and combining it with (3.68) and (3.69) gives a system of three equations for the four quantities $\frac{\mathrm{d}\rho_s}{\mathrm{d}t}$, $\left.\frac{\partial \rho}{\partial \xi}\right|_{\xi\to 1^-}$, $\left.\frac{\partial u}{\partial \xi}\right|_{\xi\to 1^-}$ and $\left.\frac{\partial T}{\partial \xi}\right|_{\xi\to 1^-}$. Thus we are free to set any one of these values in the initial condition, but the other three must satisfy this system of equations. For the sake of argument, it will be assumed that we will choose a value for $\left.\frac{\partial \rho}{\partial \xi}\right|_{\xi\to 1^-}$. Rearranging equations (3.51), (3.68) and (3.69) gives the matrix equation

$$\begin{aligned}
&\begin{bmatrix} R_s & \rho_s & 0\\ \rho_s R_s\frac{\mathrm{d}u_s}{\mathrm{d}\rho_s} & \rho_s\left(u_s-R_s'\right) & \rho_s\\ \rho_s R_s\frac{\mathrm{d}T_s}{\mathrm{d}\rho_s} & \left(\gamma-1\right)\rho_s T_s & \rho_s\left(u_s-R_s'\right)\end{bmatrix}\begin{bmatrix}\frac{\mathrm{d}\rho_s}{\mathrm{d}t}\\ \left.\frac{\partial u}{\partial \xi}\right|_{\xi\to 1^-}\\ \left.\frac{\partial T}{\partial \xi}\right|_{\xi\to 1^-}\end{bmatrix}\\
&\qquad=\begin{bmatrix}-2\rho_s u_s\\ T_s\left.\frac{\partial \rho}{\partial \xi}\right|_{\xi\to 1^-}\\ \left(\gamma-1\right)R_s Q_{Ts}-2\left(\gamma-1\right)T_s u_s\end{bmatrix}
\end{aligned}$$

which we may solve to find $\left.\frac{\partial u}{\partial \xi}\right|_{\xi\to 1^-}$ and $\left.\frac{\partial T}{\partial \xi}\right|_{\xi\to 1^-}$. Finally, evaluating equations (3.32) and (3.33) as $\xi \to 1^-$, and rearranging to solve for the appropriate

derivatives yields

$$\left.\frac{\partial X}{\partial \xi}\right|_{\xi\to 1^-} = \frac{R_s\left(Q_X - \frac{\mathrm{d}X_s}{\mathrm{d}t}\right) - X_s\left(\left.\frac{\partial u}{\partial \xi}\right|_{\xi\to 1^-} - 2u_s\right)}{u_s - R_s'}$$

and similarly for $\left.\frac{\partial A}{\partial \xi}\right|_{\xi\to 1^-}$.

3.7 Numerical Results

In the following pages we employ the method outlined in section 3.5 to model the behaviour of a reacting gas in the presence of a jump discontinuity on a selection of system parameters. For the first set of figures, the reaction parameters are chosen to be

$$\zeta = 1.25 \quad ; \quad \epsilon = 0.25 \quad ; \quad q = 1.5 \quad ; \quad \theta_a = 0.5 \quad ; \quad \gamma = 1.4$$

and with background concentrations of A and X

$$A_e = 2 \quad ; \quad X_e = 2.$$

The initial density profile is of the form

$$\rho\left(\xi, 0\right) = \rho_s\left(0\right) + a_\rho\left(\xi^2 - 1\right) + b_\rho\left(\xi^4 - 1\right),$$

wherein the coefficients a_ρ and b_ρ are constants to be chosen later. An initial condition of this form gives two degrees of freedom and, by carefully choosing the polynomial coefficients, we are able to set the density at the origin $\rho\left(0, 0\right)$. More importantly, we may also choose the spatial-derivative of the density as $\xi \to 1^-$, as per the discussion in section (3.6). The initial spectral coefficients

$\mathcal{A}_m(0)$ can then be found in closed form, by evaluating the integrals in (3.49). With a little algebra we obtain

$$\mathcal{A}_m(0) = \frac{(-1)^m}{m^2\pi^2}\left[12a_\rho + 40\left(1 - \frac{6}{m^2\pi^2}\right)b_\rho\right].$$

Similarly, we assume the velocity has an initial profile of the form

$$u(\xi, 0) = u_s(0)\,\xi + a_u\left(\xi^3 - \xi\right)$$

wherein a_u is a constant to be chosen later. Choosing such an initial condition ensures that the velocity is zero at the origin (consistent with Wood and Kirkwood [52]), that it attains the shock value u_s at $\xi = 1$ and that it has an extra degree of freedom so that we may ensure it has the correct spatial derivative as $\xi \to 1^-$. Then, evaluating the integral in equation (3.50) with $t = 0$ gives

$$\mathcal{B}_m(0) = \frac{20}{\alpha_m^2\ \sin(\alpha_m)}a_u.$$

Figure (3.3) displays the temperature as found by the numerical scheme in these conditions at times $t = 0$ to $t = 50$. Interestingly the profile flattens in the middle as time progresses, but forms a steep drop as it nears $\xi = 1$. Figure (3.4) displays the coefficients $\mathcal{C}_m$ in the spectral expansion of T at the same time steps. It's interesting to note that at first, only the coefficients corresponding to the lower-frequency modes are noticeably larger than zero, but the higher-frequency modes grow quickly thereafter. Figure (3.5) shows the shock speed produced by the scheme. The speed decreases slightly at first, before increasing quickly and continuing to accelerate at least until time $t = 50$. As such, the shock radius, as seen in figure (3.6) grows quickly from 20 units at the start, to more than 80 units at time $t = 50$.

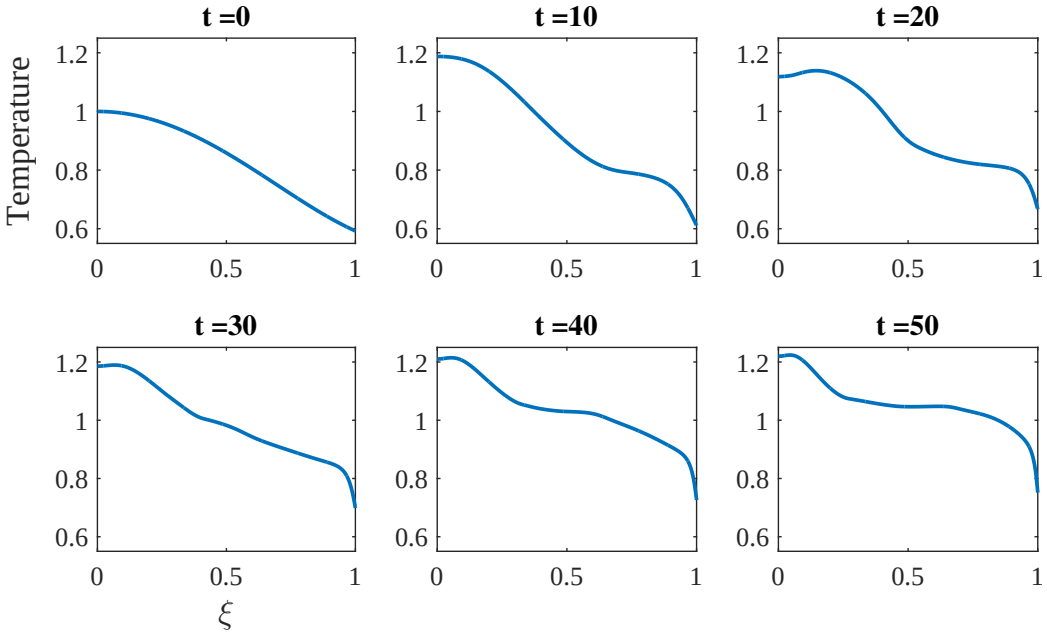

Figure 3.3: Temperature profile behind shock at regular intervals between $t = 0$ and $t = 50$, for the system parameters given in the text. Over this time frame, the shock temperature increases from about 0.59 to 0.75.

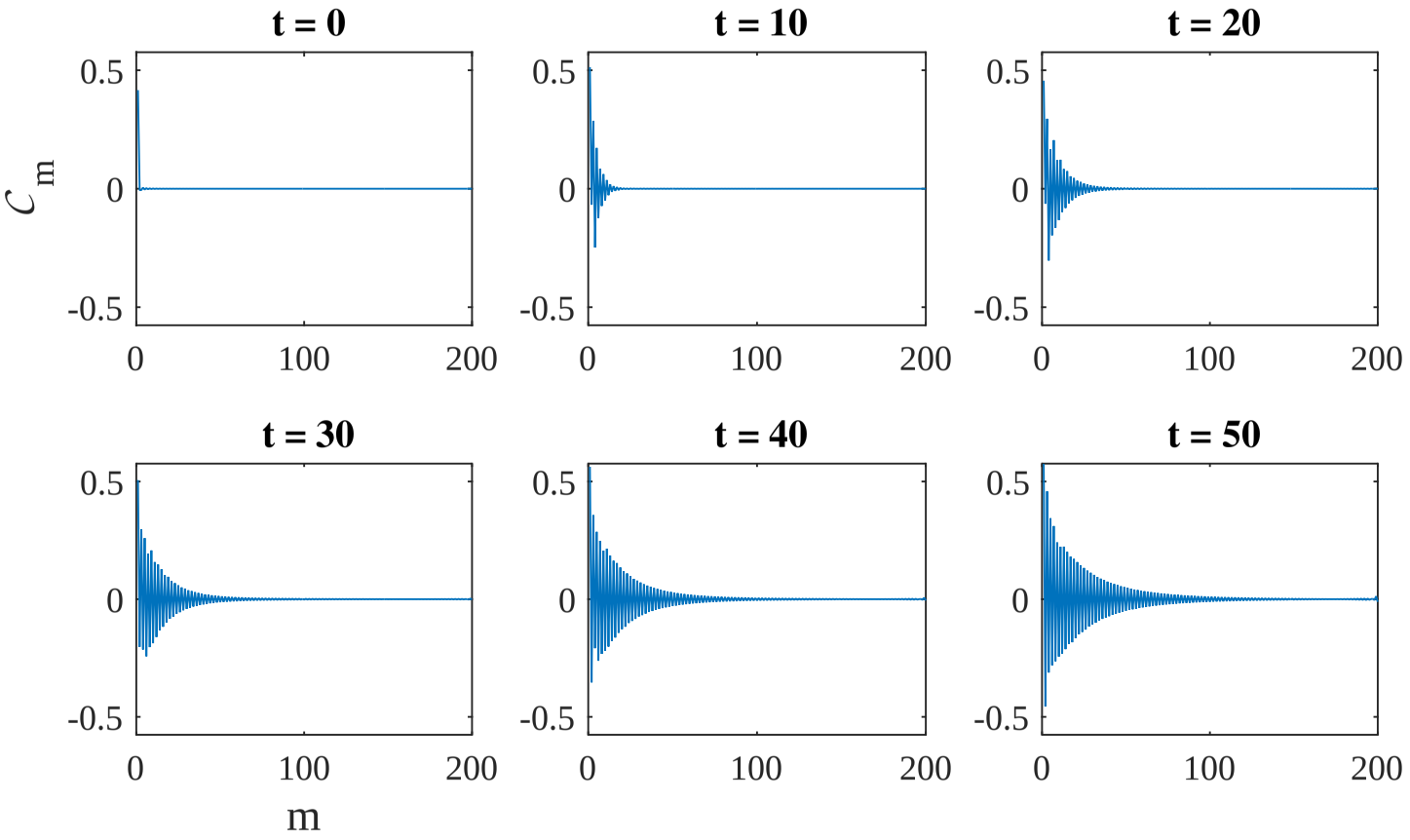

Figure 3.4: Spectral coefficients, $\mathcal{C}_m$, in the spherical-Bessel series expansion of the gas temperature behind the shock the same parameters as figure (3.3). In each snapshot, the magnitude of the coefficients appear to decrease to 0 quite quickly as m increases, but at around $t = 40$ the highest-order coefficients begin to grow in size. It seems likely that this is due to the build-up of numerical error over time.

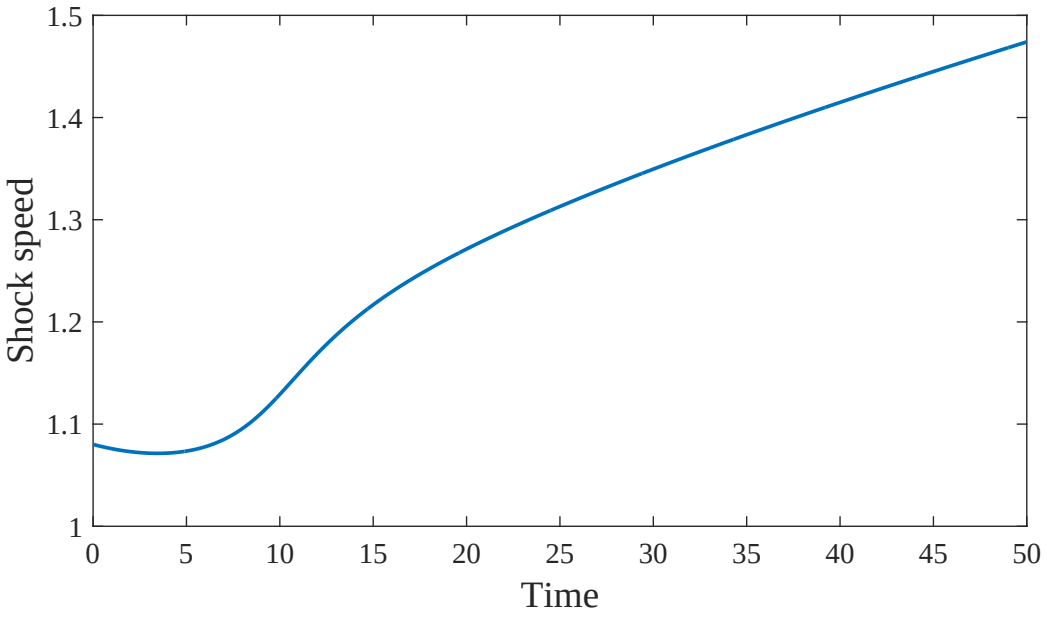

Figure 3.5: Shock speed profile for the same parameters as figure (3.3). The velocity decreases slightly at first, from approximately 1.08 at $t = 0$ to 1.07 at approximately $t = 5$ time units. It then increases steadily to a maximum of 1.47 at time $t = 50$.

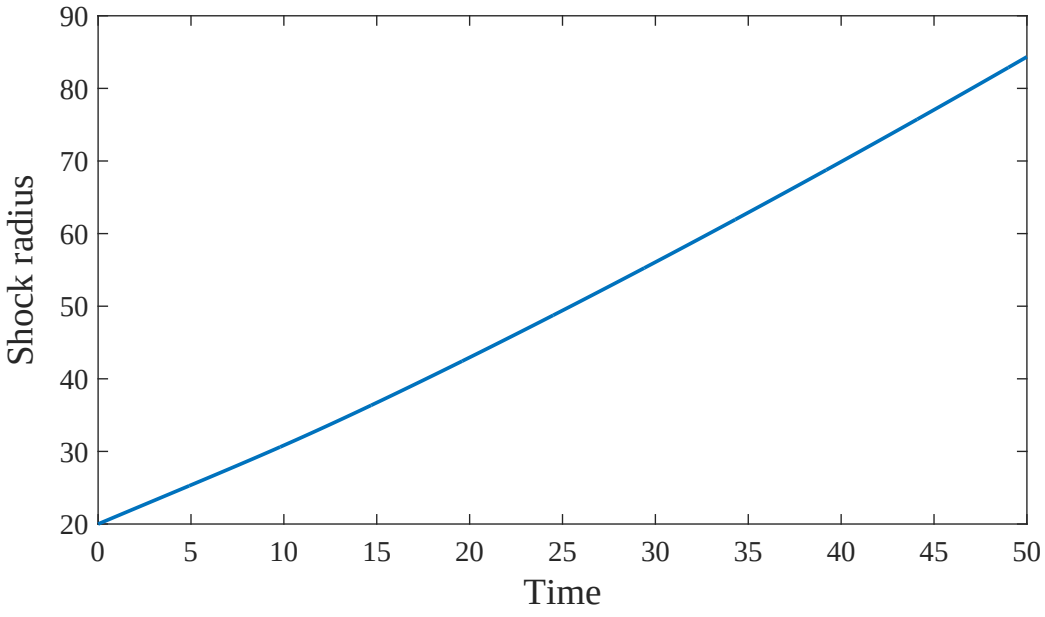

Figure 3.6: Shock radius profile for the same parameters as figure (3.3). The radius increases steadily from 20 to approximately 84 length units; more than quadrupling in size.

For many starting conditions and system parameters, the high-order modes in the spectral expansions (3.35) - (3.39) begin suddenly and rapidly to grow, causing high-frequency oscillations to form. It is not clear at this stage exactly what causes these oscillations, but the method fails soon after they appear. Figure (3.7) displays the coefficients $\mathcal{C}_m$, in the spectral expansion of temperature, clearly exhibiting rapid growth in the high-frequency modes as soon as time $t = 2$. The system parameters used in the generation of this image are

$$\zeta = 1.25 \quad ; \quad \epsilon = 0.5 \quad ; \quad q = 1.5 \quad ; \quad \theta_a = 0.5 \quad ; \quad \gamma = 1.4. \tag{3.70}$$

The background concentrations of A and X are

$$A_e = 1 \quad ; \quad X_e = 0.75. \tag{3.71}$$

while the density and its spatial derivative on the shock at time $t = 0$ are given by

$$\rho_s(0) = 3 \quad ; \quad \left.\frac{\partial \rho}{\partial \xi}\right|_{\xi \to 1^-,\, t=0} = -2.5 \tag{3.72}$$

and the shock is initially located at radius

$$R_s(0) = 4. \tag{3.73}$$

In cases such as these, we have two options: use a shock-capturing numerical method, such as a Godunov scheme; or alter the spectral method derived here, by including a small amount of diffusion and viscosity, such that the spurious growth in the high-order modes, allowing the numerical scheme to progress beyond the point that it would otherwise fail. We will do both. More precisely, we will include some "false" diffusion and viscosity into the method,

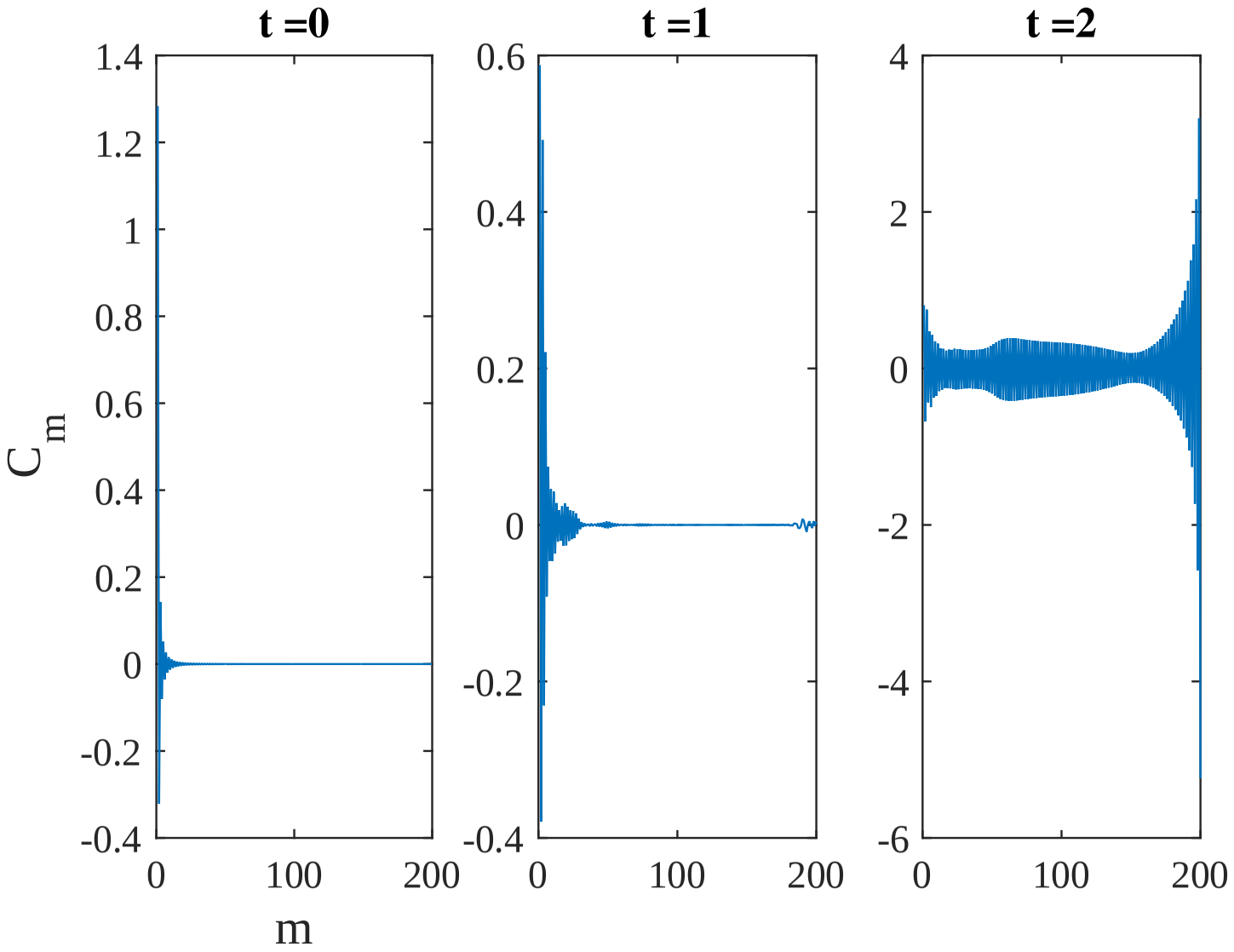

Figure 3.7: Plots of the coefficients $\mathcal{C}_m$, for the system parameter values $\zeta = 1.25$, $\epsilon = 0.5$, $q = 1.5$, $\theta_a = 0.5$, $\gamma = 1.4.$, at times $t = 0$, 1 and 2, showing rapid growth in high-order modes.

and compare the results to a shock-capturing Godunov scheme. The advantage of using the false diffusion method, as compared to a Godunov scheme, is that, as the method is shock-fitting, the shock values are all calculated as part of the method. As such, it's rather easy to track accurately the position of the shock using such a method. Conversely, a Godunov method, which is shock-capturing, will not calculate these values directly, and there will be a need to approximate them from other quantities. The disadvantage, however, is that the inclusion of false diffusion makes such a method inherently less accurate than might otherwise be the case, and it's not clear ahead of time how strong the diffusion and viscosity coefficients need to be before the scheme is able to dampen the growth of high-frequency modes.

When diffusion and viscosity are included, the governing equations to be solved become

$$\frac{\partial \rho}{\partial t} = \frac{1}{R_s}\left[(\xi R_s' - u)\frac{\partial \rho}{\partial \xi} - \frac{\rho}{\xi^2}\frac{\partial}{\partial \xi}\left(\xi^2 u\right) + \frac{\sigma}{R_s \xi^2}\frac{\partial}{\partial \xi}\left(\xi^2 \frac{\partial \rho}{\partial \xi}\right)\right] \tag{3.74}$$

$$\frac{\partial u}{\partial t} = \frac{1}{R_s}\left\{(\xi R_s' - u)\frac{\partial u}{\partial \xi} - \frac{1}{\rho}\frac{\partial p}{\partial \xi} + \frac{\nu}{R_s}\frac{\partial}{\partial \xi}\left[\frac{1}{\xi^2}\frac{\partial}{\partial \xi}\left(\xi^2 u\right)\right]\right\} \tag{3.75}$$

$$\frac{\partial T}{\partial t} = \frac{1}{R_s}\left[(\xi R_s' - u)\frac{\partial T}{\partial \xi} - (\gamma - 1)\frac{T}{\xi^2}\frac{\partial}{\partial \xi}\left(\xi^2 u\right) + \frac{\phi}{R_s \xi^2}\frac{\partial}{\partial \xi}\left(\xi^2 \frac{\partial T}{\partial \xi}\right)\right] + \frac{(\gamma - 1)}{\rho} Q_T$$

$$\frac{\partial X}{\partial t} = \frac{1}{R_s}\left[(\xi R_s' - u)\frac{\partial X}{\partial \xi} - \frac{X}{\xi^2}\frac{\partial}{\partial \xi}\left(\xi^2 u\right) + \frac{\sigma}{R_s \xi^2}\frac{\partial}{\partial \xi}\left(\xi^2 \frac{\partial X}{\partial \xi}\right)\right] + Q_X \tag{3.76}$$

$$\frac{\partial A}{\partial t} = \frac{1}{R_s}\left[(\xi R_s' - u)\frac{\partial A}{\partial \xi} - \frac{A}{\xi^2}\frac{\partial}{\partial \xi}\left(\xi^2 u\right) + \frac{\sigma}{R_s \xi^2}\frac{\partial}{\partial \xi}\left(\xi^2 \frac{\partial A}{\partial \xi}\right)\right] + Q_A. \tag{3.77}$$

Here we have marked in red the portion of each equation which differs from their respective form in equations (3.29)-(3.33). The new parameters σ and ϕ represent the artificial gaseous and thermal diffusion of the gas, whereas

ν is the artificial viscosity. These new portions are the Laplacian of the appropriate variable (or radial component of the vector Laplacian in the case of equation (3.75)), see Batchelor [49, pp.600-601], converted to the new spatial coordinate ξ.

The solution method is now much the same, and it is useful to note that the basis functions satisfy the relations

$$\frac{1}{\xi^2}\frac{\partial}{\partial\xi}\left(\xi^2\frac{\partial}{\partial\xi}j_0\left(m\pi\xi\right)\right) = -m^2\pi^2 j_0\left(m\pi\xi\right)$$

and

$$\frac{\partial}{\partial\xi}\left[\frac{1}{\xi^2}\frac{\partial}{\partial\xi}\left(\xi^2 j_1\left(\alpha_m\xi\right)\right)\right] = -\alpha_m^2 j_1\left(\alpha_m\xi\right),$$

as can be verified by application of the product rule for derivatives and the alternate forms for the basis functions in equations (3.40) and (3.41). Combining these with the spectral form of the solutions, such as in (3.35) and (3.36), yields the expressions

$$\frac{1}{\xi^2}\frac{\partial}{\partial\xi}\left(\xi^2\frac{\partial\rho}{\partial\xi}\right) = -\pi^2\sum_{m=1}^{\infty} m^2\mathcal{A}_m j_0\left(m\pi\xi\right)$$

and

$$\frac{\partial}{\partial\xi}\left[\frac{1}{\xi^2}\frac{\partial}{\partial\xi}\left(\xi^2 u\right)\right] = -\sum_{m=1}^{\infty}\alpha_m^2\mathcal{B}_m j_1\left(\alpha_m\xi\right)$$

and similarly for the respective derivatives of T, X and A. Consequently, since these expressions vanish as $\xi \to 1^-$, i.e.

$$\lim_{\xi\to 1^-}\frac{1}{\xi^2}\frac{\partial}{\partial\xi}\left(\xi^2\frac{\partial}{\partial\xi}j_0\left(m\pi\xi\right)\right) = -m^2\pi^2 j_0\left(m\pi\right) = 0$$
$$\lim_{\xi\to 1^-}\frac{\partial}{\partial\xi}\left(\frac{1}{\xi^2}\frac{\partial}{\partial\xi}\xi^2 j_1\left(\alpha_m\xi\right)\right) = -\alpha_m^2 j_1\left(\alpha_m\right) = 0,$$

we see that the equation for the derivative of the shock density is

$$\begin{aligned}\frac{\mathrm{d}\rho_s}{\mathrm{d}t} &= \lim_{\xi\to 1^-}\frac{1}{R_s}\left[\left(\xi R_s' - u\right)\frac{\partial\rho}{\partial\xi} - \frac{\rho}{\xi^2}\frac{\partial}{\partial\xi}\left(\xi^2 u\right) + \frac{\sigma}{R_s\xi^2}\frac{\partial}{\partial\xi}\left(\xi^2\frac{\partial\rho}{\partial\xi}\right)\right] \\ &= \frac{1}{R_s}\sum_{m=1}^{M}\left[\left(u_s - R_s'\right)m\pi\mathcal{A}_m\left(t\right)j_1\left(m\pi\right) - \rho_s\alpha_m\mathcal{B}_m\left(t\right)j_0\left(\alpha_m\right)\right],\end{aligned}$$

which remains identical to the previous equation in (3.52). Under this new scheme, the only somewhat substantial change is to the integrands (3.59) - (3.63) which now become

$$I_\rho = \frac{1}{R_s}\left[\left(\xi R_s' - u\right)\frac{\partial\rho}{\partial\xi} - \frac{\rho}{\xi^2}\frac{\partial}{\partial x}\left(\xi^2 u\right) + \frac{\sigma}{R_s\xi^2}\frac{\partial}{\partial\xi}\left(\xi^2\frac{\partial\rho}{\partial\xi}\right)\right] - \frac{\mathrm{d}\rho_s}{\mathrm{d}t}$$

$$\begin{aligned}I_u = \frac{1}{R_s}\Bigg\{&\left(\xi R_s' - u\right)\frac{\partial u}{\partial\xi} - \frac{T}{\rho}\frac{\partial\rho}{\partial\xi} - \frac{\partial T}{\partial\xi} + \frac{\nu}{R_s}\frac{\partial}{\partial\xi}\left[\frac{1}{\xi^2}\frac{\partial}{\partial\xi}\left(\xi^2 u\right)\right]\Bigg\} \\ &- \xi\frac{\mathrm{d}u_s}{\mathrm{d}t}\end{aligned} \tag{3.78}$$

$$\begin{aligned}I_T = \frac{1}{R_s}&\left[\left(\xi R_s' - u\right)\frac{\partial T}{\partial\xi} - \left(\gamma-1\right)\frac{T}{\xi^2}\frac{\partial}{\partial\xi}\left(\xi^2 u\right) + \frac{\phi}{R_s\xi^2}\frac{\partial}{\partial\xi}\left(\xi^2\frac{\partial T}{\partial\xi}\right)\right] \\ &+ \frac{\left(\gamma-1\right)}{\rho}Q_T - \frac{\mathrm{d}T_s}{\mathrm{d}t}\end{aligned} \tag{3.79}$$

$$\begin{aligned}I_X = \frac{1}{R_s}&\left[\left(\xi R_s' - u\right)\frac{\partial X}{\partial\xi} - \frac{X}{\xi^2}\frac{\partial}{\partial\xi}\left(\xi^2 u\right) + \frac{\sigma}{R_s\xi^2}\frac{\partial}{\partial\xi}\left(\xi^2\frac{\partial X}{\partial\xi}\right)\right] \\ &+ Q_X - \frac{\mathrm{d}X_s}{\mathrm{d}t}\end{aligned} \tag{3.80}$$

$$\begin{aligned}I_A = \frac{1}{R_s}&\left[\left(\xi R_s' - u\right)\frac{\partial A}{\partial\xi} - \frac{A}{\xi^2}\frac{\partial}{\partial\xi}\left(\xi^2 u\right) + \frac{\sigma}{R_s\xi^2}\frac{\partial}{\partial\xi}\left(\xi^2\frac{\partial A}{\partial\xi}\right)\right] \\ &+ Q_A - \frac{\mathrm{d}A_s}{\mathrm{d}t}\end{aligned} \tag{3.81}$$

and the rest of the scheme remains unchanged. As was done previously, the new additions to these expressions have been written in red to highlight the changes. While we are certainly free to choose any combination of values for σ, ϕ and ν, for ease we will choose them all to be equal, and represent

them by ϕ. The use of artificial or false diffusion or viscosity to dampen the growth of instabilities such as Gibbs phenomena is not a novel idea, and was utilised at least as early as 1950 by Von Neumann and Richtmyer [53].

3.8 Comparison with Godunov Scheme

We now employ a second numerical scheme, this time of the "shock-capturing" variety, as a means of comparison with the results of the spectral method with false diffusion. As such a scheme will require the governing equations to be in conservative form, we will solve the governing equations in $r-t$ space, instead of $\xi - t$. That is, the equations to be solved will be the partial differential equations (3.13) - (3.16), subject to the shock jump conditions (3.17) - (3.21). Godunov methods and various related shock-capturing techniques are discussed in great detail in Toro's excellent text [54], which was an invaluable reference for the writing of this section, and more briefly by Sweby [55]. The spatial domain is truncated to $[0, r_{max}]$, for some suitably large value of r_{max}, and is divided into N sub-domains of constant width $\Delta r = \frac{r_{max}}{N}$. We then introduce the discrete position value $r_i = (i - 1/2)\Delta r$ where $i = 1, 2, ..., N$, representing the centre of each sub-domain.

The governing equations may be written in general vector form as:

$$\frac{\partial \underline{\mathbf{V}}}{\partial t} + \frac{\partial}{\partial r}\underline{\mathbf{f}}\left(\underline{\mathbf{V}}\right) = \underline{\mathbf{C}}\left(r, \underline{\mathbf{V}}\right) \tag{3.82}$$

where

$$\underline{\mathbf{V}} = \begin{bmatrix} \rho \\ \rho u \\ \rho E \\ X \\ A \end{bmatrix}, \ \underline{\mathbf{f}}\left(\underline{\mathbf{V}}\right) = \begin{bmatrix} \rho u \\ \rho\left(u^2 + T\right) \\ \rho H \\ Xu \\ Au \end{bmatrix}, \ \underline{\mathbf{C}}\left(r, \underline{\mathbf{V}}\right) = \begin{bmatrix} -\frac{2\rho u}{r} \\ -\frac{2\rho u^2}{r} \\ Q_T - \frac{2\rho H u}{r} \\ Q_X - \frac{2Xu}{r} \\ Q_A - \frac{2Au}{r} \end{bmatrix}$$

subject to the initial condition $\underline{\mathbf{V}}\left(r, t_1\right) = \underline{\mathbf{V}}_0$, with the aim to calculate (or approximate) $\underline{\mathbf{V}}\left(r, t_2\right)$ at a later time $t = t_2 = t_1 + \Delta t$. As we wish to account for the presence of shock waves, an integral form of the governing equations is necessary. If equation (3.82) is integrated over the region $\left[r_{i-1/2}, \ \ r_{i+1/2}\right] \times \left[t_n, \ \ t_{n+1}\right]$, we obtain

$$\begin{aligned} \int_{r_{i-1/2}}^{r_{i+1/2}} \left(\underline{\mathbf{V}}^{n+1} - \underline{\mathbf{V}}^{n}\right) \mathrm{d}r + \int_{t_n}^{t_{n+1}} \left[\underline{\mathbf{f}}\left(\underline{\mathbf{V}}_{i+1/2}\right) - \underline{\mathbf{f}}\left(\underline{\mathbf{V}}_{i-1/2}\right)\right] \mathrm{d}t \\ = \int_{t_n}^{t_{n+1}} \int_{r_{i-1/2}}^{r_{i+1/2}} \underline{\mathbf{C}}\left(r, \underline{\mathbf{V}}\right) \mathrm{d}r\mathrm{d}t. \end{aligned} \tag{3.83}$$

We then define $\bar{\underline{\mathbf{V}}}_i$ as the spatial average of $\underline{\mathbf{V}}$ over the domain $\left[r_{i-1/2} \ \ r_{i+1/2}\right]$. That is,

$$\bar{\underline{\mathbf{V}}}_i = \frac{1}{\Delta r} \int_{r_{i-1/2}}^{r_{i+1/2}} \underline{\mathbf{V}} \mathrm{d}r$$

wherein $\Delta r = r_{i+1/2} - r_{i-1/2}$ is assumed constant for simplicity, so that equation (3.83) may be written as

$$\begin{aligned} \bar{\underline{\mathbf{V}}}_i^{(n+1)} = \bar{\underline{\mathbf{V}}}_i^{(n)} - \frac{1}{\Delta r} \int_{t_n}^{t_{n+1}} \left[\underline{\mathbf{f}}\left(\underline{\mathbf{V}}_{i+1/2}\right) - \underline{\mathbf{f}}\left(\underline{\mathbf{V}}_{i-1/2}\right)\right] \mathrm{d}t \\ + \frac{1}{\Delta r} \int_{t_n}^{t_{n+1}} \int_{r_{i-1/2}}^{r_{i+1/2}} \underline{\mathbf{C}}\left(r, \underline{\mathbf{V}}\right) \mathrm{d}r\mathrm{d}t. \end{aligned} \tag{3.84}$$

At this stage, equation (3.84) is exact, although calculating exact values for

the integral expressions $\int_{t_n}^{t_{n+1}} \left[\underline{\mathbf{f}}\left(\underline{\mathbf{V}}_{i+1/2}\right) - \underline{\mathbf{f}}\left(\underline{\mathbf{V}}_{i-1/2}\right)\right] \mathrm{d}t$ and $\int_{t_n}^{t_{n+1}} \int_{r_{i-1/2}}^{r_{i+1/2}} \underline{\mathbf{C}}\left(r, \underline{\mathbf{V}}\right) \mathrm{d}r\mathrm{d}t$ is not trivial.

To find an approximate solution, an intermediate value of $\bar{\underline{\mathbf{V}}}_i$ is first calculated as:

$$\bar{\underline{\mathbf{V}}}_i^{(n+1/2)} = \bar{\underline{\mathbf{V}}}_i^{(n)} + \frac{1}{2}\Delta t\left[\underline{\mathbf{C}}\left(r_{i-1/2}, \underline{\mathbf{V}}_{i-1/2}\right) + \underline{\mathbf{C}}\left(r_{i+1/2}, \underline{\mathbf{V}}_{i+1/2}\right)\right]$$

wherein the "correction" term is an approximation to the double integral $\frac{1}{\Delta r}\int_{t_n}^{t_{n+1/2}} \int_{r_{i-1/2}}^{r_{i+1/2}} \underline{\mathbf{C}}\left(r, \underline{\mathbf{V}}\right) \mathrm{d}r\mathrm{d}t$, making use of the trapezoidal rule to approximate the integral over r, and a forward Euler method to approximate the integral over t. The value of $\bar{\underline{\mathbf{V}}}$ at the next time step is then approximated by

$$\bar{\underline{\mathbf{V}}}_i^{(n+1)} = \bar{\underline{\mathbf{V}}}_i^{(n)} - \frac{\Delta t}{\Delta r}\left(\underline{\mathbf{F}}_{i+1/2}^{n+1/2} - \underline{\mathbf{F}}_{i-1/2}^{n+1/2}\right) + \Delta t\underline{\mathbf{C}}\left(\bar{\underline{\mathbf{V}}}_i^{(n+1/2)}\right) \tag{3.85}$$

where $\underline{\mathbf{F}}_{i+1/2}^{n+1/2}$ and $\underline{\mathbf{F}}_{i-1/2}^{n+1/2}$ are the Godunov fluxes, which represent the amount of flux into the i^{th} cell through each of the boundaries at $r = r_{i+1/2}$ and $r = r_{i-1/2}$, respectively. Operator splitting techniques such as that used to compute $\bar{\underline{\mathbf{V}}}_i^{(n+1)}$ in equation (3.85) have been utilised by, among others, Bartsch and Borzi [56] to solve numerically partial differential equations with source terms, using the method of Godunov.

To approximate the Godunov fluxes $\underline{\mathbf{F}}_{i+1/2}^{n+1/2}$ and $\underline{\mathbf{F}}_{i-1/2}^{n+1/2}$, we consider the Riemann problem, with piecewise initial data given by the value of $\bar{\underline{\mathbf{V}}}^{(n+1/2)}$:

$$\frac{\partial \bar{\underline{\mathbf{V}}}}{\partial t} + \frac{\partial}{\partial r}\underline{\mathbf{f}}\left(\bar{\underline{\mathbf{V}}}\right) = 0 \tag{3.86}$$

subject to the piecewise initial condition

$$\bar{\underline{\mathbf{V}}}\left(r, t_n\right) = \begin{cases} \bar{\underline{\mathbf{V}}}_i^{(n+1/2)} & \text{if } r < r_{i+1/2} \\ \bar{\underline{\mathbf{V}}}_{i+1}^{(n+1/2)} & \text{if } r > r_{i+1/2}. \end{cases}$$

It will also prove useful to define $\Delta\underline{\mathbf{V}}$ as the jump in $\underline{\mathbf{V}}$ across the discontinuity. Specifically, as

$$\Delta\underline{\mathbf{V}} = \underline{\mathbf{V}}_R - \underline{\mathbf{V}}_L$$

and similarly

$$\Delta\underline{\mathbf{f}} = \underline{\mathbf{f}}_R - \underline{\mathbf{f}}_L \equiv \underline{\mathbf{f}}\left(\underline{\mathbf{V}}_R\right) - \underline{\mathbf{f}}\left(\underline{\mathbf{V}}_L\right)$$

where a subscript L indicates a variable evaluated on the left side of the discontinuous interface, and a subscript R denotes a variable evaluated on the right. It is simplest then to define $V_L = V_i$ and $V_R = V_{i+1}$; however, this can lead to high-frequency Gibbs-like phenomena near areas with sharp gradients, such as around a shock. To limit these spurious oscillations, we also define piecewise linear functions in each cell, with the form $V_i + m_i\left(r - r_i\right)$ for an appropriately chosen slope m_i. Linear expressions such as this maintain the spatial average within each cell, that is

$$\frac{1}{\Delta r}\int_{r_i-\frac{1}{2}\Delta r}^{r_i+\frac{1}{2}\Delta r} V_i + m_i\left(r - r_i\right)\mathrm{d}r = V_i.$$

Then we choose

$$V_L = V_i + m_i\left(r_{i+1/2} - r_i\right) = V_i + \frac{1}{2}m_i\Delta r$$

and by a similar argument

$$V_R = V_{i+1} + m_{i+1}\left(r_{i+1/2} - r_{i+1}\right) = V_{i+1} - \frac{1}{2}m_{i+1}\Delta r.$$

A diagram of the Riemann problem, as well as the linear reconstruction technique is displayed in figure (3.8). The slopes m_i will be chosen according to the rule

$$m_i = \frac{1}{2\Delta r}\left[\sigma\left(V_{i+1} - V_i\right) + \sigma\left(V_i - V_{i-1}\right)\right]\min\left(\left|V_{i+1} - V_i\right|, \left|V_i - V_{i-1}\right|\right)$$

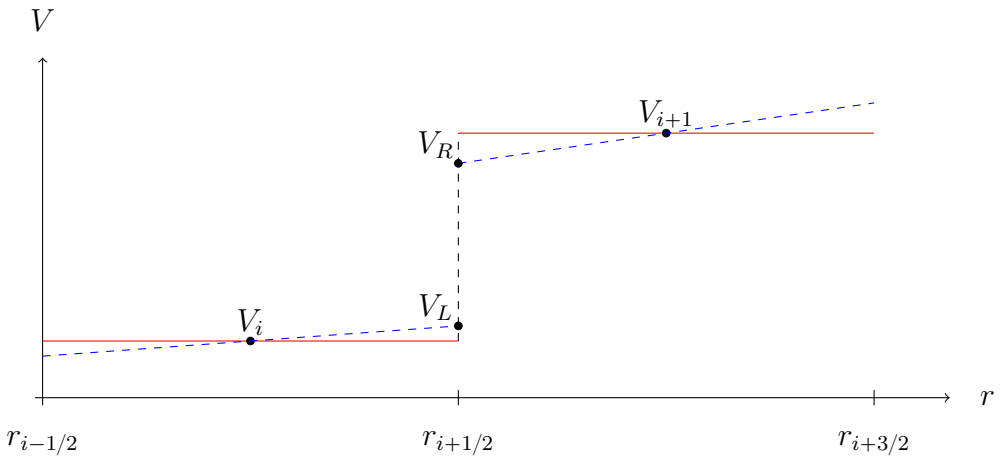

Figure 3.8: A sketch of the classic Riemann problem (solid line) and linear reconstruction (dashed line).

wherein σ denotes the sign function. That is, if the forward and backward finite difference approximations to the spatial derivative are equal in sign, the slope m_i is chosen to be equal to the one which is smallest in absolute value. Otherwise, the slope is set to zero. This is based upon the minmod slope limiter discussed by Roe [57], for example. This is a somewhat naïve method for flux limiting, but for the purposes of comparison between the two methods, it will prove sufficient. We aim to solve this problem numerically using a Roe-type method (as first described by Roe in [58]). To do so, we approximate the partial differential equation (3.86) with

$$\frac{\partial \bar{\mathbf{V}}}{\partial t} + \Omega \frac{\partial \bar{\mathbf{V}}}{\partial r} = 0 \tag{3.87}$$

where Ω is a constant matrix which satisfies three properties:

$$\begin{aligned}
&\bullet\ \Omega \text{ has all real eigenvalues and a complete set of} \\
&\quad \text{linearly independent eigenvectors. (Hyperbolicity)} \\
&\bullet\ \Omega \rightarrow \frac{\partial \underline{\mathbf{f}}}{\partial \underline{\mathbf{V}}} \text{ in the limit } \Delta\underline{\mathbf{V}} \rightarrow \underline{\mathbf{0}} \text{ (Consistency)} \\
&\bullet\ \Delta\underline{\mathbf{f}} = \Omega\Delta\underline{\mathbf{V}} \text{ (Conservation)}
\end{aligned} \tag{3.88}$$

A method for finding such a matrix is also described by Roe [58], and we now introduce a parameter vector $\boldsymbol{\omega}$, which will assist in finding such a matrix, defined as such:

$$\boldsymbol{\omega} = \begin{bmatrix} \sqrt{\rho} \\ \sqrt{\rho}u \\ \sqrt{\rho}H \\ \frac{X}{\sqrt{\rho}} \\ \frac{A}{\sqrt{\rho}} \end{bmatrix}. \tag{3.89}$$

With $\boldsymbol{\omega}$ defined as in (3.89), every element of $\underline{\mathbf{V}}$ (ρ, ρu, ρE, X and A) can be expressed as quadratics in the elements of $\boldsymbol{\omega}$. Denoting the first element of the vector $\boldsymbol{\omega}$ as ω_1, the second as ω_2 and so on, we have the result

$$\underline{\mathbf{V}} = \begin{bmatrix} \rho \\ \rho u \\ \rho E \\ X \\ A \end{bmatrix} = \begin{bmatrix} \omega_1^2 \\ \omega_1\omega_2 \\ \frac{\gamma-1}{2\gamma}\omega_2^2 + \frac{1}{\gamma}\omega_1\omega_3 \\ \omega_1\omega_4 \\ \omega_1\omega_5 \end{bmatrix},$$

For convenience, we now define $\bar{\omega}_1 = \frac{1}{2}(\omega_{1L} + \omega_{1R})$, that is, as the average of ω_1 on each side of the discontinuity, with similar definitions for $\bar{\omega}_2$, $\bar{\omega}_3$ and

so on. Then we have

$$\Delta\underline{\mathbf{v}} = \begin{bmatrix} 2\bar{\omega}_1 & 0 & 0 & 0 & 0 \\ \bar{\omega}_2 & \bar{\omega}_1 & 0 & 0 & 0 \\ \frac{1}{\gamma}\bar{\omega}_3 & \frac{\gamma-1}{\gamma}\bar{\omega}_2 & \frac{1}{\gamma}\bar{\omega}_1 & 0 & 0 \\ \bar{\omega}_4 & 0 & 0 & \bar{\omega}_1 & 0 \\ \bar{\omega}_5 & 0 & 0 & 0 & \bar{\omega}_1 \end{bmatrix} \Delta\boldsymbol{\omega}. \tag{3.90}$$

Similarly, every element of $\underline{\mathbf{f}}$, i.e ρu, $\rho\left(u^2+T\right)$, ρH, uX and uA, can also be written as quadratics in the elements of $\boldsymbol{\omega}$:

$$\underline{\mathbf{f}} = \begin{bmatrix} \rho u \\ \rho\left(u^2+T\right) \\ \rho u H \\ uX \\ uA \end{bmatrix} = \begin{bmatrix} \omega_1\omega_2 \\ \frac{\gamma+1}{2\gamma}\omega_2^2 + \frac{\gamma-1}{\gamma}\omega_1\omega_3 \\ \omega_2\omega_3 \\ \omega_2\omega_4 \\ \omega_2\omega_5. \end{bmatrix}$$

This then allows us to write

$$\Delta\underline{\mathbf{f}} = \begin{bmatrix} \bar{\omega}_2 & \bar{\omega}_1 & 0 & 0 & 0 \\ \frac{\gamma-1}{\gamma}\bar{\omega}_3 & \frac{\gamma+1}{\gamma}\bar{\omega}_2 & \frac{\gamma-1}{\gamma}\bar{\omega}_1 & 0 & 0 \\ 0 & \bar{\omega}_3 & \bar{\omega}_2 & 0 & 0 \\ 0 & \bar{\omega}_4 & 0 & \bar{\omega}_2 & 0 \\ 0 & \bar{\omega}_5 & 0 & 0 & \bar{\omega}_2 \end{bmatrix} \Delta\boldsymbol{\omega}. \tag{3.91}$$

It is useful here to introduce the "Roe-averaged values", each given by

$$
\begin{aligned}
u^* &\equiv \frac{\bar{\omega}_2}{\bar{\omega}_1} = \frac{\sqrt{\rho_L}u_L + \sqrt{\rho_R}u_R}{\sqrt{\rho_L} + \sqrt{\rho_R}} \\
H^* &\equiv \frac{\bar{\omega}_3}{\bar{\omega}_1} = \frac{\sqrt{\rho_L}H_L + \sqrt{\rho_R}H_R}{\sqrt{\rho_L} + \sqrt{\rho_R}} \\
X^* &\equiv \frac{\bar{\omega}_4}{\bar{\omega}_1} = \frac{\frac{X_L}{\sqrt{\rho_L}} + \frac{X_R}{\sqrt{\rho_R}}}{\sqrt{\rho_L} + \sqrt{\rho_R}} \\
A^* &\equiv \frac{\bar{\omega}_5}{\bar{\omega}_1} = \frac{\frac{A_L}{\sqrt{\rho_L}} + \frac{A_R}{\sqrt{\rho_R}}}{\sqrt{\rho_L} + \sqrt{\rho_R}} \\
s^* &\equiv \sqrt{(\gamma-1)\left[H^* - \frac{1}{2}\left(u^*\right)^2\right]}
\end{aligned}
$$

then, combining equations (3.90) and (3.91), we have:

$$
\begin{aligned}
\Delta\underline{\mathbf{f}} &= \begin{bmatrix}
\bar{\omega}_2 & \bar{\omega}_1 & 0 & 0 & 0 \\
\frac{\gamma-1}{\gamma}\bar{\omega}_3 & \frac{\gamma+1}{\gamma}\bar{\omega}_2 & \frac{\gamma-1}{\gamma}\bar{\omega}_1 & 0 & 0 \\
0 & \bar{\omega}_3 & \bar{\omega}_2 & 0 & 0 \\
0 & \bar{\omega}_4 & 0 & \bar{\omega}_2 & 0 \\
0 & \bar{\omega}_5 & 0 & 0 & \bar{\omega}_2
\end{bmatrix}
\begin{bmatrix}
2\bar{\omega}_1 & 0 & 0 & 0 & 0 \\
\bar{\omega}_2 & \bar{\omega}_1 & 0 & 0 & 0 \\
\frac{1}{\gamma}\bar{\omega}_3 & \frac{\gamma-1}{\gamma}\bar{\omega}_2 & \frac{1}{\gamma}\bar{\omega}_1 & 0 & 0 \\
\bar{\omega}_4 & 0 & 0 & \bar{\omega}_1 & 0 \\
\bar{\omega}_5 & 0 & 0 & 0 & \bar{\omega}_1
\end{bmatrix}^{-1} \Delta\underline{\mathbf{v}} \\
&= \begin{bmatrix}
0 & 1 & 0 & 0 & 0 \\
-\frac{1}{2}(3-\gamma)\left(u^*\right)^2 & (3-\gamma)u^* & \gamma-1 & 0 & 0 \\
\frac{1}{2}(3-\gamma)\left(u^*\right)^3 - u^*H^* & H^* - (\gamma-1)\left(u^*\right)^2 & \gamma u^* & 0 & 0 \\
-u^*X^* & X^* & 0 & u^* & 0 \\
-u^*A^* & A^* & 0 & 0 & u^*
\end{bmatrix} \Delta\underline{\mathbf{v}}.
\end{aligned}
$$

The eigenvalues of this matrix are

$$
\begin{aligned}
\lambda_1 &= u^* + s^* \\
\lambda_2 &= u^* - s^* \\
\lambda_3 = \lambda_4 = \lambda_5 &= u^*
\end{aligned}
\tag{3.92}
$$

with corresponding eigenvectors

$$\underline{\mathbf{K}}_1 = \begin{bmatrix} 1 \\ u^* + s^* \\ H^* + s^* u^* \\ X^* \\ A^* \end{bmatrix}, \; \underline{\mathbf{K}}_2 = \begin{bmatrix} 1 \\ u^* - s^* \\ H^* - s^* u^* \\ X^* \\ A^* \end{bmatrix}$$
$$\underline{\mathbf{K}}_3 = \begin{bmatrix} 1 \\ u^* \\ \frac{1}{2}\left(u^*\right)^2 \\ 0 \\ 0 \end{bmatrix}, \; \underline{\mathbf{K}}_4 = \begin{bmatrix} 0 \\ 0 \\ 0 \\ 1 \\ 0 \end{bmatrix}, \; \underline{\mathbf{K}}_5 = \begin{bmatrix} 0 \\ 0 \\ 0 \\ 0 \\ 1 \end{bmatrix} \tag{3.93}$$

It is rather straight-forward to show that the eigenvalues in (3.92) are real. We may also see that the eigenvectors in (3.93) satisfy

$$\left\| \underline{\mathbf{K}}_1 \quad \underline{\mathbf{K}}_2 \quad \underline{\mathbf{K}}_3 \quad \underline{\mathbf{K}}_4 \quad \underline{\mathbf{K}}_5 \right\| = \frac{2\left(s^*\right)^3}{\gamma - 1}$$

and thus are linearly independent and the hyperbolicity condition in (3.88) is met if $s^* \neq 0$. We then expand $\Delta \underline{\mathbf{V}}$ as a linear combination of the eigenvectors in (3.93), in the form

$$\Delta \underline{\mathbf{V}} = \sum_{j=1}^{5} a_j \underline{\mathbf{K}}_j = \left[\underline{\mathbf{K}}_1 \quad \underline{\mathbf{K}}_2 \quad \underline{\mathbf{K}}_3 \quad \underline{\mathbf{K}}_4 \quad \underline{\mathbf{K}}_5 \right] \underline{\mathbf{a}}.$$

Here $\underline{\mathbf{a}}$ is the 5×1 column vector with entries a_1, a_2 etc. Then the coefficients are given by the equation

$$\begin{aligned}\underline{\mathbf{a}} &= \left[\underline{\mathbf{K}}_1 \quad \underline{\mathbf{K}}_2 \quad \underline{\mathbf{K}}_3 \quad \underline{\mathbf{K}}_4 \quad \underline{\mathbf{K}}_5\right]^{-1} \Delta \underline{\mathbf{V}} \\ &= \frac{\gamma - 1}{(s^*)^2} \begin{bmatrix} \frac{1}{2}u^*\left(\frac{1}{2}u^* - \frac{s^*}{\gamma-1}\right) & \frac{1}{2}\left(\frac{s^*}{\gamma-1} - u^*\right) & \frac{1}{2} & 0 & 0 \\ \frac{1}{2}u^*\left(\frac{1}{2}u^* + \frac{s^*}{\gamma-1}\right) & -\frac{1}{2}\left(\frac{s^*}{\gamma-1} + u^*\right) & \frac{1}{2} & 0 & 0 \\ \frac{(s^*)^2}{\gamma-1} - \frac{1}{2}(u^*)^2 & u^* & -1 & 0 & 0 \\ -\frac{1}{2}(u^*)^2 X^* & u^* X^* & -X^* & \frac{(s^*)^2}{\gamma-1} & 0 \\ -\frac{1}{2}(u^*)^2 A^* & u^* A^* & -A^* & 0 & \frac{(s^*)^2}{\gamma-1} \end{bmatrix} \Delta \underline{\mathbf{V}}.\end{aligned}$$

Then, we may calculate the approximate Godunov fluxes, given by

$$\underline{\mathbf{F}}_{i+1/2} = \frac{1}{2}\left(\underline{\mathbf{F}}_L + \underline{\mathbf{F}}_R\right) - \frac{1}{2}\sum_{j=1}^{5} a_j \left|\lambda_j\right| \underline{\mathbf{K}}_j.$$

This scheme can be iterated repeatedly, at time steps of size Δt until the final, required time is reached, ensuring that the Courant-Friedrichs-Lewy condition is satisfied. That is, we require:

$$\Delta t < \frac{1}{2}\frac{\Delta r}{\max\limits_i ||\lambda_i||}$$

to ensure that no two characteristics of the partial differential equation (3.87) may intersect (see Toro, [54, p.216]). As mentioned previously, a disadvantage of the Godunov scheme over the spectral solution is that the position of the shock and the value of the various system variables thereon are not produced naturally from the method. For comparison purposes, however, we need to determine, at least approximately, the values of these properties. In the particular case to be discussed in the remainder of this section, this is achieved simply by locating the position of the global maximum value of the

initial reagent A. Figure (3.9) displays the concentration of A as produced by the spectral method, with false diffusion parameter $\phi = 2.5 \times 10^{-3}$, with the rest of the system parameters as were used in producing figure (3.7). Note that it appears to attain a global maximum at $\xi = 1$, at each time step. This means that, at least in this particular case, the position of the maximum value of A can be used as a proxy for the shock location. Approximate values for the remaining shock properties can then be calculated from the relations in (3.22) - (3.26). Figure (3.10) compares the shock radius as predicted by the Godunov method described above (in the blue, solid line) with that predicted by the spectral method with various values of the false diffusion coefficient ϕ, between the times $t = 0$ and $t = 50$. Both numerical methods were run with 10^4 nodes over the spatial domain [0, 100] in the case of the Godunov method, and the usual domain of $[0,\ 1]$ for the spectral method. As with previous results, the spectral method used a total of 200 coefficients, as this was deemed sufficient to attain the required accuracy. When $\phi = 2.5 \times 10^{-3}$ (plotted in the red, dashed line) the shock radius is almost indistinguishable from that produced by the Godunov method. As ϕ increases to $\phi = 2.5 \times 10^{-2}$ (plotted in the black, dot-dashed line) the solutions are noticeably different from around the time $t = 25$, but still remain very close until $t = 50$. When $\phi = 2.5 \times 10^{-1}$ (magenta, dotted line) the spectral method deviates from the Godunov scheme much more quickly, with a noticeable difference forming around the $t = 15$ mark. Figure (3.11) shows the temperature profiles produced by each of the Godunov scheme (blue, solid line) and the spectral method with false diffusion coefficients given by $\phi = 2.5 \times 10^{-3}$ (in the red, dashed line), for the same parameters as given in

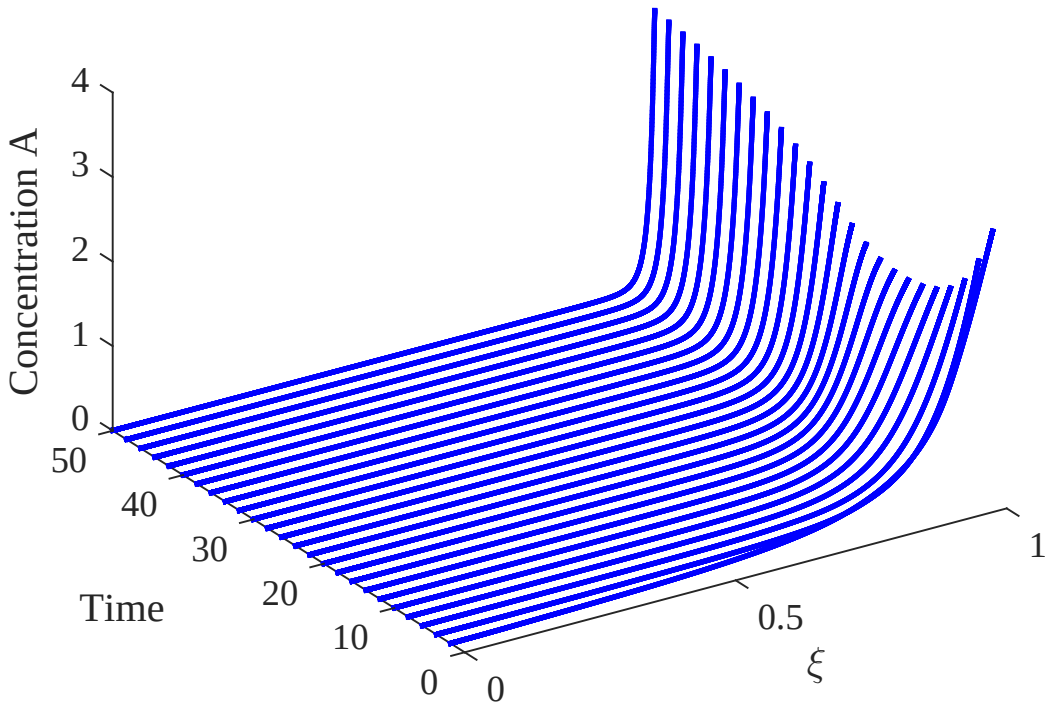

Figure 3.9: A plot of the concentration of reagent A, as given by the spectral method with parameters the same as in figure (3.7), with false diffusion $\phi = 2.5 \times 10^{-3}$, until time $t = 50$. Note that the concentration appears to attain its global maximum value on the shock at $\xi = 1$.

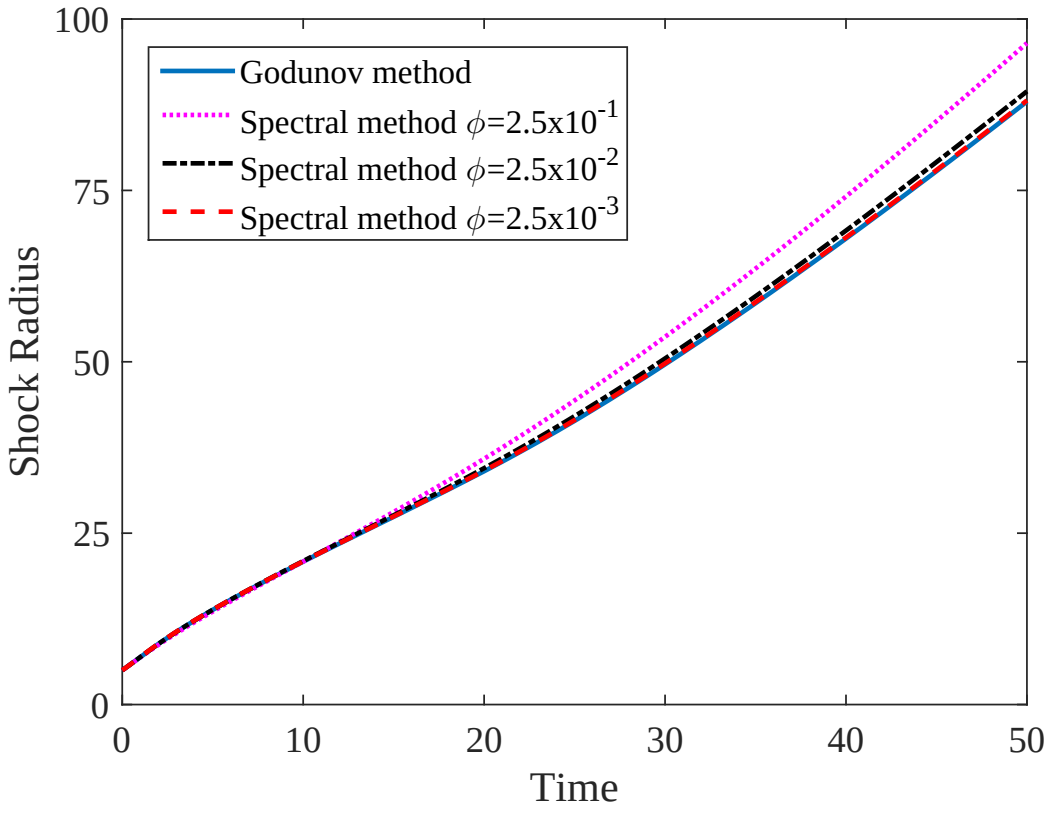

Figure 3.10: A comparison of the shock radius as predicted by the Godunov scheme and spectral method with parameters the same as in figure (3.7) and varying diffusion strengths. The disagreement between the Godunov scheme (blue, solid line) and the spectral method increases as the diffusion parameter increases from $\phi = 2.5 \times 10^{-3}$ (red, dashed line), to $\phi = 2.5 \times 10^{-2}$ (black, dot-dashed line) and finally $\phi = 2.5 \times 10^{-1}$ (magenta, dotted line)

(3.70)-(3.73) above. Both numerical schemes were able to produce this output in similar amounts of time, with the Godunov scheme running in about 30 minutes and the spectral method 25. The spectral method, however, produces better spatial resolution, as every one of the 10^4 nodes lies within the area of interest behind the shock. Conversely, the Godunov scheme "wastes" some computation time and resolution on the unburnt gas, where no change is expected, though it is possible that a more complex shock-capturing scheme may be able to overcome this inefficiency.

3.9 Conclusion

In this chapter we have developed a spectral method to model the evolution of a reacting gas behind a shock. This new shock-fitting technique ties together two separate sub-problems; on the shock a system of coupled ordinary differential equations govern the size and propagation speed of the shock, and in the remainder of the domain the reaction is governed by a system of highly non-linear, coupled partial differential equations. It is shown that these two problems are inextricably linked, and careful consideration of the initial conditions is needed to ensure that the two solution sets are compatible with each other. We then presented a novel spectral method which builds the shock values in the general solution to each reaction variable, and the partial differential equations are solved numerically in the transformed spectral variable. Some numerical solutions are then presented, but it is seen that the scheme is susceptible to the rapid growth of numerical instabilities in some parameter regimes, as high-frequency spectral modes grow rapidly

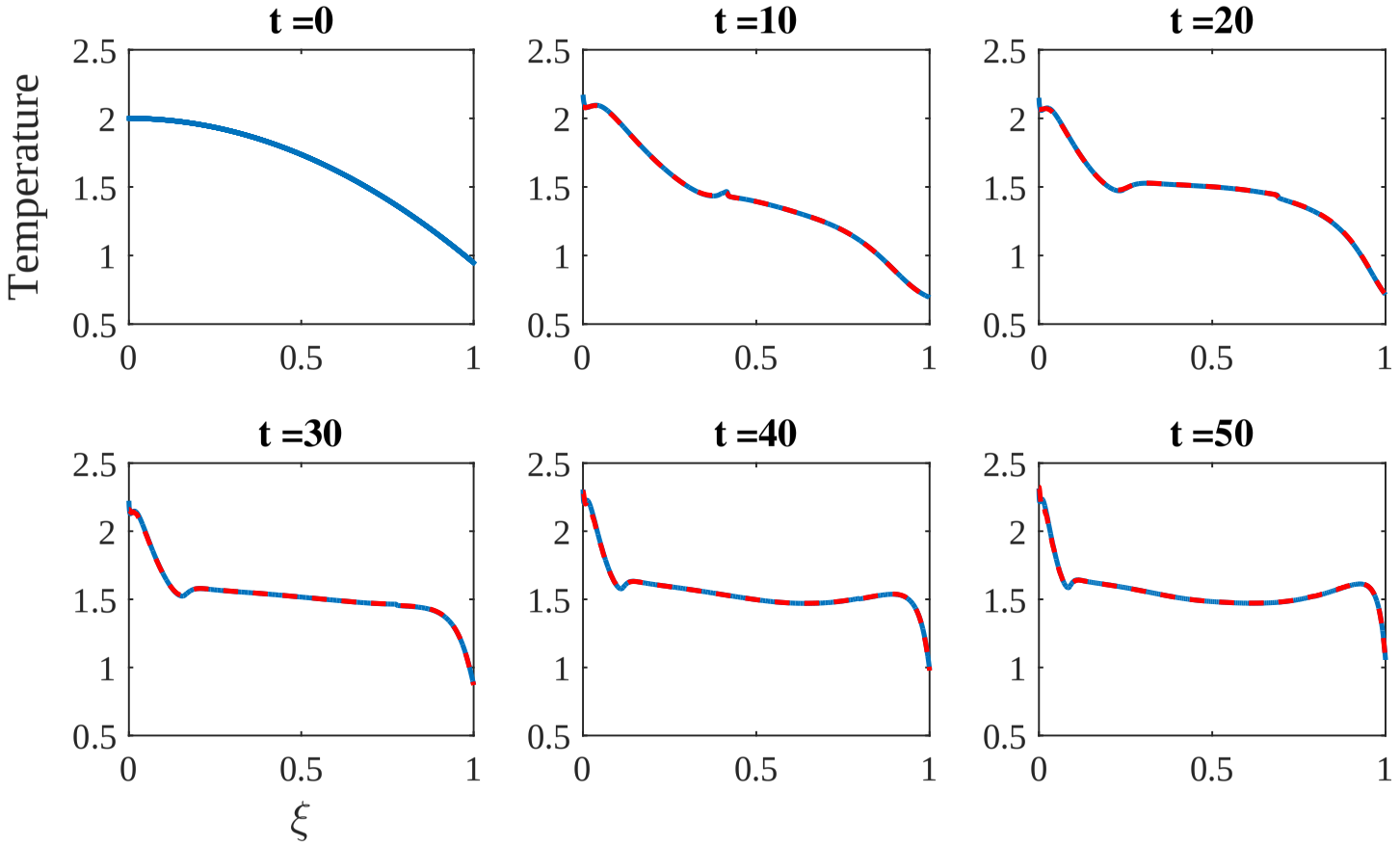

Figure 3.11: Temperature profiles at times $t = 0$, 10, 20, 30, 40 and 50 time units for the spectral method with parameters the same as in figure (3.7) and false diffusion coefficient $\phi = 2.5 \times 10^{-3}$ (red, dashed line) and Godunov scheme (blue, solid line), normalised to the domain $[0, 1]$, demonstrating the very close agreement between the two techniques.

in value. These high order modes are damped out with the addition of a small amount of artificial viscosity and diffusion, which allow the numerical scheme to progress beyond the formation of these high-frequency oscillations. This new scheme is then compared with the results of a classical Godunov method, and the two show remarkable agreement, even when the artificial viscosity parameter is moderately high.

3.10 Appendix

The previous sections of this chapter rely heavily on the orthogonality of the basis functions $j_0(m\pi z)$ and of $j_1(\alpha_m z)$. These orthogonality conditions are given, without proof, in equations (3.47) and (3.48). These expressions are derived in full in this appendix. It will be useful in each proof to recall the trigonometric identity:

$$\sin(a)\sin(b) = \frac{1}{2}\left[\cos(a-b) - \cos(a+b)\right]. \tag{3.94}$$

3.10.1 Proof of orthogonality of $j_0(m\pi z)$

We first aim to prove the result stated in equation (3.47), that is

$$I_1(m,n) \equiv \int_0^1 z^2 j_0(m\pi z)\, j_0(n\pi z)\, \mathrm{d}z = \frac{1}{2m^2\pi^2}\delta_{mn}. \tag{3.95}$$

where δ_{mn} is the Krönecker delta and takes the value 1 if $m = n$ and zero otherwise. To do so, we first make use of the trigonometric expressions for

j_0, as in equation (3.40), and simplify, so that we have

$$\begin{aligned} I_1(m,n) &= \int_0^1 z^2 \frac{\sin(m\pi z)}{m\pi z} \frac{\sin(n\pi z)}{n\pi z} \mathrm{d}z \\ &= \frac{1}{mn\pi^2} \int_0^1 \sin(m\pi z) \sin(n\pi z)\, \mathrm{d}z. \end{aligned}$$

Recalling the trigonometric identity in equation (3.94), the integral in question becomes

$$I_1(m,n) = \frac{1}{2mn\pi^2} \int_0^1 \{\cos[(m-n)\pi z] - \cos[(m+n)\pi z]\}\, \mathrm{d}z.$$

Assuming first that $m \neq n$, we have

$$I_1(m,n) = \frac{1}{2mn\pi^2} \left[\frac{\sin[(m-n)\pi z]}{(m-n)\pi} - \frac{\sin[(m+n)\pi z]}{(m+n)\pi} \right]_0^1 \mathrm{d}z = 0$$

as both m and n are non-zero integers. If $m = n$, then the integral is instead

$$\begin{aligned} I_1(m,n) &= \frac{1}{2m^2\pi^2} \int_0^1 [1 - \cos(2m\pi z)]\, \mathrm{d}z \\ &= \frac{1}{2m^2\pi^2} \left[z - \frac{\sin(2m\pi z)}{2m\pi} \right]_0^1 \mathrm{d}z \\ &= \frac{1}{2m^2\pi^2}, \end{aligned}$$

thus completing the result.

3.10.2 Proof of orthogonality of $j_1(\alpha_m z)$

We now prove the result stated in equation (3.48) on the orthogonality of the basis functions $j_1(\alpha_m z)$:

$$I_2(m,n) \equiv \int_0^1 z^2 j_1(\alpha_m z)\, j_1(\alpha_n z)\, \mathrm{d}z = \frac{\sin^2(\alpha_m)}{2\alpha_m^2} \delta_{mn}.$$

where δ_{mn} is the Krönecker delta and takes the value 1 if $m = n$ and zero otherwise. This time we begin with the derivative relations presented in equation (3.44) and (3.45), so that integration by parts yields

$$\begin{aligned} I_2(m,n) &= -\frac{1}{\alpha_n}\int_0^1 z^2 j_1(\alpha_m z)\,\frac{\mathrm{d}}{\mathrm{d}z}\left[j_0(\alpha_n z)\right]\mathrm{d}z \\ &= \frac{1}{\alpha_n}\left\{\int_0^1 j_0(\alpha_n z)\,\frac{\mathrm{d}}{\mathrm{d}z}\left[z^2 j_1(\alpha_m z)\right]\mathrm{d}z \right. \\ &\qquad\qquad \left. -\left[z^2 j_1(\alpha_m z)\, j_0(\alpha_n z)\right]_0^1\right\} \\ &= \frac{1}{\alpha_n}\int_0^1 j_0(\alpha_n z)\,\frac{\mathrm{d}}{\mathrm{d}z}\left[z^2 j_1(\alpha_m z)\right]\mathrm{d}z \\ &= \frac{1}{\alpha_n}\int_0^1 z^2 j_0(\alpha_n z)\,\frac{1}{z^2}\frac{\mathrm{d}}{\mathrm{d}z}\left[z^2 j_1(\alpha_m z)\right]\mathrm{d}z \\ &= \frac{\alpha_m}{\alpha_n}\int_0^1 z^2 j_0(\alpha_n z)\, j_0(\alpha_m z)\,\mathrm{d}z \\ &= \frac{1}{\alpha_n^2}\int_0^1 \sin(\alpha_n z)\sin(\alpha_m z)\,\mathrm{d}z. \end{aligned} \tag{3.96}$$

The equality of the second and third lines of equation (3.96) above follows from the definition of α_m as a solution to $j_1(\alpha_m) = 0$, so that the quantity in brackets vanishes. The remainder of this proof continues similarly to the previous proof, and we make use of the trigonometric identity in (3.94), yielding

$$I_2(m,n) = \frac{1}{2\alpha_n^2}\int_0^1 \left[\cos(\alpha_m - \alpha_n) - \cos(\alpha_m + \alpha_n)\right]\mathrm{d}z. \tag{3.97}$$

Assuming that $m \neq n$ (and therefore that $\alpha_m \neq \alpha_n$), integral (3.97) becomes

$$\begin{aligned} I_2(m,n) &= \frac{1}{2\alpha_n^2}\left[\frac{\sin(\alpha_m - \alpha_n)}{\alpha_m - \alpha_n} - \frac{\sin(\alpha_m + \alpha_n)}{\alpha_m + \alpha_n}\right] \\ &= \frac{\alpha_m \sin(\alpha_n)\cos(\alpha_m) - \alpha_n \sin(\alpha_m)\cos(\alpha_n)}{2\alpha_n^2(\alpha_n^2 - \alpha_m^2)}. \end{aligned}$$

Here we have used another trigonometric identity:

$$\sin(a \pm b) = \sin(a)\cos(b) \pm \sin(b)\cos(a) \tag{3.98}$$

to simplify the result of the integration step. Finally, since $\alpha\cos(\alpha) = \sin(\alpha)$, as follows from equation (3.42), we have

$$\begin{aligned} I_2(m,n) &= \frac{\alpha_m \sin(\alpha_n)\cos(\alpha_m) - \alpha_n \sin(\alpha_m)\cos(\alpha_n)}{2\alpha_n^2(\alpha_n^2 - \alpha_m^2)} \\ &= \frac{\sin(\alpha_n)\sin(\alpha_m) - \sin(\alpha_m)\sin(\alpha_n)}{2\alpha_n^2(\alpha_n^2 - \alpha_m^2)} \\ &= 0. \end{aligned}$$

We now consider the case that $m = n$, or, equivalently, that $\alpha_m = \alpha_n$. We have from integral (3.97):

$$\begin{aligned} I_2(m,n) &= \frac{1}{2\alpha_m^2}\int_0^1 [1 - \cos(2\alpha_m)]\,\mathrm{d}z \\ &= \frac{1}{2\alpha_m^2}\left[1 - \frac{\sin(2\alpha_m)}{2\alpha_m}\right] \\ &= \frac{1}{2\alpha_m^2}\left[1 - \frac{\cos(\alpha_m)\sin(\alpha_m)}{\alpha_m}\right] \\ &= \frac{1}{2\alpha_m^2}\left[1 - \frac{\sin^2(\alpha_m)}{\alpha_m^2}\right] \\ &= \frac{1}{2\alpha_m^2}\left[\sin^2(\alpha_m) + \cos^2(\alpha_m) - \frac{\sin^2(\alpha_m)}{\alpha_m^2}\right] \\ &= \frac{\sin^2(\alpha_m)}{2\alpha_m^2}. \end{aligned}$$

The equivalence of the two final lines follows directly from equation (3.42):

$$\begin{aligned} \cos^2(\alpha_m) - \frac{\sin^2(\alpha_m)}{\alpha_m^2} &= -\alpha_m\left[\frac{\sin(\alpha_m)}{\alpha_m^2} - \frac{\cos(\alpha_m)}{\alpha_m}\right]\left[\cos(\alpha_m) + \frac{\sin(\alpha_m)}{\alpha_m}\right] \\ &= 0. \end{aligned}$$

Thus we have the final result.

Chapter 4

Conclusion

4.1 Discussion

In this thesis we have examined the mechanics by which a two-step reaction, according to the Sal'nikov model, propagates through a combustible gas of various geometries and properties. While rather simple, Sal'nikov's combustion model is capable of producing highly complex behaviour, as each step is thermally sensitive, forming intricate feedback loops between reagent concentration and temperature.

In chapter 1, a reaction through an infinite pipe is considered, and the gas properties are assumed to depend only on a single Cartesian spatial coordinate. A weakly non-linear approximation is made to the governing equations, and using the method of multiple time scales, it is seen that the gas velocity must satisfy the familiar wave equation in the shorter time scale, and Burgers' equation in the longer one. Travelling-wave solutions are sought in the two time scales, and it is then shown that, regardless of the strength of gaseous diffusion and viscosity, the reaction induces a thermal soliton with a sech-squared profile in temperature, which propagates with speed equal to the square root of the ambient temperature. The solutions to these weakly non-linear approximations to the full, non-linear governing equations are then compared to a rather straight-forward numerical scheme based on the method of lines, and are shown to agree closely with the numerical results, at least up to $t = 50$ time units. The numerical scheme was then used to investigate further behaviour of the system not covered by the weakly non-linear analysis, and pulsatile travelling wave solutions were detected. These waves spread out from the point of initial ignition, with periodically-varying amplitude and propagation speed. These waves spark new points of ignition in

turn, which spread throughout the domain.

A similar combustion model is then considered in chapter 2; however, the reaction is assumed to emanate from an initial perturbation at the centre of a spherically-symmetric cloud of gas. As such, the only spatial variable of interest is the radial distance from the centre of reaction. Despite the apparently minor difference in the geometry of the model compared to that considered in chapter 1, the weakly non-linear method used previously is not found to be necessary, and linear solutions are presented instead. It is then shown that the form of the linear solutions is dependent on a single parameter, denoted Ω, representing the net amount of heat produced by the reaction at the linear level. When this parameter is zero, the reaction front is shown to progress as a travelling wave with propagation speed equal to the speed of sound in the ambient gas, and with a steady burnt-distribution which remains after the reaction front passes. However, while every other variable is stable under this regime, the concentration of the intermediate reagent, X, is almost unconditionally unstable, growing or decaying at a rate directly proportional to the time t. When the parameter Ω is non-zero, solutions to the linearised equations are found via an integral transform over a basis of spherical Bessel functions. This reduces the problem to a system of five linear, ordinary differential equations in time for each value of the transformation variable m. Assuming exponential forms for the temporal functions reduces the problem further to a system of algebraic equations for the exponential parameter, which is found to satisfy a cubic polynomial. Finally, the solutions are reconstructed from the initial conditions, with special care taken to ensure convergence at the origin. By a simple argument based on

the Routh-Hurwitz criterion, it is then shown that the stability of these solutions depend only on the same reaction parameter Ω; stable when $\Omega < 0$ and unstable otherwise. Then the linearised solutions are compared to a numerical solution, again based on the method of lines, verifying their accuracy. In the final section of this chapter, we provide a brief extension of the spectral method to a diffusive gas. It is again shown that the solution is stable when $\Omega \leqslant 0$, and unstable otherwise, independent of the strength of the diffusion, though the travelling wave solutions are no longer present.

Finally, chapter 3 models the combustion reaction behind an out-ward moving spherical shock, where the reaction variables return abruptly to their background values with an infinitely steep gradient. As in chapter 2, the gas is assumed to be spherically-symmetric, depending only on the distance r from the reaction centre. Behind the shock, the combustion progresses according to the same governing equations modelled in chapter 2. These are coupled with five algebraic conditions on the density, gas velocity, temperature and concentration of the reactants A and X, as well as the shock propagation speed. These governing equations are then solved numerically using a novel scheme, which builds the jump-conditions into a spectral method based on a set of orthogonal spherical Bessel functions. While this method is shown to model successfully the dynamics of the reacting gases in some parameter spaces, in others high-frequency oscillations may cause the scheme to diverge rapidly from the correct solution. In such cases, some small artificial diffusion and viscosity are then built into the model, smoothing out any erratic behaviour in high-frequency spectral modes, which allows the numerical scheme to progress far beyond the point at which it would other-

wise fail. This new spectral scheme is then compared to a Godunov method, using a Roe type Riemann solver, and the two schemes show remarkably close agreement, even when artificial diffusion is necessary. As well as accurately modelling the shock problem, the spectral method developed in this chapter solves directly for each of the shock values, including the speed and position of the shock front; something which the Godunov method does not natively achieve. Moreover, this new method is capable of achieving much higher spatial resolution behind the shock, as it devotes the entirety of its computational power to the region of interest, and to do so in less time.

4.2 Future Work

While this thesis focuses specifically on Sal'nikov's reaction scheme, there is no reason as to why the analyses contained within cannot be applied to a range of different chemical systems. It would be of interest to investigate a range reaction pathways in this way, allowing for more complex interactions between reaction steps.

Similarly, the range of geometries considered herein is also far from exhaustive. As such there is room for future research in adapting the various methods described in the preceding chapters to unexplored geometric conditions, such as allowing for variation in a second or third spacial dimension, or in considering boundaries which are a finite distance from the reaction centre. In this latter case, perhaps the most interesting feature will be in the interaction of a reaction front with a finite boundary.

Finally, it would be of interest to see the numerical algorithm discussed in

chapter 3 adapted to allow for more sophisticated techniques to solve numerically the flow equations in the domain $0 < \xi < 1$. Such methods may be less prone to developing the high-frequency oscillations to which the stated method is shown to be susceptible, and may even avoid them altogether. It may also be worthwhile to analyse these techniques in more detail, so as to understand their stability and convergence rates, and to compare them with other shock fitting methods.

Bibliography

[1] IYe Sal'nikov. Contribution to the theory of the periodic homogeneous chemical reactions. *Zh Fiz Khim*, 23:258–272, 1949.

[2] BF Gray and MJ Roberts. Analysis of chemical kinetic systems over the entire parameter space I. The Sal'nikov thermokinetic oscillator. *P Roy Soc A*, 416(1851):391–402, 1988. doi: 10.2307/2398066.

[3] BF Gray and MJ Roberts. Analysis of chemical kinetic systems over the entire parameter space II. Isothermal oscillators. *P Roy Soc A*, 416(1851):403–424, 1988. doi: 10.1098/rspa.1988.0041.

[4] LK Forbes. Limit-cycle behaviour in a model chemical reaction: The Sal'nikov thermokinetic oscillator. *P Roy Soc A*, 430(1880):641–651, 1990. doi: 10.1098/rspa.1990.0110.

[5] DP Coppersthwaite, JF Griffiths, and BF Gray. Oscillations in the hydrogen + chlorine reaction: Experimental measurements and numerical simulation. *J Phys Chem*, 95(18):6961–6967, 1991. doi: 10.1021/j100171a043.

[6] G Barenblatt, YaB Zel'dovich, VB Librovich, and GM Makhviladze. *The Mathematical Theory of Combustion and Explosions*. Springer, 1985.

[7] RA Fisher. The wave of advance of advantageous genes. *Annals of Eugenics*, 7(4):355–369, 1937. doi: 10.1111/j.1469-1809.1937.tb02153.x.

[8] A Kolmogorov, I Petrovskii, and N Piskunov. Study of a diffusion equation that is related to the growth of a quality of matter and its application to a biological problem. *Mosc Univ Math Bull*, 1:1–26, 1937.

[9] BJ Matkowsky and GI Sivashinsky. Propagation of a pulsating reaction front in solid fuel combustion. *SIAM J Appl Math*, 35(3):465–478, 1978. doi: 10.2307/2100631.

[10] RO Weber, GN Mercer, HS Sidhu, and BF Gray. Combustion waves for gases (Le = 1) and solids (Le$\rightarrow \infty$). *P Roy Soc A*, 453(1960):1105–1118, 1997. doi: 10.1098/rspa.1997.0062.

[11] H Byrne, J Norbury, and J Ward. Travelling combustion waves in porous media. *Math Eng Ind*, 6:39–62, 1997. doi: 10.1007/978-3-663-09834-8_15.

[12] LK Forbes and W Derrick. A combustion wave of permanent form in a compressible gas. *ANZIAM J*, 43(1):35–58, 2001. doi: 10.1017/S144618110001141X.

[13] LK Forbes. Thermal solitons: Travelling waves in combustion. *P Roy Soc A*, 469(2150), 2013. doi: 10.1098/rspa.2012.0587.

[14] A Bayliss and BJ Matkowsky. Fronts, relaxation oscillations, and period doubling in solid fuel combustion. *J Comput Phys*, 71(1):147–168, 1987. doi: 10.1016/0021-9991(87)90024-6.

[15] RA Paul and LK Forbes. Travelling waves and oscillations in Sal'nikov's reaction in a compressible gas. *ANZIAM J*, 56:233–247, 2015. doi: 10.1017/S1446181114000479.

[16] GI Sivashinsky. On a converging spherical front. *Int J Heat Mass Tran*, 17:1499–1506, 1974. doi: 10.1016/0017-9310(74)90060-X.

[17] M Frankel and GI Sivashinsky. On quenching of curved flames. *Combust Sci Technol*, 40:257–268, 1984. doi: 10.1080/00102208408923809.

[18] PD Ronney and GI Sivashinsky. A theoretical study of propagation and extinction of nonsteady spherical flame fronts. *SIAM J Appl Math*, 49: 1029–1046, 1989. doi: 10.1137/0149062.

[19] Y Wu and Z Chen. Asymptotic analysis of outwardly propagating spherical flames. *Acta Mech Sinica*, 28:359–366, 2012. doi: 10.1007/s10409-012-0008-8.

[20] RA Paul and LK Forbes. Combustion waves in Sal'nikov's reaction scheme in a spherically symmetric gas. *J Eng Math*, 101(1):29–45, 2016. doi: 10.1007/s10665-016-9843-0.

[21] WJM Rankine. On the thermodynamic theory of waves of finite longitudinal disturbances. *Philos T Roy Soc A*, 160:277–288, 1870. doi: 10.1098/rstl.1870.0015.

[22] H Hugoniot. Sur la propagation du mouvement dans les corps et spcialement dans les gaz parfaits. *J Ecole Polytechnique*, 58:1–125, 1889. doi: 10.1098/rstl.1870.0015.

[23] DL Chapman. VI. on the rate of explosion in gases. *Lond Edinb Dubl Phil Mag*, 47(284):90–104, 1899. doi: 10.1080/14786449908621243.

[24] É Jouguet. On the propagation of chemical reactions in gases. *J Math Pures Appl*, 1:347–425, 1905.

[25] YaB Zel'dovich. On the theory of the propagation of detonation in gaseous systems. *Zh Eksp Teor Fiz*, 1940.

[26] J Von Neumann. Theory of detonation waves. *OSRD*, 1942.

[27] W Döring. On detonation processes in gases. *Ann Phys*, 1943.

[28] G Taylor. The formation of a blast wave by a very intense explosion I. theoretical discussion. *P Roy Soc A*, 201(1065):175–186, 1950. doi: 10.1098/rspa.1950.0050.

[29] MH Rogers. Similarity flows behind strong shock waves. *Q J Mech Appl Math*, 11(4):411–422, 1958. doi: 10.1093/qjmam/11.4.411.

[30] LI Sedov. *Similarity and Dimensional Methods in Mechanics*. Academic Press, 1959.

[31] G Taylor. The formation of a blast wave by a very intense explosion II. the atomic explosion of 1945. *P Roy Soc A*, 201(1065):159–174, 1950. doi: 10.1098/rspa.1950.0049.

[32] SK Godunov. A difference method for numerical calculation of discontinuous solutions of the equations of hydrodynamics. *Mat Sb*, 89(3): 271–306, 1959.

[33] JD Anderson. *Modern Compressible Flow with Historical Perspective*. McGraw-Hill, 2003.

[34] GB Whitham. *Linear and Nonlinear Waves*. Wiley-Interscience, New York, 1974.

[35] SK Scott. *Chemical Chaos*. Oxford University Press, 1993.

[36] T Stocker. *Introduction to Climate Modelling*. Springer, 2011.

[37] HW Liepmann and A Roshko. *Elements of Gasdynamics*. Wiley, New York, 1957.

[38] FA Williams. *Combustion theory: The fundamental theory of chemically reacting flow systems*. Addison-Wesley Publishing Company, 1965.

[39] WF Ames. *Numerical methods for partial differential equations*. Academic Press, 1977.

[40] The Mathworks, Inc. MATLAB and Statistics Toolbox Release 2012b.

[41] LK Forbes and BF Gray. Forced oscillations in an exothermic chemical reaction. *Dynamics and Stability of Systems*, 9(3):253–269, 1994. doi: 10.1080/02681119408806181.

[42] M Abramowitz and IA Stegun. *Handbook of Mathematical Functions*. Dover Publications, New York, 1964.

[43] GB Arfken. *Mathematical Methods for Physicists*. Academic Press, London, 1985.

[44] EJ Routh. *Stability of Motion*. Halsted Press, London, 1975.

[45] D Zwillinger. *CRC Standard Mathematical Tables and Formulae, 30th Edition*. CRC Press, New York, 1995.

[46] B Fornberg. Generation of finite difference formulas on arbitrarily spaced grids. *Math Comput*, 51:699–706, 1988. doi: 10.1090/S0025-5718-1988-0935077-0.

[47] JEA John. *Gas Dynamics*. Allyn and Bacon, 1969.

[48] G von Winckel. Legendre-Gauss quadrature weights and nodes, 2004. URL `http://www.mathworks.com/matlabcentral/fileexchange/4540-legendre-gauss-quadrature-weights-and-nodes`.

[49] GK Batchelor. *An Introduction to Fluid Dynamics*. Cambridge University Press, London, 1967.

[50] LK Forbes and OA Krzysik. Shock–jump conditions in a general medium: Weak-solution approach. *Shock Waves*, pages 1–10, 2016. doi: 10.1007/s00193-016-0695-3.

[51] R Courant and KO Friedrichs. *Supersonic Flow and Shock Waves*. Springer-Verlag, 1948.

[52] WW Wood and JG Kirkwood. Diameter effect in condensed explosives. The relation between velocity and radios of curvature of the detonation wave. *J Chem Phys*, 22(11):1920–1924, 1954. doi: 10.1063/1.1739940.

[53] J Von Neumann and RD Richtmyer. A method for the numerical calculation of hydrodynamic shocks. *J Appl Phys*, 21(3):232–237, 1950. doi: 10.1063/1.1699639.

[54] EF Toro. *Riemannn Solvers and Numerical Methods for Fluid Dynamics*. Springer-Verlag, 2009.

[55] PK Sweby. Godunov methods. *Godunov methods: Theory and Application*, pages 879–898, 2001. doi: 10.1007/978-1-4615-0663-8_85.

[56] P Bartsch and A Borzi'. A new reconstruction technique for the Euler equations of gas dynamics with source terms. *Godunov methods: Theory and Application*, pages 77–88, 2001. doi: 10.1007/978-1-4615-0663-8_7.

[57] PL Roe. Characteristic-based schemes for the Euler equations. *Annu Rev Fluid Mech*, 18:337–365, 1986. doi: 10.1146/annurev.fl.18.010186.002005.

[58] PL Roe. Approximate Riemannn solvers, parameter vectors, and difference schemes. *J Comput Phys*, 43(2):357–732, 1981. doi: 10.1016/0021-9991(81)90128-5.